DRIPPING DYNAMICS
FROM A TILTED NOZZLE

AMARAJA TAUR

DISSERTATION SUBMITTED IN FULFILMENT OF THE REQUIREMENTS FOR THE DEGREE OF MASTERS OF ENGINEERING SCIENCE

CHEMICAL ENGINEERING DEPARTMENT,
FACULTY OF ENGINEERING
UNIVERSITY OF MALAYA
KUALA LUMPUR
2014

UNIVERSITI MALAYA

<u>Original Literary Work Declaration</u>

Name of Candidate: **AMARAJA TAUR**   (Passport No: **k418494**)

Matric No: KGA120063

Name of Degree: KGA-MASTERS OF ENGINEERING SCIENCE

Title of Thesis ("this work"):

DRIPPING DYNAMICS FROM A TILTED NOZZLE

Field of Study: CHEMICAL ENGINEERING – EXPERIMENTAL FLUID DYNAMICS

I do solemnly and sincerely declare that:

(1) I am the sole author/writer of this Work;
(2) This Work is original;
(3) Any use of any work in which copyright exists was done by way of fair dealing and for permitted purposes and any excerpt or extract from, or reference to or reproduction of any copyright work has been disclosed expressly and sufficiently and the title of the Work and its authorship have been acknowledged in this Work;
(4) I do not have any actual knowledge nor do I ought reasonably to know that the making of this work constitutes an infringement of any copyright work;
(5) I hereby assign all and every rights in the copyright to this Work to the University of Malaya ("UM"), who henceforth shall be owner of the copyright in this Work and that any reproduction or use in any form or by any means whatsoever is prohibited without the written consent of UM having been first had and obtained;
(6) I am fully aware that if in the course of making this Work I have infringed any copyright whether intentionally or otherwise, I may be subject to legal action or any other action as may be determined by UM.

Candidate's Signature: Date:

Subscribed and solemnly declared before,

Witness's Signature: Date

Name:

Designation:

ABSTRACT

The dripping dynamics of Newtonian liquids emanating from a tilted nozzle is studied. A high speed camera is employed to observe the drop breakup process. The level of viscosity, flow rate, nozzle diameter, and nozzle inclination angle had been varied independently. The drop break up time t_b, which is the time interval between two subsequent drops, and the different modes of dripping have been identified. The new experiments reveal that increasing the nozzle inclination angle results in lowering the drop breakup times for all viscosities and nozzle diameters investigated, suggesting that the surface tension forces cannot hold the drops longer despite the weakened effective gravitational pull. This counter-intuitive finding is further corroborated by pendant drop experiments and computations. In the modes of dripping, as the liquid flow rate increases, the system transitions from period-1(P1) dripping to limit cycle (LC) before showing chaotic (C) responses. A phase diagram showing the transition between the different dripping modes for different nozzle inclination angle is constructed in the (We, Ka) space, where We (Weber number) measures the relative importance of inertia to surface tension force and Ka (Kapitza number) measures the relative importance of viscous to surface tension forces. At low values of We and Ka, the system shows a transition from period-1 to limit cycle before chaos. The limit cycle region narrows down with increase in inclination. Further increase in the values of We and Ka gives a direct transition from period-1 to chaos. The experimental volumes of primary drops by image analysis show good agreement with the volumes obtained from the correlation developed, showing a maximum of 15% error. The experimental data obtained from image analysis

further suggest that, in the P1 regime the pendant drop volume varies such that the trend

of the primary drop volume differs significantly from that of the breakup time.

ABSTRAK

Dinamik penitisan cecair Newtonian berpunca daripada muncung condong dikaji. Sebuah kamera berkelajuan tinggi digunakan untuk memerhatikan proses pemecahan titisan. Tahap kelikatan, kadar aliran, diameter muncung, dan sudut muncung telah diubah secara bebas. Penurunan masa pemechan t_b, iaitu selang masa di antara dua titik yang berikutan, dan pelbagai mod penitisan telah dikenalpasti. Ujikaji baru mendedahkan bahawa peningkatan sudut muncung cenderung menurunkan selang masa perpecahan titisan untuk semua kelikatan dan diameter muncung disiasat, seterusnya mencadangkan bahawa daya ketegangan permukaan tidak boleh memegang titisan lebih lama walaupun tarikan graviti berkesan yang lebih lemah. Penemuan lawan jangkaan ini disokong lagi oleh ujikaji titisan tergantung bebas dan pengiraan. Dalam mod penitisan, dengan kenaikan kadar aliran, sistem beralih dari kitaran-1 (P1) kepada kitaran terhad (LC) sebelum menunjukkan gejala huru-hara (C). Gambar rajah fasa yang menunjukkan peralihan antara mod penitisan yang berbeza untuk sudut muncung yang berbeza dibina dalam ruang (We, Ka), di mana We (nombor Weber) mengukur kepentingan relatif inersia kepada daya tegangan permukaan dan Ka (nombor Kapitza) mengukur kepentingan relatif kelikatan ke daya ketegangan permukaan. Pada kadar aliran cecair yang rendah dan kelikatan rendah, sistem ini menunjukkan peralihan daripada kitaran-1 kepada kitaran terhad. Rejim kitaran terhad menjadi lebih sempit dengan peningkatan sudut muncung. Peningkatan dalam nilai-nilai Ka dan We memberikan peralihan terus dari tempoh-1 ke huru-hara. Isipadu titisan utama melalui analisis imej ujikaji menunjukkan persetujuan yang baik dengan isipadu yang diperolehi daripada sekaitan yang dicadangkan, dengan menunjukkan ralat maksimum 15%. Data ujikaji yang diperolehi daripada analisis imej mencadangkan bahawa dalam rejim P1, isipadu titisan tergantung berubah sedemikian sehingga pola isipadu titisan utama berbeza dengan ketara dengan masa perpisahan.

ACKNOWLEDGEMENT

Place:

_____

Dated: Amaraja Taur
                                                                Dept of Chemical Engineering
                                                                University of Malaya

TABLE OF CONTENTS

Chapter	Topic	Page no

LIST OF FIGURES

Figure No	Title	Page No

LIST OF TABLES

Table No	Title	Page No

LIST OF SYMBOLS AND ABBREVIATIONS

Symbols

Roman alphabets

g Acceleration due to gravity

G Bond number

Ka Kapitza number

Q   Liquid flow rate

R   Radius of the nozzle

$\tilde{t}_b$ Drop breakup time

t_b Dimensionless drop breakup time

v Velocity of the liquid

$\tilde{V}$ Drop volume

V   Dimensionless drop volume

We Weber number

Greek alphabets

θ Nozzle inclination angle from the vertical

ρ Density of the liquid

σ Surface tension of the liquid

Abbreviations

C   Chaos

LC   Limit cycle

P1   Period-1

SE   Surface evolver

N1   Nozzle-1

N2   Nozzle-2

N3   Nozzle-3

S0   0% glycerol in water glycerol solution

S20   20% glycerol in water glycerol solution

S40   40% glycerol in water glycerol solution

S80   80% glycerol in water glycerol solution

1 Introduction

1.1   Research Background

Drop formation from a nozzle is phenomenon ubiquitous in nature and industries. The phenomenon of drop breakup, drop collision, and drop formation involving free surface flow is not only beautiful, but also is a challenging physical problem for researchers. The drop formation process in the nature has been observed and the richness in the physics of the drop formation has been identified which attracted the attention of scientist and engineers over the years.

A drop may form when liquid accumulates at the lower end of a tube or other surface boundary. Drop may also form by the condensation of a vapor or by atomization of a larger mass of liquid. Rain drop formation is the best example of drop formation seen in the nature, where the liquid droplets formed from the condensation of atmospheric water vapor get precipitated, which later becomes heavy enough to fall under gravity. Another example is the water in the form of small droplets that is generally seen on thin, exposed surfaces in the morning or evening as a result of water vapor condensation called dew. The large surface area of the exposed surface aids the radiation process cooling the exposed surface which helps in the condensations of the atmospheric moisture, resulting in the formation of droplets. The drop formation resulting from the dripping of water from the roof and tap are also interesting examples which clearly show the individual events of detaching drops.

The description of the flow and drop formation process shown in the Figure 1.1 would be more complicated than one might think. Instead, it is much more useful to focus on the

individual events of drop formation, to gain some general insight into the dynamics which can help to investigate the global behaviour of the process.

Figure 1.1 A dolphin in the New England Aquarium in Boston, Massachusetts; Edgerton (1977). [Adapted from Eggers (1997)]

A simple way to form a drop is to allow liquid to flow slowly from the lower end of a vertical nozzle of small diameter. The surface tension of the liquid tries to minimize the liquid drop interfacial tension which allows the liquid volume to hang at the lower end of the nozzle. This hanging drop is called pendant drop. Later the pendant drop becomes unstable when drop volume exceeds a certain limit. The drop later detaches under the influence of gravitation pull. The detached drop is called as primary drop and the small drop volume produced during the detachment process which is undesirable for industrial application is called satellite drop. This drop formation process from a vertical nozzle has been an interesting area because of many industrial

applications such as ink-jet printing (Le, 1998), silicone microstructure array (Laurell et al., 2001), emulsion formation (Sachs et al., 1994), 3D micro-printing (Walstra, 1993), microencapsulation etc (Freitas et al., 2005).

In most of the applications the most desired drop formation process should give uniform size distribution and fast production rate. Even though the drops generically results from the motion of free surfaces, it is not easy to predict their size distribution and the dynamics involved in the process. The key parameters which controls this drop formation process are physical properties of liquid, size and shape of nozzle, liquid ejection velocity etc. The physical properties of the liquid consist of the surface tension, density and viscosity of the liquid. Whereas the different shapes of nozzle can be flat nozzle or obliquely cut nozzle. The slow drop formation can be observed at very low liquid ejection velocity, whereas at high velocity the liquid can eject as a column of the liquid which subsequently breaks into drops. The detailed studies of the dynamics involved in the drop formation process were not possible before high-speed digital cameras could be used for the photography in the experiments and powerful computers for the simulations.

Drop formation thus results in an extremely broad spectrum of different droplet sizes. The distribution of sizes was first time noticed 200 years ago by Felix Savart (1833) in Paris. He observed that the water jet emanating from a small diameter orifice separates in to tiny droplets in the span of perhaps a $1/100^{th}$ of a second. Drop formation sequences are shown in the Figure 1.2, where the jet of water is being ejected from a vertical nozzle with primary and satellite drop formation. Generally the formation of droplet is periodic in nature, but sometimes with primary drop, a

smaller "satellite" drop is seen as a result of drop breakup process. This satellite drop formation is undesirable because they are far more readily misdirected by aerodynamic and electrostatic forces and can thereby degrade the printing resolution. Yet another example is the formation of satellite drops during crop spraying. The lighter satellite drops of herbicides or pesticides are more easily transported to the site other than that intended (spray drift). Beside waste and inefficiency spray drift from pesticides and herbicide application exposes people and the environment to residues that causes undesired health and environmental effects (Dravid, 2006).
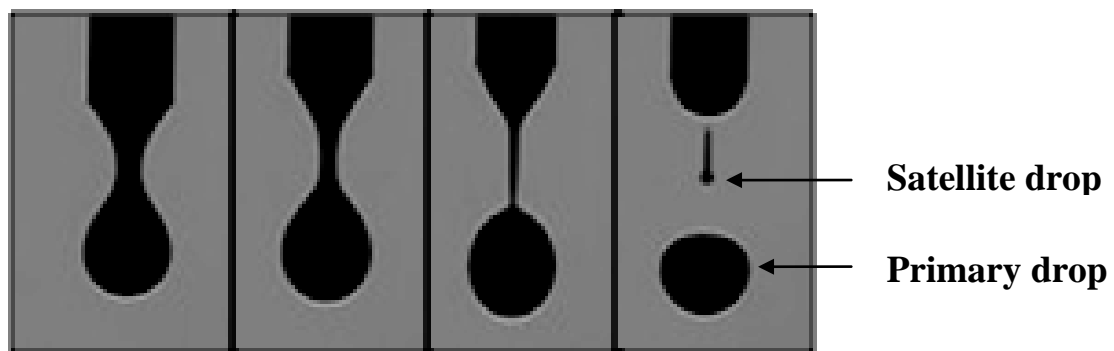
Figure 1.2 Drop formation sequences showing primary and satellite drop.

Thus the arrival of ink-jet printing technology, that the consequences of Savart's observations were fully appreciated. Ink-jet printing has been implemented in many different designs and has a wide range of potential applications. Ink-jet is a non-impact dot-matrix printing technology in which droplets of ink are jetted from a small aperture directly on a targeted object on a specified media to create an image (Le, 1998). Thus the technical importance of the drop formation process and its continuous study from last 300 years (Eggers, 1997) led to intense development in ink-jet printing technology. For example, in the printing applications of integrated circuits the ink is replaced by solder (Liu and Orme, 2001). In biotechnology, thousands of DNA-filled water drops can be analyzed in parallel, by placing them in

4

an array on a solid surface (Basaran, 2002). All these techniques rely on the production of drops of well-controlled size, and satellite drops are highly detrimental to the quality of the product.

Many liquid dosage forms in the pharmaceutical and biotech industries are based on micro droplets (Kippax and Fracassi, 2003). The liquid pharmaceutical dosages in aerosol form are directly sprayed on affected areas. The individual liquid drop sizes and the amount of the liquid dosage sprayed on the affected area decide the amount of drug absorbed, hence controlling these parameters becomes very important in the pharmaceutical industries. The same efforts have been made to control the liquid drop size distribution and their velocities in the agricultural sprays in order to increase the efficiency (Lake, 1977).

Fundamentally the process of drop formation can be broken down in to dripping, jetting and drop on demand. The first two methods occur under the action of gravity, where dripping is the phenomenon of ejection of liquid from a nozzle to form droplets when flow rate is sufficiently low, while jetting is phenomenon at high flow rates in which liquid flows out as a continuous stream to form a jet which subsequently breaks up in to small droplets. The third method i.e. drop on demand involves external electrical force to control the drop formation process.

A Newtonian liquid having viscosity μ, density ρ, and surface tension σ, flowing through a nozzle of radius R, at flow rate Q is the most commonly investigated configuration for drop formation studies as shown in Figure 1.3. For a vertical nozzle the dripping dynamics are governed by three dimensionless groups (Subramani et al., 2006; and Basaran, 1995; Clasen et al., 2009): Weber number We$= \rho v^2 R/\sigma$ that

5

measures the relative importance of inertial to surface tension force, a Bond number

$G = \rho g R^2 / \sigma$, where g is the acceleration due to gravity, that measures the relative

importance of body force to surface tension force, and Kapitza number $Ka = (\mu^4 g /$

$\rho\sigma^3)^{1/3}$ or Ohnesorge number $Oh = \mu/(\rho R \sigma)^{1/2}$, both measures the relative importance of

viscous force to surface tension force.
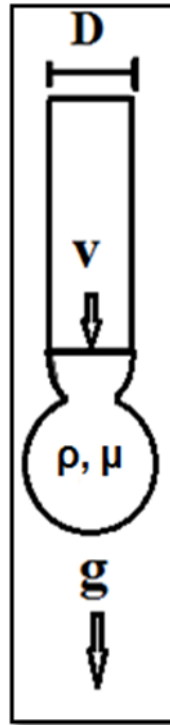
Figure 1.3 Drop formation from a vertical nozzle.

The quantitative studies usually focus on the measurement of volumes of the liquid

droplets (Subramani et al., 2006), the liquid thread length before breakup (Zhang and

Basaran, 1995), and time interval between two drop breakups (Clasen et al., 2009).

1.2 Motivation

As addressed before the increased technological applications of drop formation grabbed the attention of scientist to get enough inside in to the drop formation process. Drop formation from a nozzle or an orifice has been the subject of numerous theoretical and experimental studies (Eggers, 1997). Most of the attention to date has focused on studies of the drop formation from a vertical nozzle, where the studies are done either by changing the liquid properties or by changing the liquid flow rate (Zhang and Basaran, 1995; Ambravaneswaran et al., 2000). In some of the studies the effect of nozzle size and shape is also studied (Zhang and Basaran, 1995; D'Innocenzo et al., 2004). Though the large number of studies shows that there has been enough research done on the drop formation, but a lot is to be explored which is explained in the paragraph below.

Despite the considerable amount of efforts devoted to droplet formation studies, there has been a little attention directed towards drop formation studies from an inclined nozzle. In this system, the nozzle is inclined at an angle θ and liquid is passed through a nozzle to form small liquid droplets. The introduction of asymmetrical perturbations, by tilting the nozzle at an angle θ (Reyes et al., 2002) breaks the cylindrical symmetry and found strong changes in dripping dynamics when compared with those obtained from a vertical nozzle. In the experiments on dripping from a tilted nozzle, it is showed that the inclination angle can constitute an effective control parameter by breaking the axis symmetry thus adding the asymmetric perturbations. However, previous studies are far from being comprehensive, thus unable to provide the proper explanations on the general behaviour of drop formation from a tilted nozzle.

However, so far, there are no reports on the general behaviour of different modes of drop formation from an inclined nozzle. The reported data only showed the strong change in the dripping behaviour of an inclined nozzle even for small nozzle inclination angle $\theta = 5°$ (Reyes et al., 2002). To this end it is highly desirable to know the details about the general behaviour of drop formation from an inclined nozzle.

1.3   Objectives of Present Work

In this work, focus will be given on the drop formation study from an inclined nozzle and the results will be compared with its behaviour when nozzle is in vertical position. Some of the results will be further highlighted and compared with the computations. As the details about the general behaviour of drop formation process from an inclined nozzle is not provided before, the results obtained in this work will provide useful information. The main objectives of this work are summarized as follow:

a) To investigate the different dripping modes by investigating the drop breakup time t_b, for different θ and We values. The different modes of dripping are shown on the phase diagrams which are constructed in (We, Ka) space for all G and θ values. The effect of θ on the formation of satellite drops is also highlighted in the phase diagram.

b) To investigate the effect of We, Ka, G and θ on the dripping time t_b. This finding was summarized in a correlation for the dimensionless breakup volume V over wide ranges of *G*, *Ka* and θ.

c) To investigate the breakup volumes of the drop from tilted nozzle dripping experiments using image analysis.

1.4   Outline of the research approach

- In Chapter 2, a literature review is presented. A brief history of drop formation study presented followed by detailed review with their key findings and recent development in same area is given.

- In Chapter 3, a brief introduction about the methodology is provided followed by the experimental setup with the fluid characterization and properties. In the same chapter the experimental procedure is given followed by details on image analysis method and breakup time calculations.

- In Chapter 4, results on different dripping modes for both vertical and inclined nozzle are presented and also the modes of dripping are shown on phase diagrams. The effect of θ on drop breakup time in the P1 regime are presented for a wide range of parameters and results obtained on the same are corroborated with some experiments and computer simulations which later gives a correlation for drop breakup volume. The breakup volumes of primary drops by image analysis also compared with that obtained from the correlation developed.

- The conclusions are given in chapter 5.

2 Literature Review

2.1   History of Drop Formation

Early experiments of Savart (1833) demonstrated that the liquid jet flowing out from nozzle first decays in to small undulations and then droplets. Savart illuminated the liquid jet as shown in Figure 2.1 by using a light source. He simply assumed liquid jet as a circular cylinder and observed that the tiny undulations grow on liquid jet. These undulations then grow large enough and results in to droplets. Without photography, it was very difficult to make experimental observations, since the time scale at which the drop breakup occurs is very small. Yet Savart was able to extract a remarkably accurate and complete picture of the actual breakup process using his naked eye alone. The observations on drop breakup process are well summarized in Figure 2.2 (Eggers, 2006). To the left side of the figure, one sees a continuous jet of the liquid near the exit of nozzle. Growing perturbations are seen next to the continuous jet until the point labelled as 'a', where drops start breaking up. The elongated liquid thread near 'a' later becomes part of the droplet. Both primary and tiny satellite drops are visible in the figure. The fast moments involved in the drop formation process were not clearly resolved in the figure.
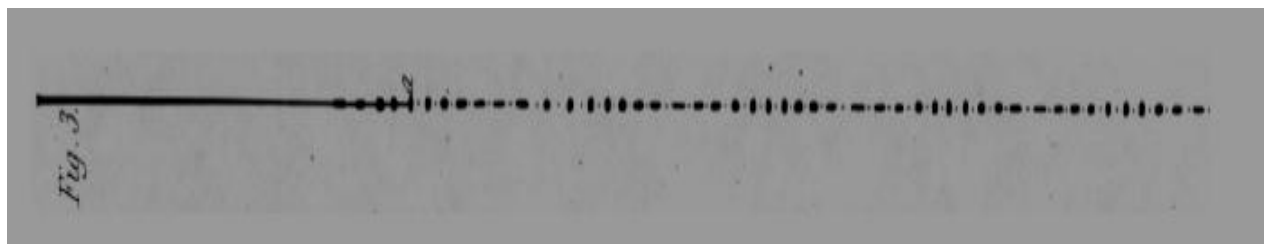
Figure 2.1 Drop breakup process of a liquid jet 6 mm in diameter showing main drops and satellite drops (Eggers, 2006).

Some of the Savart's observations are summarized as: (i) the liquid jet breakup is independent of direction of gravity, physical properties of liquid, the diameter of liquid jet and jet velocity; (ii) the tiny undulations always results from the perturbations received by the liquid jet from the nozzle tip when it emanates from nozzle. Savart assumed that the drop formation process involves balance between inertial and gravity force.

A few years later Plateau (1843) discovered that it's surface tension which causes liquid jet perturbations to reduce its surface area by collecting the liquid in to one sphere in order to maintain smallest surface to volume ratio. Identification of the surface tension force was missing in Savart's study, however he made a reference to mutual attraction of molecules which prefers to form a sphere of the liquid, around which the oscillations take place. But the crucial role of the surface tension was identified by Plateau only. With this results it follows as well whether the perturbations imposed on the liquid jet will grow or not. The perturbations that will undergo reduction of surface area favored by surface tension, and will thus grow.

Following up on Plateau's insight, Rayleigh (Rayleigh, 1879, Rayleigh and Strutt, 1879) in 1879 studied the linear stability of liquid jet, where he noticed that, the surface tension has to work against inertia, which opposes fluid motion over long distance. Rayleigh assumed an infinitely long, initially stationary, circular, inviscid liquid jet of radius r and the calculation made by this linear stability analysis allowed him to describe the initial growth of instabilities as they initiate near the nozzle and continuous length of jet. Rayleigh found that there is an optimal wavelength $\lambda = 9r$ at which perturbations grow faster, and which sets the typical size of drops. Rayleigh confirmed his theory within 3% with the data Savart got 50 years before.
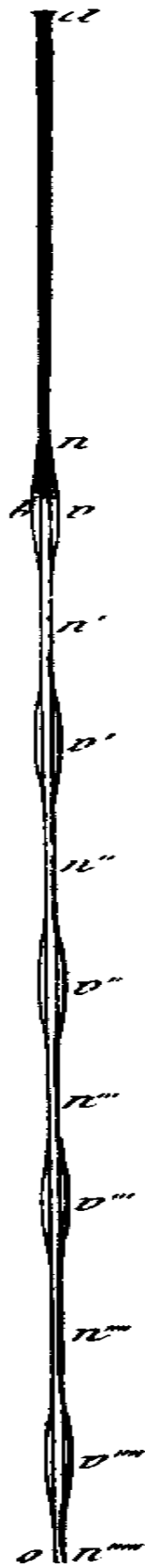
Figure 2.2 Growing perturbations on a jet of water [adopted from (Eggers, 1997)]

In the second half of the 19th, many researchers had focus on the surface tension related phenomenon, whereas different parameters affecting on drop dynamics was studied in 20th century both experimentally and theoretically.

2.2   Drop formation dynamics

When the flow rate is small, a pendant drop hanging at the nozzle tip can detach when a critical volume is reached resulting into primary drop. A small volume of liquid drop can also results in the process of drop breakup giving satellite drop. Conceptually, drop formation process can be divided into two stages: The first one corresponds to the growth of the liquid at the end of the nozzle tip and second one corresponds to the necking and breaking of the drop which may form only primary drop or both primary or satellite drop depending upon the experimental parameters. A static description of the droplet breakup patterns, neck formation, shape and size of the droplets are useful in the study and given in the following subsections.

2.2.1   Primary drop formation

Historically, research on the drop formation was motivated mostly by engineering applications, hence the liquid drop shape and a size has given more attention in the study. When liquid is released slowly through a vertical nozzle, initially the surface tension forces are in balance with the gravitational force. When inertia does not play any role, one can easily see that the hanging drop goes through a sequence of equilibrium shapes. These sequences of liquid drops are carefully studied by Worthington in 1881 (Worthington, 1881). Worthington noticed that, in the previous dripping experiments carried by Guthrie (1863), the drop sizes were calculated based on the weight of the droplets. But this study lacks the most important information of the liquid drops i.e. shape and size of the droplet when it falls and goes thrugh the number of sequences.A simple experimental technique allowed Worthington to observe the drop sequences, but the observations are made without photographic technique hence the results were not quantitative in nature.

The first quantitative experiments were done by Haenlein (1931) in 1931 using different liquids having different densities, surface tension, viscosities, jet diameters and jet velocities. The liquids tested were water, gas oil, glycerine and castor oil. A simple apparatus was used to produce the liquid jet of 0.1 to 1 mm diameter with velocities ranging from 2 to 70 m/s. The observations were made by using shadow pictures by means of electric spark. Haenlein observed the disintegration time for different kinds of liquid jets, where he found different patterns of disintegration of liquid jet: drop formation without air influence, drop formation with air influence, formation of waves, and complete disintegration of jet. These were the primary dripping experiments where the primary drops were quantitatively observed for different experimental parameters. A step ahead, Ohnesorge (McKinley and Renardy, 2011) used sophisticated spark flash timing and variable exposure system, where the quality of the images and temporal resolution was improved. The liquids of different physical properties were ejected from the nozzle at different flow rates. Four important regimes were observed in the drop breakup process in his experiments namely: Slow dripping, breakup of cylindrical jet by axisymmetric perturbations, breakup by skew like perturbations, and atomization of jet. Takahashi and Kitamura (1969) also carried out the dripping and jetting experiments on liquids like water, kerosine, and glycerine surrounded air and immicible liquid and he observed that the break up pattern in both the system are analogous to each other. Takahashi observed that as the ejection velocity increased all the liquids shows dripping, laminar jetting, and turbulant flow patterns.

A fascinating demonstration of Shi and Brenner (Shi et al., 1994) by experiments and computations, using the one dimensional equation developed by Eggers and DuPont (1994), that liquid thread or liquid neck can spawn a series of smaller necks with even

thinner diameters was a very important contribution in the study of secondary necks. In the study, the different shapes of hanging drops for different liquid viscosities close to drop breakup were focused, where they observed the dramatic change in primary drop shape for different viscosities. As the value of viscosity increases the neck of the liquid drop elongates and forms structure that is not seen in case of pure water. They observed some secondary neck formations at the break up points for high viscosity liquids which occurs by initial thinning near the drop followed by rapid extension of the neck upward away from the drop as shown in the figure 2.3 (a-c). As the liquid neck becomes sufficiently thin, it undergoes finite amplitude instabilities may be due to the thermal noise. As a result of this, a secondary neck grows on a primary neck having self-similar form. These observations were experimentally possible by high speed photography where they could see the multiple stages of necking process before actual break up. Simulation results on the same also shows that the near the bottom of the long neck there is a region where the thickness of the neck decreases forming a secondary neck.
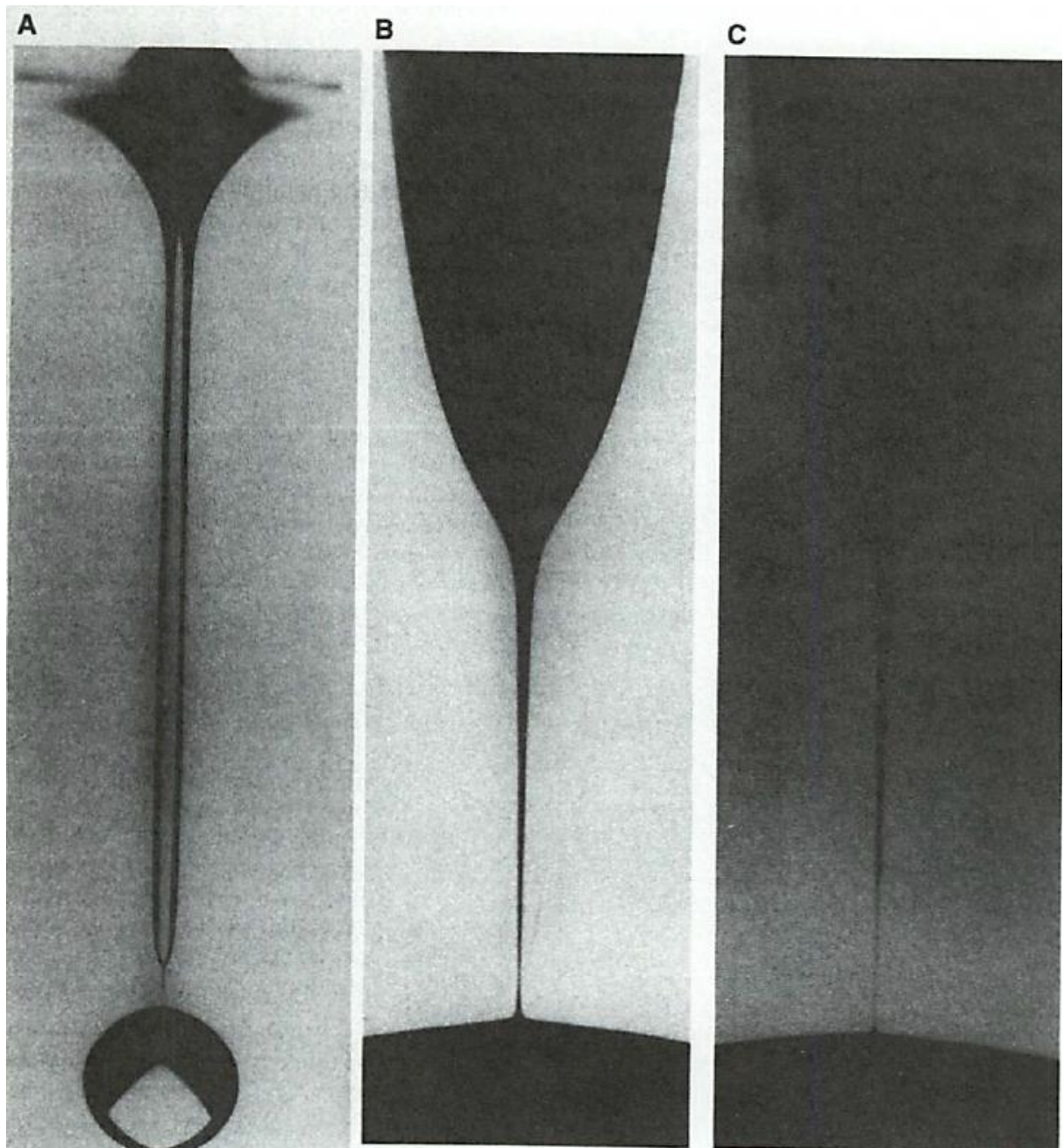
Figure 2.3   Secondary neck formations for water glycerol mixture (85%).   (A) The elongated liquid thread forms a secondary neck just above the primary drop (B) A magnified region near breakup point (C) Same region as in (B), very near to breakup process (Shi et al., 1994).

A detailed experimetal study by Zang and Basaran (1995) investigated the effect of all relevant parameters on the drop breakup length for first time in the study.   Figure 2.4 shows the evolution of liquid thread connecting the main drop and the remaining liquid for water.   It is very clear from the figure that during necking the portion of main drop

takes spherical shape and the remaining liquid thread looks like a liquid cone. Later the liquid thread thins, and at certain neck diameter it detaches from the spherical drop which later oscillates in vertical direction by changing its shape as seen in Figure 2.3 (l, m). However the braking process can result in to formation of satellite drop as seen in Figure 2.3(m). Comparisons of the primary drop breakup volume measured in the experiments are compared with predicted volume obtained from the empirical model of Scheele and Meister (1968). The volumes measured experimentally are smaller than the predicted and more deviation is seen at higher flow rates with maximum relative deviation of 25%, showing relatively good agreement between experimental and predicted volume. In same study Zhang and Basaran obtained a detailed phase diagram for different viscosity, flow rate and nozzle radius. The phase diagram details about main drop, satellite drop size and neck length.

a   b   c   d   e   f   g   h   i   j   k   l   m
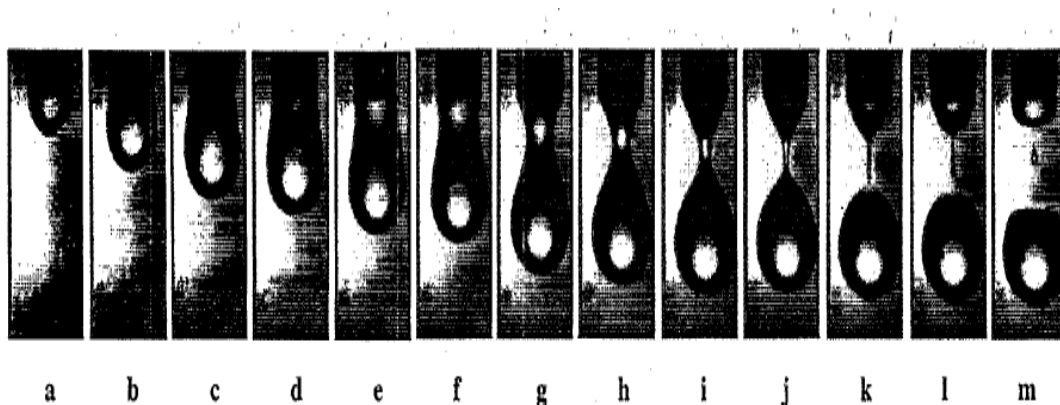
Figure 2.4 Drop shapes of water dripping from a nozzle of diameter 0.16 cm at the liquid flow rate 1ml/min, taken at different time intervals (Zhang and Basaran, 1995).

The predictions of the computations made by Wilkes *et al*. (1999) made by using a 3D, axisymmetric or 2D finite element algorithm have been shown to agree with couple of per

cent with the experimental results which confirms the high degree of accuracy in the calculations. The volumes of the drops are found to mostly affected by the interplay between gravity and surface tension force. The computed shapes of the drop are overlaid on experimental shapes of the drops showing a very good agreement in figure 2.5. In the same study, the algorithm developed is used for calculating limiting length and primary drop volume for a wide range of parameter space spanned by relevant dimensionless group.
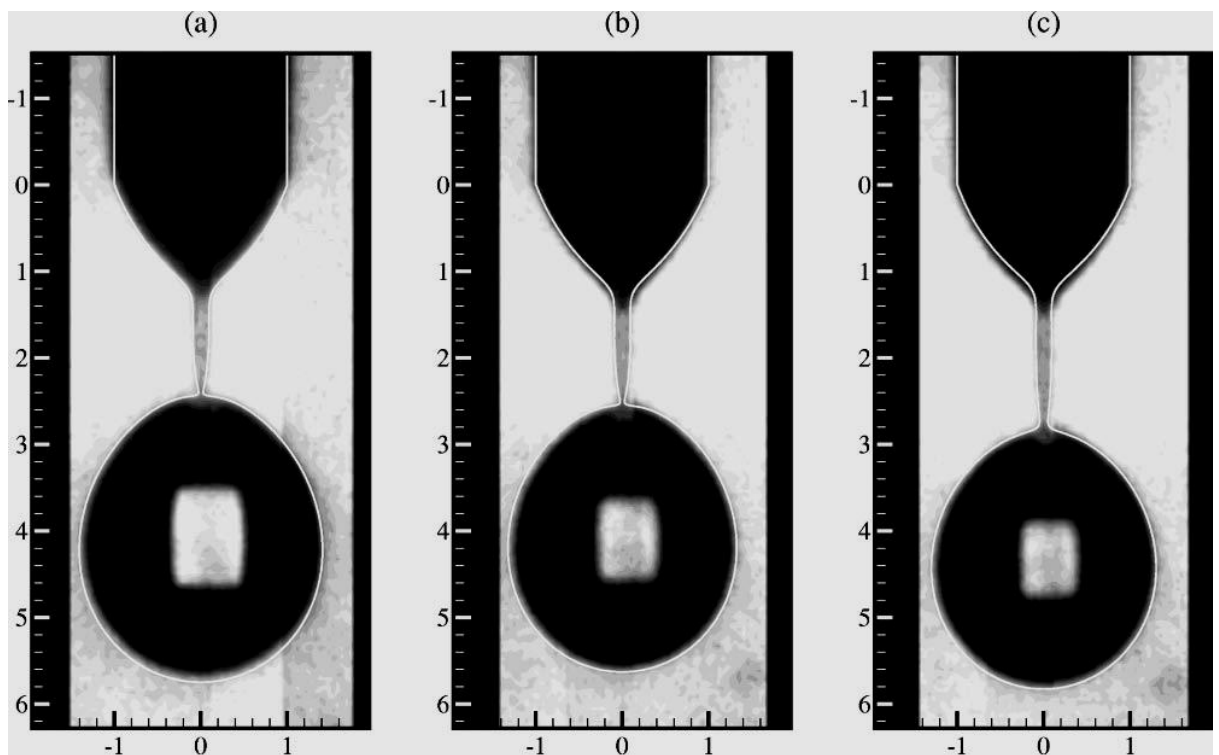
Figure 2.5 Computed shapes of drops, solid white curves, overlaid on experimentally recorded images of identical drops of glycerine–water mixtures at near the drop breakup. The viscosity of the liquid increases from left to right (Wilkes et al., 1999).

2.2.2 Satellite drop formation

In the drop formation process, the primary drop does not form alone in some cases, a undesirable form of a small drop volume also results in the breakup process called "satellite drop". These satellite drops actually decay the printing quality, as drop of different size are deflected differently by an electric field. Hence understanding the cause of satellite drop formation and possible control has been attracted the attention of researchers in the field of drop formation.

The satellite drop formation was first observed by Savart in 1833 (Eggers, 2006). Figure 2.1 given in the above sub section 2.1, shows that the small satellite drops in between two primary drops results during the liquid jet breakup. Later Plateau (1849) also included some experimental sketches as shown in the figure 2.6 for oil suspended in to water alcohol mixture. The nonlinear dynamics of drop liquid jet breakup of a viscous liquid first goes through the elongation of the liquid thread and then tiny perturbations grows forming minima at many places. The final stage of the breakup includes the formation of primary and satellite droplets where he observed that the satellite drop is not alone formed at the center of two primary drop, but also even smaller satellite drops are formed at right and left of the satellite drop which indicates that the final stage of the breakup is much more complicated that one would think. Without photography and with air as media surrounding the drop, it was very difficult to observe the existence of the satellite drops in the dripping experiments. Having these difficulties did not escape the attentive eyes of Guthrie (Guthrie, 1863) in satellite drop observation. The kind of drops he observed were the one which moves upward once they formed as a result of pinch off process.
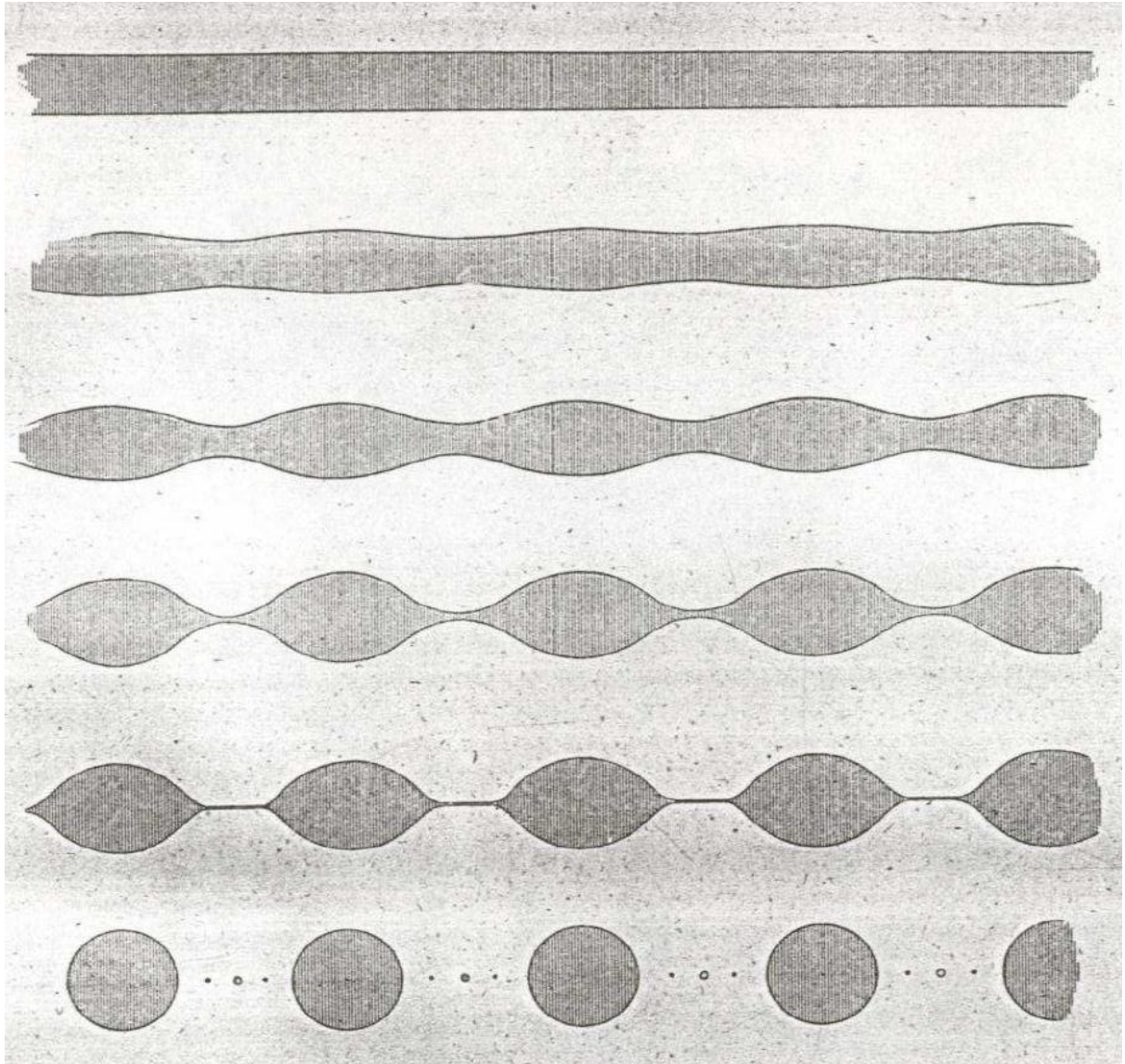
Figure 2.6 Breakup sequences of oil column suspended in a mixture of water and alcohol (obtained from (Eggers, 2006)).The small perturbations grow on liquid cylinder which grows giving minima and maxima on the liquid thread to result in to three small satellites at each breakup.

The stroboscopic method used by Lenard (1887) enabled him to take an entire sequence to see the dynamics near the drop breakup with the time resolution that would otherwise be impossible to achieve.   These sequences first time showed the appreciable results for satellite drop formation. In the satellite drop formation: first liquid neck breaks near to the primary drop, but before it snap back it also thins near the pendant drop which later breaks forming the satellite drop. These sequences are shown in the figure 2.7.
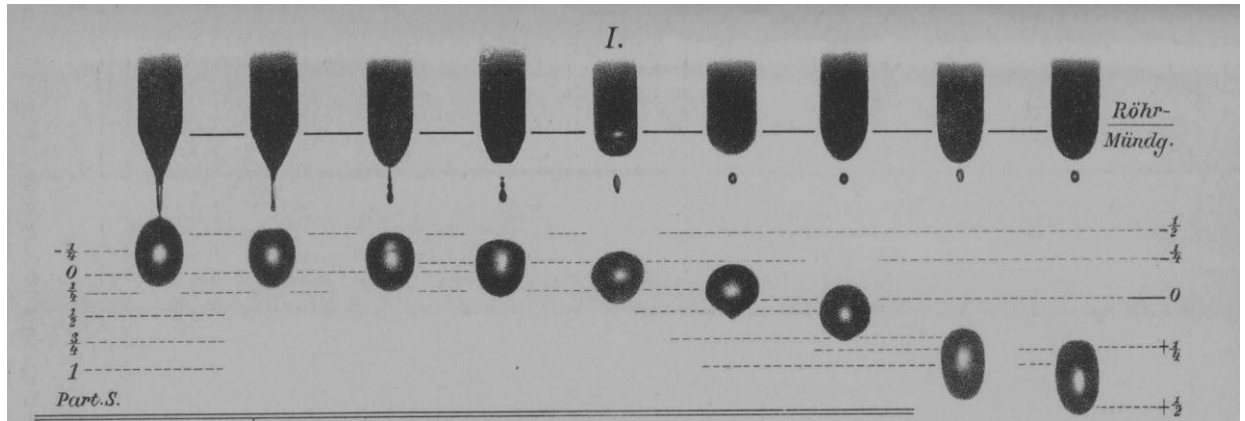
Figure 2.7 A sequence of drop formation from a pipette, where both satellite and primary drops are visible (Lenard 1887, obtained from ref (Eggers, 2006)). For the first time, the sequence of events leading to satellite formation can be appreciated.

A detailed study on nonlinear effect of liquid jet breakup and complex behaviour of the satellite drop formation was experimentally was by Goedde &Yuen (1970). Figure 2.8 taken from their paper shows that the process of satellite drop formation is very complicated. The observations showed that the first breakup always happens at lower end of the liquid thread as it gets more time to thin as shown in the figure 2.8 (a-d). Later experimental results showed that there is a quite possibility that the ligament first breaks at upper end of the liquid thread. The other observation that they made was that the satellite drop size increases with decreasing wave number which can help reducing the satellite drop formation simply by adjusting the amplitude of applied disturbance. The experimental results on satellite drop size were concluded by Rutland & Jameson (1971), where they showed that the satellite drop size actually increases with decrease in wave number. The results on satellite drop size by the disturbance amplitude contradicted the findings of Goedde &Yuen (1970), showing that the satellite drop size is unaffected by the disturbance amplitude.
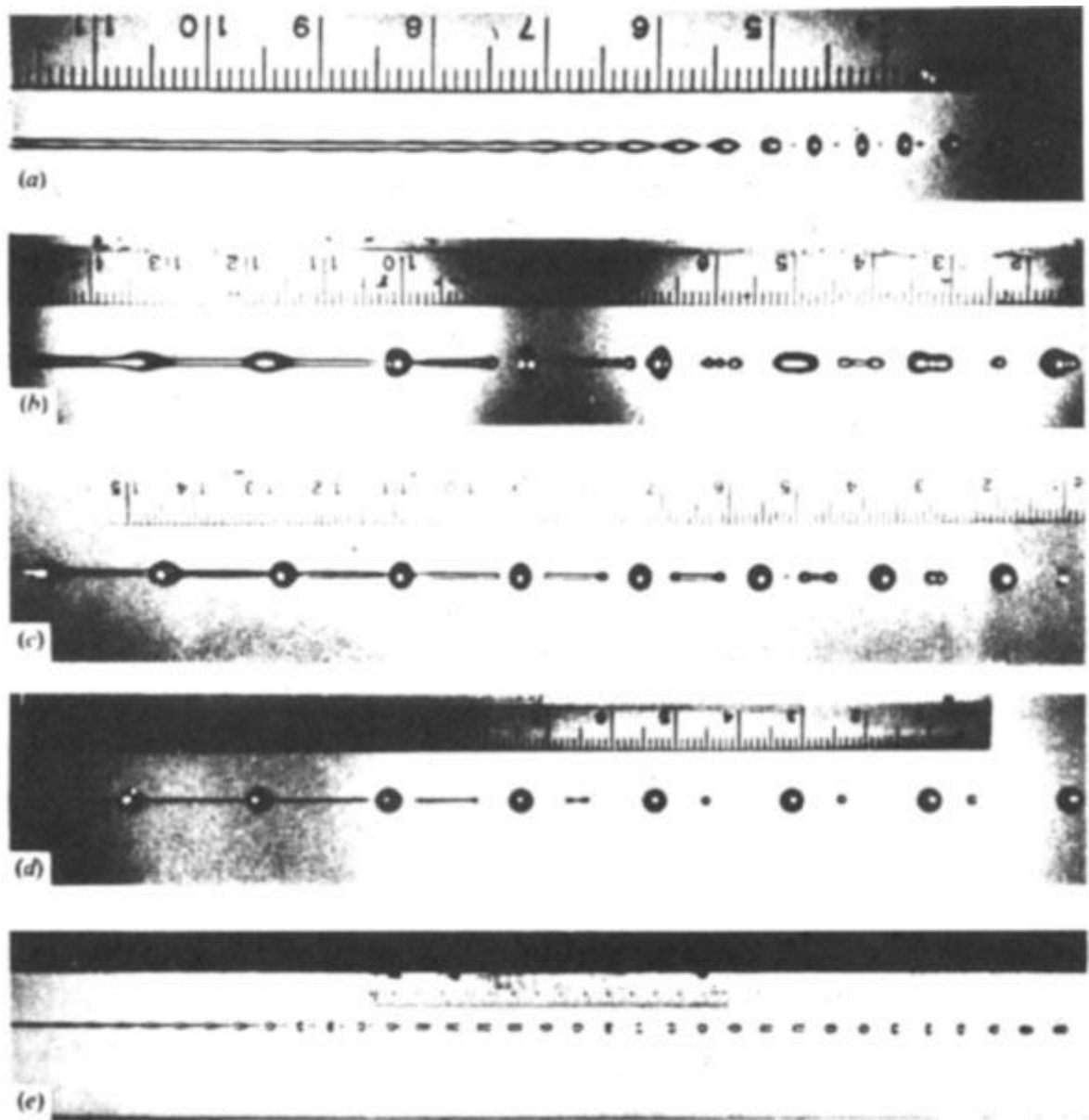
Figure 2.8 Typical sequences of drop formation for water and glycerine (Goedde and Yuen, 1970).

A new experimental results on satellite drop breakup revealed that the liquid thread may break at upper side of ligament first, lowers side of ligament side or simultaneously at both the end (Pimbley and Lee, 1977). The best example of ligament breaking first at upper side of the liquid thread is shown in the figure 2.9, taken from their paper. Another observation they made was that the satellite drop may merge forward or backward

depending upon the disturbance amplitude. If the satellite is formed by breakup of liquid thread due to breakup at both the ends simultaneously then the satellite drop speed remains equal to the speed of primary drop and this condition of breakup is called "infinite satellite condition".

This is the first reported experimental observation that contradicts the observations made by Goedde and Yuen (1970) that the liquid thread always breaks at lower end in the satellite drop formation process.
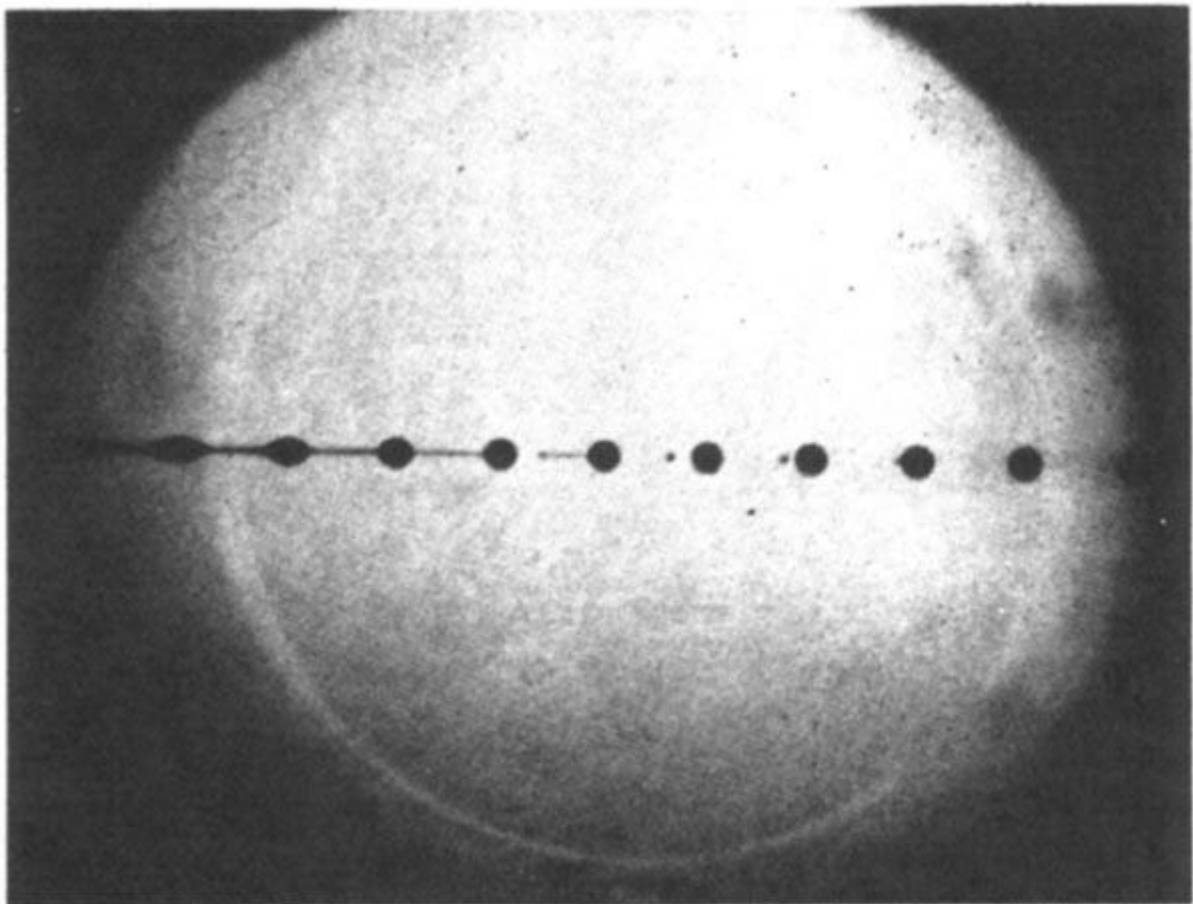
Figure 2.9 Stroboscopic microphotograph of liquid thread breaking at upper end of the liquid jet (From Pimbley & Lee, 1977.)

In the later part of the twentieth century, the effects of different experimental parameters like nozzle dimensions, flow rate, rheological properties, and physical properties of the liquid on the satellite and primary drop formation was investigated. The next subtopic

gives the literature review on the effect of these parameters on the drop formation dynamics.

2.3 Effects of experimental parameters on drop formation

2.3.1 Physical properties of the liquid

The physical properties of the liquids like viscosity, surface tension, and density can have some effect on the drop formation dynamics. As the viscosity of the liquid is varied, the changes in liquid drop shape were investigated both experimentally and computationally (Shi et al., 1994). Figure 2.10 shows photographic events of the shape and length of the liquid length change near the drop breakup for different viscosities. The viscosity of the liquid increases from A-E in figure 2.10, where A and E represents pure water and pure glycerol respectively. By mixing the water with glycerol, the viscosity of the liquid can be varied by 10^3 times and the surface tension was not varied more than 15% so that the effect of viscosity was more visible. As seen in the figure 2.10, the liquid thread length increases as the viscosity of the liquid increases from A-E. Also they observed that, as the value of viscosity increases the neck of the liquid drop elongates and forms structure that is not seen in case of pure water. Another distinct feature observed for high viscosity liquid drop, as discussed earlier, the high viscosity liquid shows secondary neck formations at the break up points which occurs by initial thinning near the drop followed by rapid extension of the neck upward away from the drop. The simulation results obtained for drop shapes were found to be very similar to the photographic events obtained near the drop breakup.

Building on the previous findings of Shi *et al*. (1994), Zhang and Basaran (1995) demonstrate the important role played by viscosity on the necking and drop breakup dynamics of the forming drop. Aside from the noticeable difference in the size of the

27

drop near to the drop breakup, Zhang and Basaran demonstrate the variation of

dimensionless drop
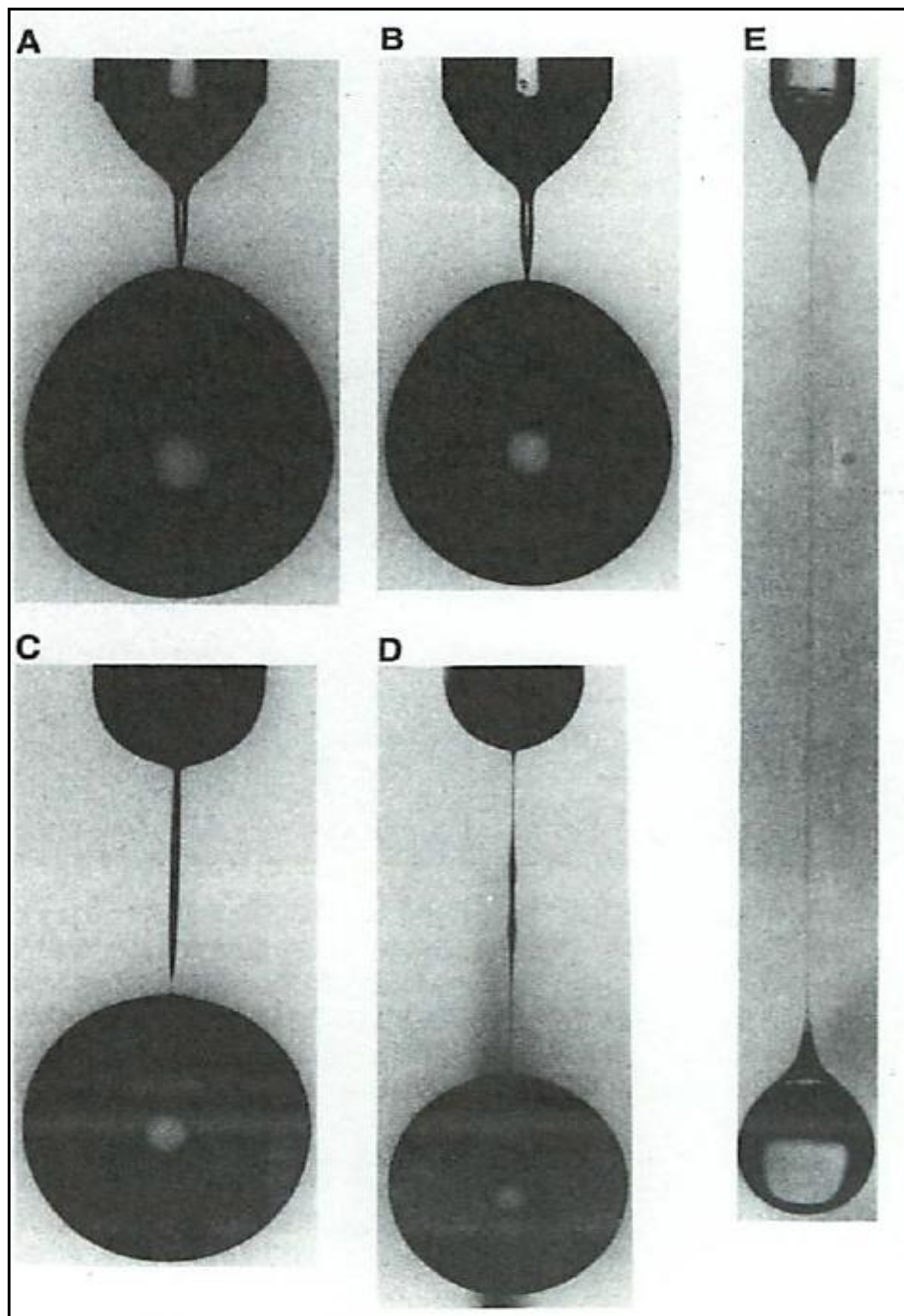
Figure 2. 10 Shapes of liquid drop from a nozzle having diameter 1.5 mm close to break up times for the liquids with increasing viscosity from A to E (Guthrie, 1863). The liquids are water glycerol mixtures having viscosities 0.01 P (A), 0.1 P (B), 1 P (C), 2 P (D), 12 P (E).

elongation i. e. neck length with relative time for pure water and 85% water glycerol mixture. In the same study the drop volumes and neck lengths for 20%, 50%, 70%, and 80% water glycerol solutions are investigated. Viscosity plays a very important role in stabilizing the grooving drop which makes possible larger drop elongation by damping and it eliminating the interfacial oscillations, but has virtually no effect on drop size. The finding here on the drop stabilizing due to viscosity has found to have two important aspects in the drop formation. First, viscosity promotes the damping of interfacial oscillations remained on pendant due to the breakup of previous drop and second, the viscosity keeps the about to fall primary drop nearly spherical in shape. These observations are important in the area of polymer beads formation, where the drop sphericity has a prime importance.

Zhang and Basaran (1995) in the same study investigated the effect of surface active agent on the drop formation dynamics. By just adding different concentration of the surface active agent like triton, can change the surface tension of the liquid by keeping density and viscosity of the liquid virtually constant. So the role played by surface tension in the dynamics of the drop formation was easily identified. The drop breakup volume of the pure water and 0.01 and 0.05 % triton solution is compared. The results accords well with the intuition that at low flow rate the breakup volume of primary drops decrease with increase in surfactant concentration. Consequently, because of the reduction in the volume of the primary drops, the limiting length also decreases with increase in surfactant concentration. The similar experiments are performed for the high flow rates and the surface dilation occurs at high rate giving increasing primary drop breakup volume and breakup length values as surfactant concentration increases. The volumes of satellite drops also compared in the same study. The volume of satellite drops found to increase with increase in surfactant concentration. The well-known facts about

the surfactant are that the surfactant greatly damp and suppress the surface waves stabilizing the growing and stretching liquid thread. This leads to increase in the liquid volume of a thread and hence satellite drop volume.

2.3.2 Liquid rheology

Rheology of the liquid may complicate the drop formation, when it is compared to its Newtonian counterparts. The rheology of the fluid can be changed by addition of micron size particles to the Newtonian liquid. Furbank and Morris (2004) studied the particles effect on drop formation, where the particles used were in micron size suspended in viscous liquid. The density of particles and the surrounding liquid was matched to make the system neutrally buoyant so that one can neglect the settling effect. The suspensions were investigated for different volume fractions and dripping experiments were performed for three different nozzle sizes. The typical drop formation process for a neutrally buoyant suspension system from a nozzle is shown in the Figure 2.11. The dripping behaviour for low volume fraction ϕ shows the similar behaviour as that of pure liquid, but at high volume fraction ϕ the dripping behaviour is markedly different. The addition of particles in the liquid suppress the number of satellite drop formation at higher volume fraction, but few satellite drops were still noticed having size much larger than in pure liquids. The dripping to jetting transition was observed at small flow rate for a fine value of volume fraction, but at high volume fraction ϕ the transition becomes less abrupt and difficult to identify.
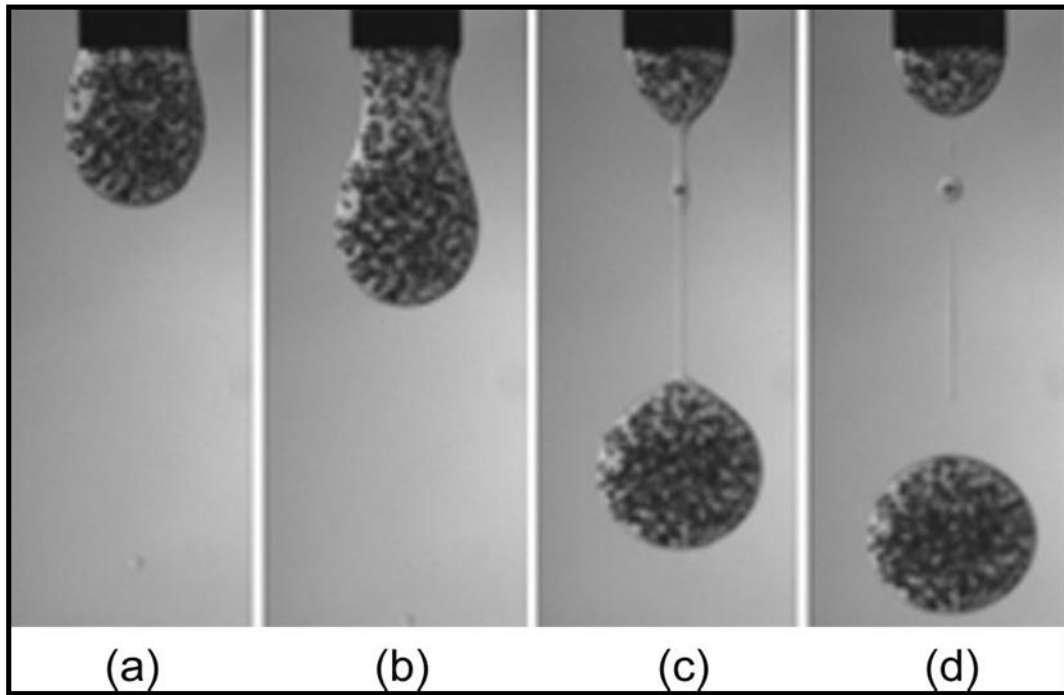
Figure 2. 11 Typical drop formation process for a neutrally buoyant suspension system from a nozzle of diameter d=0.32 cm. The surrounding liquid is silicone oil and the suspended particles has diameter d=212-250 μm (Furbank and Morris, 2004).

Cooper-White *et al.*(2002) investigated the effect of liquid elasticity on dripping dynamics, where two types of fluids having similar viscosity,density, and surface tension but different elasticity were studied for dripping experiments. The results showed similar behaviour till the formation of lower pinch region for all types of liquids regardless of elasticity, which gives proper justification for importance of capillary and inertial forces before lower pinch occures. But once the lower pinch is occurred, the break up time for elastic liquid is increased compared to Newtonian liquid. This break up time increases with increase in fluid elasticity. Later in 2008 Li and Sundararaj (2008) studied the breakup mechanism for viscoelastic liquid drop. They found that the drop size of a viscoelastic fluid determines the drop breakup mechanism and also the critical point where the mechanism changes. The small drops break in the direction which is perpendicular to the flow direction and large drops break along the flow direction.

Breakup of capillary jet of dilute polymer solution showing gobbling phenomenon which is the result of the dynamic interaction of capillary breakup in a falling viscoelastic jet with a large terminal drop that serves as a sink for the mass and momentum of the incoming fluid is studied. The gobbling phenomenon which is observed near the transition from dripping to jetting and the thinning process of the ligament connecting the main drop and pendant drop for a viscoelastic polymer solution is explained (Clasen *et al*., 2009). The high speed photography technique used to observe the gobbling phenomena showed that the gobbling is actually a form of delayed dripping process and the thinning process of the ligaments that are subjected to a constant axial force is driven by surface tension and resisted by the viscoelasticity of the dissolved polymeric molecules.

The later work of Clasen *et al.* (2011) focus on the dispensing behaviour of rheologically complex fluids and its behaviour is compared with their Newtonian counterparts.The properties of liquid that they varied are fluid viscosity, elsticity, and the degree of shear thinning. The drop break up mechanism, drop volumes, and break up times have been observed using high-speed video-microscopy. To predict the thinning and dispensing behaviour of rheologically complex fluids, different nondimensional groups which defines the relative importance of different forces involved, that is, the Ohnesorge, elasto-capillary number, and Deborah number have been defined. With the different values of these nondimensional numbers in the experiments one can to identify the dominant mechanism resisting breakup and its corresponding critical dimensionless number. These critical values also allow one to identify the filament life times. German and Bertola (2010) experimentally investigated the formation and detachment of liquid drops from a capillary nozzle for Newtonian fluids of variable viscosity, shear-thinning fluids, and viscoplastic or yield-stress fluids. The experimental results showed that the behaviour of

Newtonian and shear-thinning drops is qualitatively similar, and leads to the formation of spherical drops, viscoplastic drops exhibit strongly prolate shapes and a significantly different breakup dynamics of the capillary filament.

2.3.3 Liquid flow rate

The complexity in the dripping behaviour can be seen by increasing the flow rate of the dispensing liquid. The different modes of dripping seen in the experiments include period-1 dripping where every drop is of equal size, period-n (n=2,3,4…..) dripping where every n-th drop is identical, and higher odd-period or chaotic mode of dripping (Subramani et al., 2006; Zhang and Basaran, 1995; Clasen et al., 2009; Ambravaneswaran et al., 2000; Scheele and Meister, 1968; Wilkes et al., 1999). Wilkes *et al*. (1999) studied low viscosity Newtonian fluids at low flow rate, where the dripping behaviour changes from Period-1 to some complex dripping, chaotic responses and then at high flow rates the transition takes place from complex dripping to jetting. But high viscosity liquids shows direct transition from simple dripping to jetting as flow rate increases.

Ambravaneswaran *et al*. (2004) investigated this transition at different flow rates and at different viscosities. For constant viscosity and constant nozzle size, the different regimes of drop formation are explained in Figure 2.12 where the flow rate is increasing from left to right. At low flow rate the dripping with satellite drop formation is observed and with increasing flow rate the observed region is the dripping region without satellite drop formation (Figure 2.12 (b)) which can be simply a Period-1 or complex dripping or chaotic behaviour. Further increase in flow rate gives jetting behaviour in the system where the droplets detach from the end of long liquid thread as shown in Figure 2.12 (c). In the same study, phase diagrams were constructed in (*We*, *Ka*) space shows the

transition between different modes of dripping. As an extension of this work, the critical *We* for transitions from one mode to another were estimated by scaling arguments and shown to accord well with simulations (Subramani *et al.*, 2006). Initially the phase diagram developed in (*We*, *Oh*) space was constructed for a moderate value of G=0.5 (Subramani *et al.*, 2006), but the reponse if the value of *G* varies was unknown. This unexplored dripping dynamics for a wider range of *G* was later studied by Subramani *et al.* (2006). It was found that at high values of *G*, the dripping dynamics is richer and tends to become chaotic at lower values of *We*. In the same study they found that, at very low flow rates, a tiny satellite drop often follows the primary drop. If the viscosity of the dispensing liquid is increased (high *Oh*), the dripping behaviour simplifies to either P1 with satellites or jetting (Subramani *et al.*, 2006). A detailed phase diagram showing transitions from complex to simple dripping and jetting in the (*We*, *Oh*) space had been reported (Subramani *et al.*, 2006).
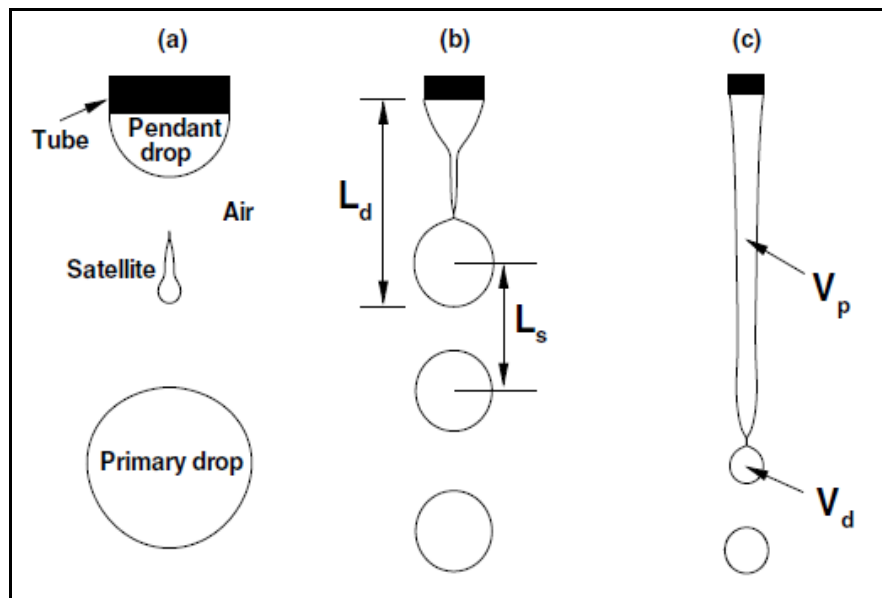
Figure 2.12 Different regimes of drop formation, (a) Dripping with satellite formation, (b) Dripping without satellite drop formation, (c) Jetting, The flow rates increases from left to right (Scheele and Meister, 1968).

2.3.4 Nozzle geometry

If the liquid wets the entire thickness of the nozzle, the radius of the contact circle equals the outer radius of the nozzle in all the experiments. Even if R is considered as a radius of contact circle, it is important to know the effect of ratio R_i/R (where R_i is the inner radius of the nozzle) on the drop formation dynamics. The variation of drop volume and drop breakup length with R_i/R is investigated by keeping flow rate and viscosity constant (Zhang and Basaran, 1995). As ratio R_i/R decreases i.e. as the thickness of the nozzle increases, the elongation of drop at drop breakup increases giving increased length of the liquid thread and hence the drop breakup volume decreases. The further decrease in the ratio R_i/R diminishes the effect of wall thickness on drop volumes and liquid thread length at some critical value of $R_i/R>0.2$. At this critical value, the drop volumes, liquid thread length and even the shapes of the liquid drops are found within experimental error to be identical to those obtained when the nozzle has virtually zero thickness. This finding helps to choose the proper nozzle in the experiments where one can simply neglect the effect of wall thickness.

The critical role of nozzle geometry was investigated by changing the two parameters in the experiments: first the inner nozzle diameter and second the nozzle shape (D'Innocenzo et al., 2002). The dripping dynamics found to be almost similar for relatively large values of the inner nozzle width. In addition, radical changes in the dripping dynamics were found when the nozzle shape changes from a flat tip to a bevelled shape. Dripping dynamics of relatively narrow internal diameter changes considerably for different nozzle shapes. In particular, the observation shows that the inner diameter can have a control parameter to change the dripping dynamics of the nozzle. A very useful finding on nozzle thickness showed that, the wall dimension of the

nozzle influences substantially the dripping behaviour, for the nozzles with a ratio of thickness of the wall to inner radius ≤ 0.2. The satellite drop formation for beveled tips nozzle is found to be notable reduced. As an extension of this work a detailed study on the effect of different nozzle geometry on dripping behaviour is done by D'Innocenzo *et al.* (2004). Two types of nozzle geometries, flat and obliquely shaped cut tip nozzle he considered for dripping experiments. For same flow rate and viscosity the dripping behaviour for these two different nozzles is compared. The obtained result shows the dramatic change in the dripping behaviour when nozzle shape changes from flat to obliquely cut shape. They found that the added degree of freedom produces a transversal oscillation of a pending drop, which couples with a vertical oscillation which is the result of the break off of the previous drop. As a result of that the dripping times are found to be shortened and dripping patterns are more regularize. This results into the decreased frequency of the vertical oscillations of the residue and reduced contact circle. They observed a very complex liquid flow patterns and eddies of different amount. The frequency of drop oscillations decreased going from the flat nozzle tip to the bevelled nozzle tip and to the obliquely cut nozzle (D'Innocenzo et al., 2004). It was claimed that this was due to wetting characteristics of the liquid with the wall of the nozzle as it determines three phase contact line affecting the dripping time series behaviour (D'Innocenzo et al., 2004).

2.3.5 Nozzle inclination

The introduction of asymmetrical perturbations, by tilting the nozzle at an angle θ with the vertical breaks the cylindrical symmetry and induced strong changes in dripping dynamics (Reyes et al., 2002). The topological considerations to characterize heteroclinic scenario uniquely from the time series of the dripping faucet experiment are used to investigate the influence of the nozzle inclination, representing symmetry breaking in the system, and generating heteroclinic tangle. In the experiments on dripping from a tilted nozzle, the measured time (T_n) between the nth and (n+1)th drop were plotted, giving time return maps for different nozzle inclination angle θ. The obtained time return maps showed that even for small inclination angle θ=5°, the system symmetry breaks and dripping behaviour changes dramatically. The results showed strong changes in the attractor topology, suggesting that inclination angle can be an effective control parameter for the dripping dynamics (Reyes et al., 2002).

Despite the rich dynamics of dripping from a tilted nozzle, we failed to uncover any other articles in the English literature. Due to the limited range of parameters studied previously (Reyes et al., 2002), the more general behaviour of dripping from a tilted nozzle remains unknown. The main goal of this paper is to develop a comprehensive picture of the dripping dynamics from a tilted nozzle. In order to achieve that goal, (a) dripping dynamics will be explored through the study of the breakup time $\tilde{t}_b$, which is the time interval between two subsequent drop breakups, and (b) dripping phase diagrams for different values of θ will be constructed.

3 Research Methodology

3.1 Introduction

The experiments are designed to obtain the quantitative information on the drop breakup time and the drop breakup volume. Attention is also paid in the experiments to the satellite drop formation for different experimental conditions. The experiments are performed by varying liquid viscosity, flow rate, nozzle size, and nozzle inclination angle.

3.2 Experimental setup

The experimental setup is depicted in figure 3.1. It consists of a nozzle through which liquid flows to form drops. The liquid was delivered to the nozzle by using a MeditechJZB-1800D Syringe Pump which is capable of providing range of flow rate from 0.00167 to 30 mL/min with an accuracy of ±2%. Stainless steel dispensing nozzles (P-30619-06, P-30619-01, and P-30619-07) were obtained from Cole-Parmer. The outer radii of the nozzles are 0.625 mm (N1), 1.00 mm (N2), and 1.96 mm (N3). The ratio of the inner radius to outer radius is <0.2, hence the effect of nozzle thickness on the interface dynamics can be safely neglected (Zhang and Basaran, 1995). A protractor is provided to adjust the tilt angle of the nozzle. A transparent shield is provided to reduce draft that can perturb the drop formation process.

The high speed camera is Casio EX-FH100 capable of recording 30 to1000 frames per second. A planar white LED backlight measuring 10 cm × 10 cm (model LFL-Si100-W-IP65) with adjustable brightness was obtained from Falcon Illumination (M) Pte. Ltd. The sharpness of the images can be adjusted via the intensity of the backlight, the focal

length and digital zoom of the camera. All parts of apparatus except the syringe pump were kept on a 0.3m×0.3m×0.06m aluminium optical base plate inside the transparent shield.
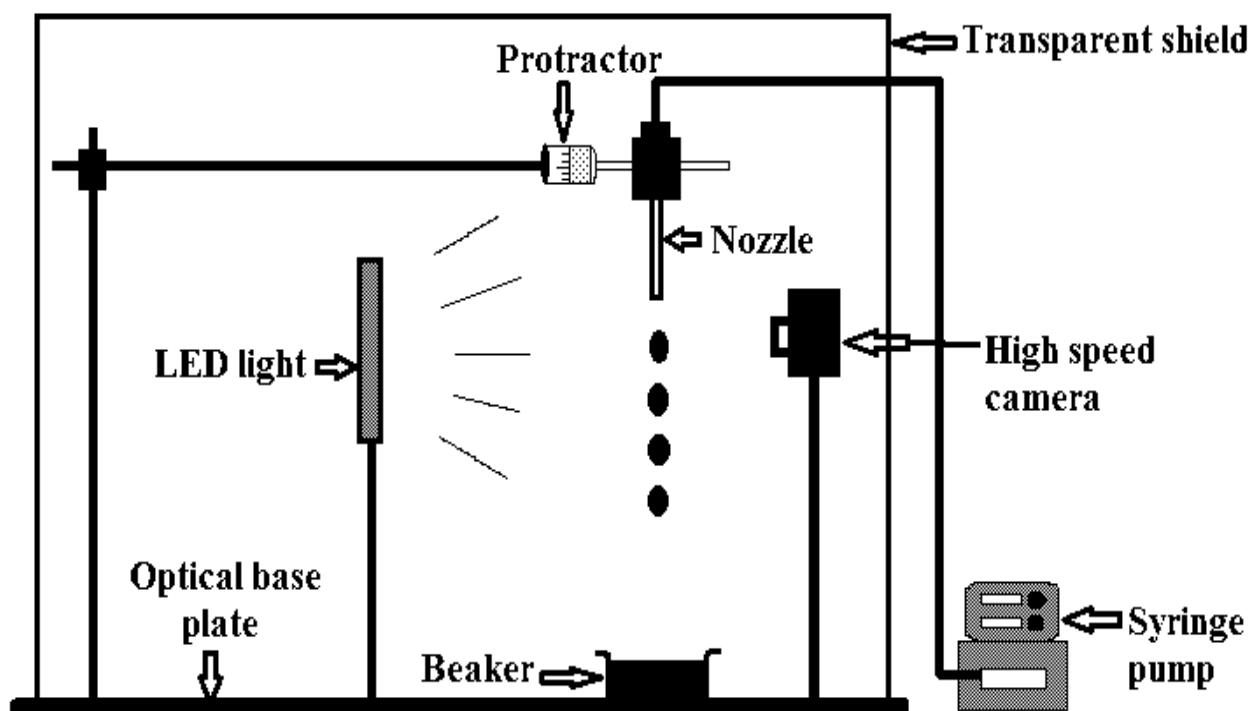
Figure 3.1 Schematics of the experimental setup.

3.3   Fluid Characterization

Mixtures of water and glycerol were chosen because their surface tension and densities are almost similar to that of pure water, but their viscosities can be made to vary three orders of magnitude. The 99% pure glycerol obtained from R and M Chemicals, CAS NO [56-81-5], and used as obtained. Distilled water was used to the make water glycerol mixtures. The physical properties of these water glycerol mixtures are taken from the literature (Physical properties of glycerine and its solution. 1967) and are listed in Table

3.1. Silicone oil (Dow Corning® 111 Valve Lubricant and Sealant) was used to prevent wetting of the outer nozzle surface.

The image captured by using just water-glycerol mixtures showed a color gradient within the drop area, which was inconvenient for the subsequent automated image analysis. To minimize the colour gradient within the drop area, methylene blue dye was added in the water glycerol mixture. Analyzing the images for the dyed solution showed that 0.5 wt% was the minimum required. The surface tensions of the dyed water-glycerol solutions were measured using Langmuir Blodgett trough from KSV instruments. The viscosity measurements were carried using an ARES rheometer equipped with the cup and bob geometry. The liquid densities were measured using the known volume of liquid using a weighing balance, AND model GF-300. All the physical property measurements for the dyed water-glycerol mixtures were performed at 25±1°C. The measurement errors for density, surface tension and viscosity were within ±1% accuracy. These measurements showed that the effect of dye on the physical properties of the water-glycerol solutions could be safely neglected within experimental error.

Table 3.1 Physical properties of water glycerol mixtures (Physical properties of glycerine and its solution. 1967).

Solution	Wt. % glycerol	ρ (kg/m^3)	μ (mPa.s)	σ (mN/m)
S0	0	1000	1	72
S20	20.0	1044	1.5	69.5
S40	40.0	1095	3.2	68.4
S80	80.0	1205	45.9	64.7

3.4   Experimental procedure

The experimental run began with applying a thin layer of silicone oil on the outer wall of the nozzle. This pinned the liquid to the outer sharp edge of the nozzle tip even at inclined positions. The verticality of the nozzle was checked with two perpendicularly mounted pendulums. Following this, the tilt angle was adjusted using a protractor. The prepared solution was drawn into the syringe and any bubble present in the syringe or tube was purged off. A desired flow rate was then set on the syringe pump. The drop formation sequences were recorded at 240-420 frames per second depending upon the liquid flow rate. The recorded videos were first converted into images with the ImageJ software (ImageJ software, retrieved on 10 August 2012), then analyzed using an algorithm written in MATLAB^{TM} software to detect the drop breakup and to calculate the breakup time between two successive drops.

In this work, the experiments were performed at different values of *We* (5×10^{-4} to 0.45) by varying the liquid flow rate *Q*, *Ka* (3.22×10^{-4} to 0.0526) by changing the viscosity μ of the liquid, *G* (0.053 to 0.70) by using three different nozzle radius R, and θ (0°, 30°, and 60°). All the experiments were carried out at room temperature (25±1°C).

3.5   Image Analysis Methods

3.5.1   Breakup Time Calculations

The images so retrieved are analyzed using an algorithm written in MATLAB (Appendix A.1) software to detect the drop breakup and to calculate the breakup time t_b between two successive drops. The MATLAB algorithm takes the images of a set of experiments. These images are first read in to the MATLAB, which are later converted in to black and white (BW) images. MATLAB reads these images in three dimensional matrix forms, where each pixel value in the corresponding direction is assigned to the row and columns of the matrix. The images we have are the two dimensional images, which has the pixel values in 'x' and 'y' direction only, which assigns these values in column vector and row vector of the matrix respectively, and the third dimension of the matrix is always kept constant. Once the images are converted in to BW image, there are only two different pixel values, that is '1' and '0' as shown in Figure 3.2 (b), where pixel value '1' corresponds to the dark part of the image and '0' corresponds to the bright part of the image. We have intensity threshold, which has to be given before we convert a RGB image to BW image. Deciding the value of intensity threshold is very important in the process as it decides the part of the image which has to consider as black or white, hence it needs some trial and error experiments. Once the images are converted in to BW form, the drop break up is detected on the basis of intensity difference near nozzle area. If the intensity difference values are changed from 1-1-1 (Figure 3.2 (a)) to 1-0-1 (Figure 3.2 (b)), then the very first image is detected as drop breakup image.
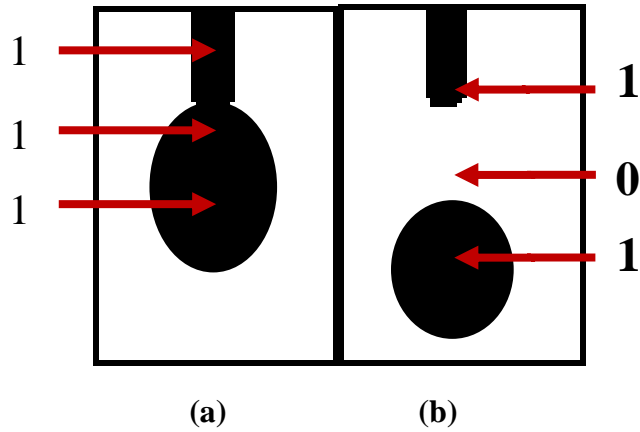
Figure 3.2 Image analysis of drop breakup process. Intensity value '1' represents black part and '0' represents white part of the image.

Some of the sequences of drop formation from a vertical nozzle are shown in the Figure 3.3, where the image sequence (c) and (f) represents the drop breakup instant and hence drop breakup image on the basis of intensity difference criteria explained in the previous paragraph. Once the drop breakup image numbers are detected, the breakup time t_b is calculated on the basis of image number and frame rate of the camera. The time interval between these two image sequences ((c) and (f)) represents the drop breakup time t_b.
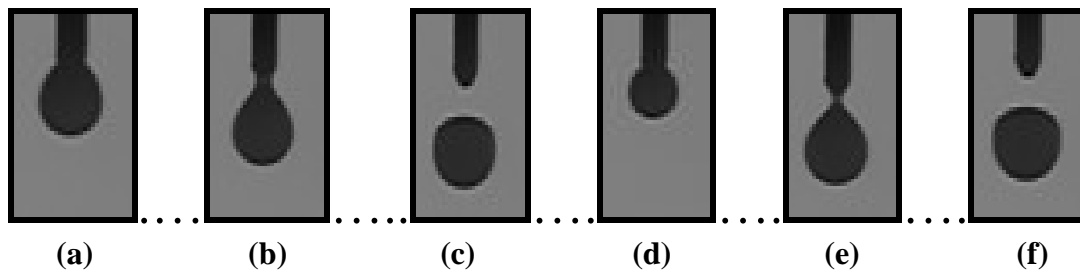
Figure 3.3 Drop breakup sequences. The time interval between sequence (c) and (f) is the breakup time t_b (Resolution: 0.21 mm/pixel).

3.5.2   Primary Drop Volume Calculation

3.5.2.1   For the Vertical Nozzle

The volumes of primary drops are also measured using the same images obtained for the t_b calculations using a MATLAB code (Appendix A.2). For the experiments from a vertical nozzle, the liquid drop is symmetric in shape. So the images of the liquid drops from one fixed angle using just one camera are taken as shown in Figure 3.4. The drop breakup images initially detected were further sent to MATLAB for volume calculation. These images are initially converted in to BW format and value of one pixel is initially calculated by the dimensions of a reference object (In our experiments the nozzle diameter was the reference dimension to convert pixels into centimeters). To measure the drop volume for each image, initially we assumed each drop as a symmetric shape akin to an ellipsoid. The drop is then divided in two vertical sections along the major axis as shown in figure 3.5. Each vertical section has 'n' number of radius equal to the number of pixels on a vertical axis. The radius is measured by calculating the number of pixels on a horizontal line representing a radius at a particular location. The different radii are shown in figure 3.5. At the same position, the value of the radius used for volume calculations is the average values for two radii. By using combined Simpsons 1/3 rd and 3/8 th rule for numerical integration over the entire asymmetric shape, the volume for a drop from one angle is calculated. For the same experiments, the error in the measurement is calculated by weighing 10 drops from the similar experiments. The average weight of the 10 drops (14 mg) was then converted to volume via the density of the water-glycerol solution. The error between the weighed drop volumes and volumes obtained from image analysis was within 3%.

44
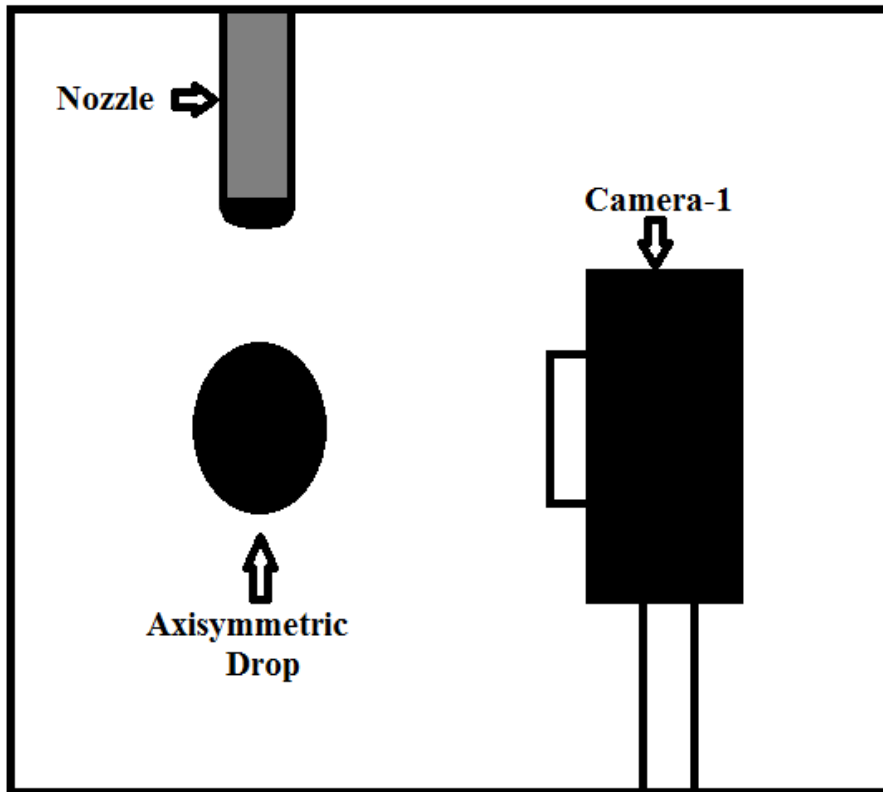
Figure 3.4 Experimental setup for vertical nozzle dripping experiments for volume measurements
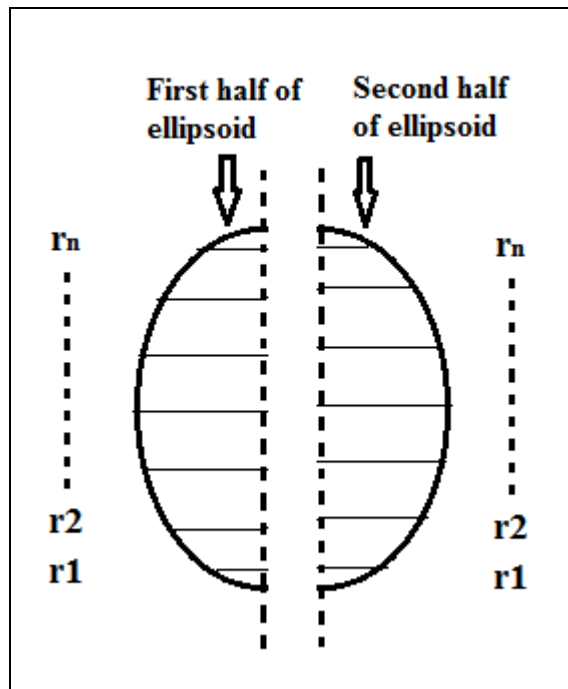
Figure 3.5 Volume measurement method for a axisymmetric drop

3.5.2.2 For an Inclined Nozzle

In the experiments of dripping from a inclined nozzle, the images of drop sequences are taken from two angles placed at 90° to each other so that even if the drop is asymmetric in shape, we can measure the drop diameters from two different angles to have more accurate estimates of the volumes of the drops. These two drop breakup images taken from two different angles are detected and sent to the MATLAB programme (Appendix A.2) for volume calculations. The method of volume calculation is similar to the method mentioned above for vertical nozzle, but for inclined nozzle experiments there are two images at same instant. Though these two images are taken from two different angles as shown in figure 3.6, the major axis of the asymmetric drop shape is a vertical axis which is clearly understood in figure 3.7 snapshots taken for similar drops from two different angles. As vertical axis is common in both the images, the two images can be easily

46

correlated for the volume calculations. These two images are analyzed the same way mentioned above and the average volume of these two images is taken to be the volume of asymmetric drop. The volumes obtained from the image analysis for asymmetric drops was verified with the volume calculated from a drop weighing method and found to be within a maximum of 5% error.
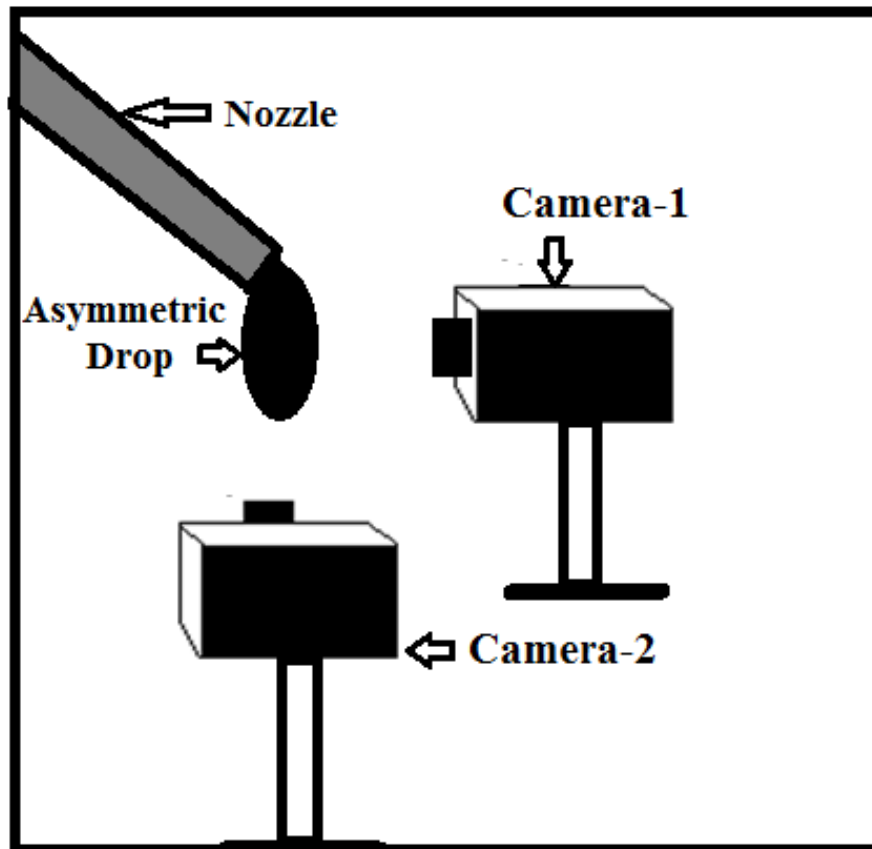
Figure 3.6 Experimental setup for vertical nozzle dripping experiments for volume measurements.
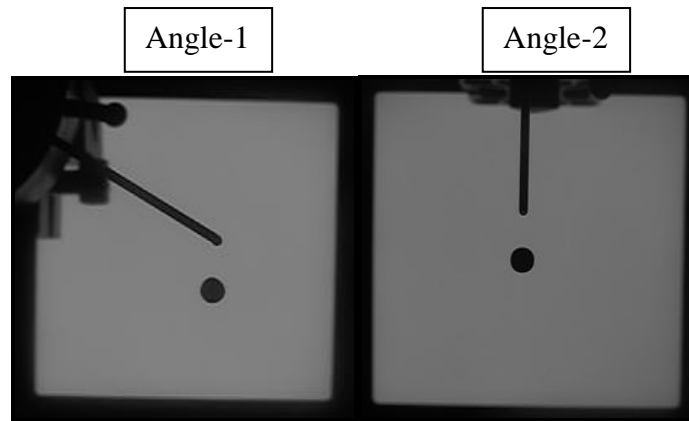
Figure 3.7 Images taken from two cameras kept at 90° to each other.

4 Results and Discussion

In the section below, the different modes of dripping for a vertical nozzle are identified on the basis of drop breakup times and their evaluation with total time. Some other approaches to identify the dripping modes are also given. Similarly the dripping modes for different θ are identified and a phase diagram for each θ value in (*We, Ka*) space is given in the following section. In the next section, a similar phase diagram showing the effect of θ on satellite drop formation is constructed. Later the effect of θ on dripping time is also shown section followed by the computational approach to confirm the obtained results. The drop volume measurements for primary drops and its comparison with drop breakup time is given in the following sub section.

4.1 Dripping modes

Experiments with a vertically oriented nozzle illustrate the various dripping modes observed. The breakup time, $\tilde{t}_b$ was made dimensionless using capillary time $\sqrt{\rho R^3 / \sigma}$. Throughout the remainder of this report, a variable with a tilde designates a dimensional variable while one without denotes the dimensionless counterpart of the same variable. Fig. 4.1 shows the variation of the dimensionless breakup time t_b, with drop numbers. As depicted in Fig. 4.1, values of t_b decreases with increase in Weber number. Based on this, three different dripping regimes were encountered, namely period-1 (P1), limit cycle (LC), and chaos (C). At low Weber numbers, every droplet had the same t_b value, and this mode was denoted as the period-1 dripping (P1). At moderate Weber numbers, the t_b

trajectory repeated itself, showing low amplitude and low frequency oscillations around the average. This was denoted as the limit cycle (LC) behaviour. The chaotic (C) behaviour was seen at high Weber numbers, where the t_b trajectory did not repeat itself, showing disorderly long term evolution.

Figure 4.1 Variation of the dimensionless dripping time with drop number. Three different dripping behaviors are seen as *We* increased, namely P1 (□ *We*=0.05), LC (♦ *We*=0.15), and C (▲ *We*=0.30). Here *G*=0.057, Ka=0.000562

Figure 4.2 Variation of the dimensionless dripping time with drop number. Three different dripping behaviors are seen as *We* increased, namely P1 (⬜ *We*=0.05), LC (◆ *We*=0.15), and C (△ *We*=0.30). Here *G*=0.057, Ka=0.000562
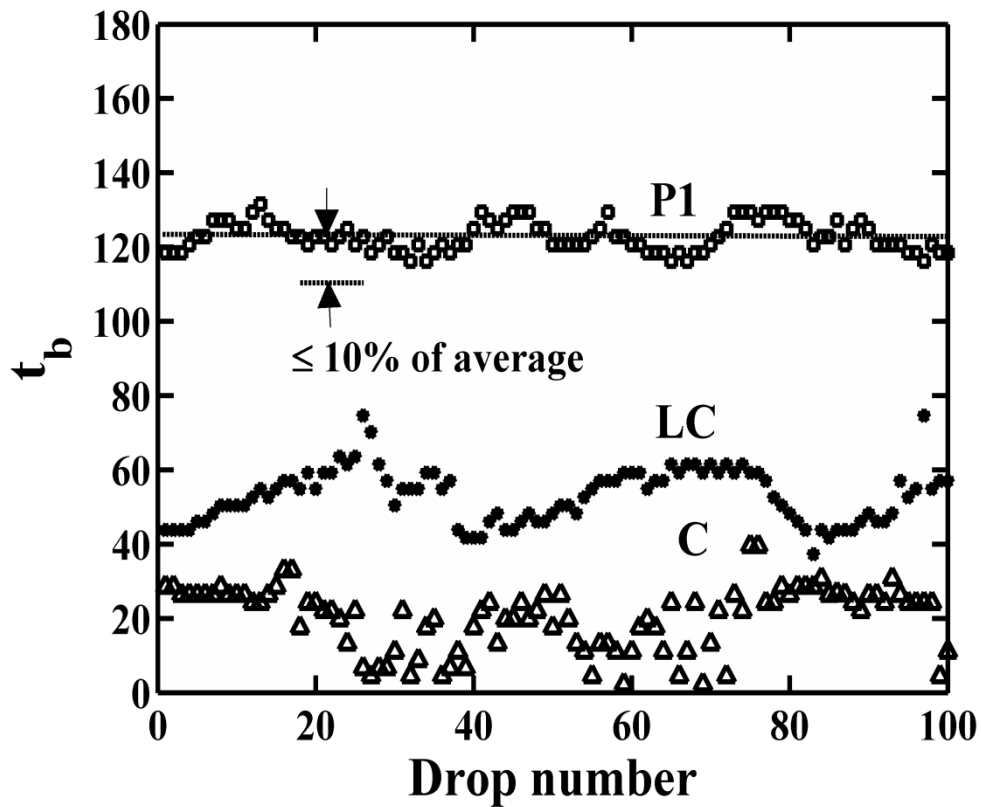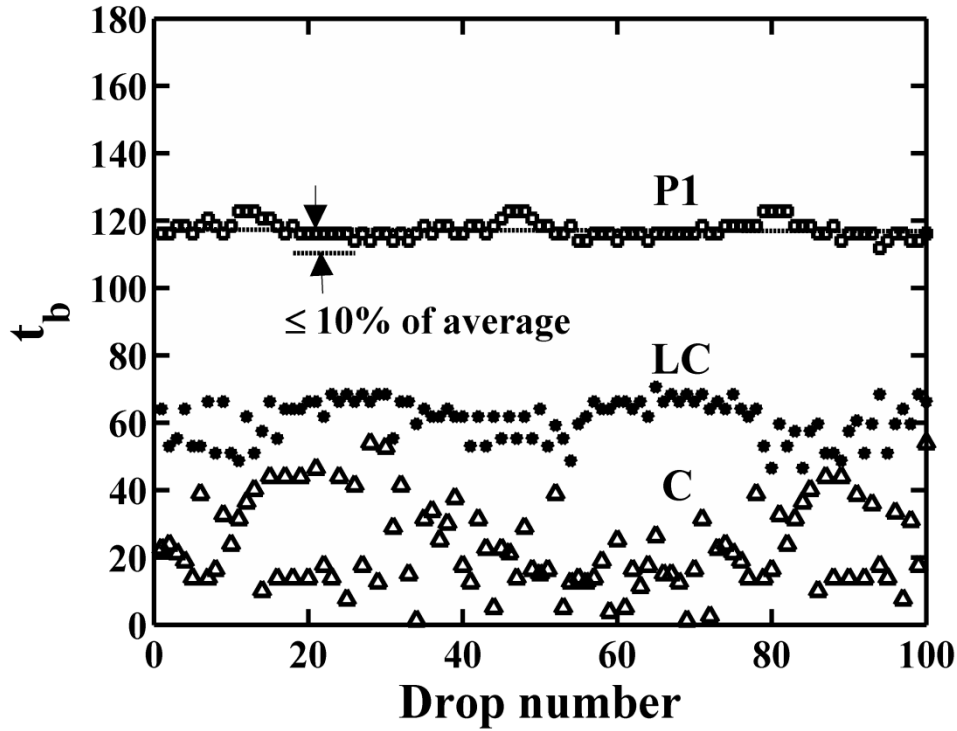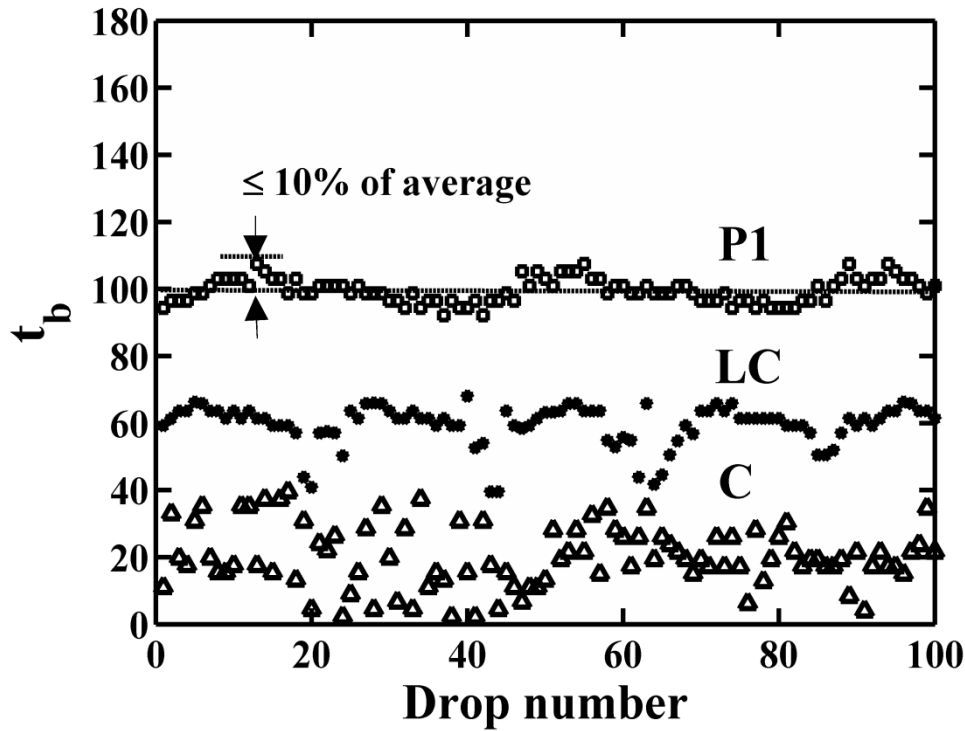

Figure 4.3 Variation of the dimensionless dripping time with drop number. Three different dripping behaviors are seen as *We* increased, namely P1 (⬜ *We*=0.05), LC (◆ *We*=0.15), and C (△ *We*=0.30). Here *G*=0.057, Ka=0.000562

Raising the angle of tilt to $\theta = 30^o$ and 60°, at constant *We*, *Ka*, and *G*, the evolution of t_b with drop number and the time return map is shown in Fig.4.2 and 4.3 respectively. The features remain qualitatively identical. This is notable as the extent of asymmetry in the liquid meniscus is significant at this inclination. It suggests that inclination probably exerts higher order effects on the dripping dynamics. Nevertheless, comparing Figs. 4.1 and 4.3, the values of t_b for the P1 regime decrease noticeably with an increase in θ, whereas the values for t_b for the LC and the C modes of dripping are relatively independent of θ. Since the flow rate remains identical, the droplets formed from the inclined nozzle in the P1 regime must be smaller than their counterparts in the vertical case. This opens up another avenue to regulate drop volumes.

The breakup time data obtained here for different experimental parameters can be analyzed in different ways to identify the dripping behaviour. Some of the efforts made to analyze the same are given in subsections below.

4.1.1   Time series analysis

To extract more meaningful statistical results from the data of drop breakup time, the time series analysis is used. This is the first ever attempt made to identify the nature of the phenomenon represented by the sequence of observations. In the time series analysis, MATLAB algorithm for Fast Fourier Transform (FFT) (Appendix A.3) to compute the Discrete Fourier Transform (DFT) is used to convert time data to frequency. The FFT allows us to look at the data in frequency domain rather than in the time domain (Bloomfield, 2004). The converted frequency domains are analyzed here to find out the dominant frequency that may be present in the data and the patterns obtained may allow

us to identify and decide more efficiently the modes of dripping. If the obtained plots shows any patterns, one can easily predict whether the time series obtained in dripping experiments are of periodic nature (P-n, where n=1,2,....n) or chaotic in nature. Following three FFT plots for time data are for P1, LC, and C behaviour respectively.
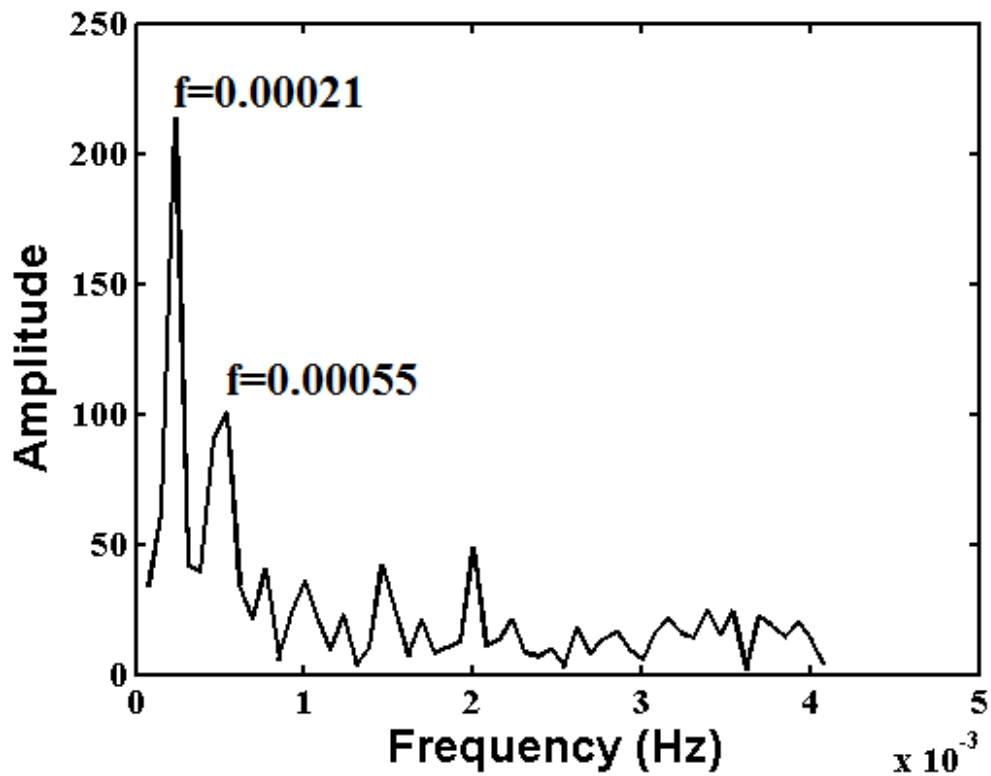
Figure 4.4 FFT plot for time data having P1 behaviour. Here *We*=0.05,*G*=0.057, *Ka*=0.000562
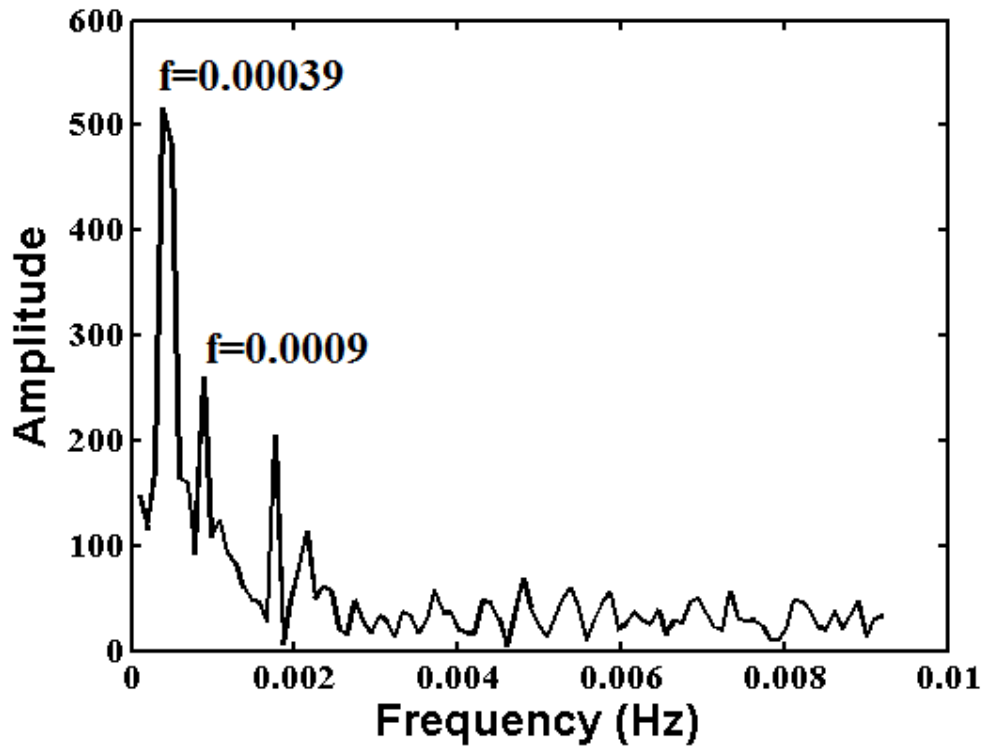
Figure 4.5   FFT plot for time data having LC behaviour. Here *We*=0.15,*G*=0.057, *Ka*=0.000562
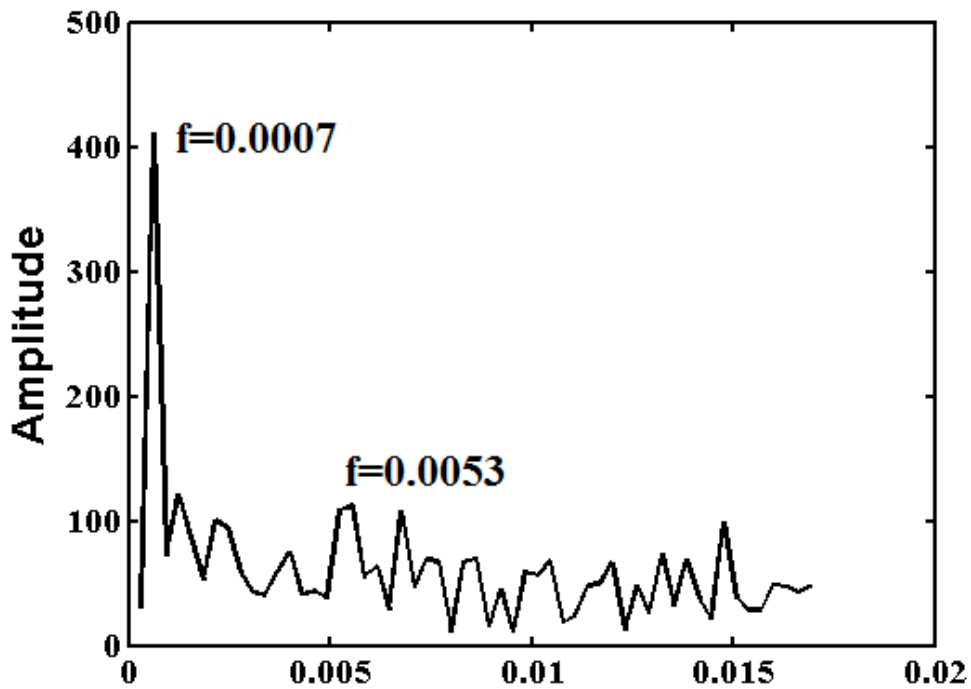
Figure 4.6 FFT plot for time data having C behaviour. Here *We*=0.3,*G*=0.057, *Ka*=0.000562

The FFT plots for P1, LC, and C time series data shown in figure 4.4, 4.5, and 4.6 respectively shows one dominant frequency peak. For P1 and LC plot, the plot has two sub frequency peaks. The plots clearly do not show the frequency patterns to identify the modes of dripping.

The data points for breakup time data are not equally spaced. So the more accurate FFT method for non-equally spaced data points is Lomb Scargle method (Ruf, 1999) which estimates a frequency spectrum based on a least squares fit of sinusoid called power spectral density (PSD) normalized over frequency. A MATLAB algorithm is used to obtain the periodogram for the same method (lomb.m file Appendix A.4). The plots given in Figure 4.7 (a-f) shows the Lomb Scargle periodogram for P1 (a, b), LC (c, d), and C (e, f) behaviour respectively.
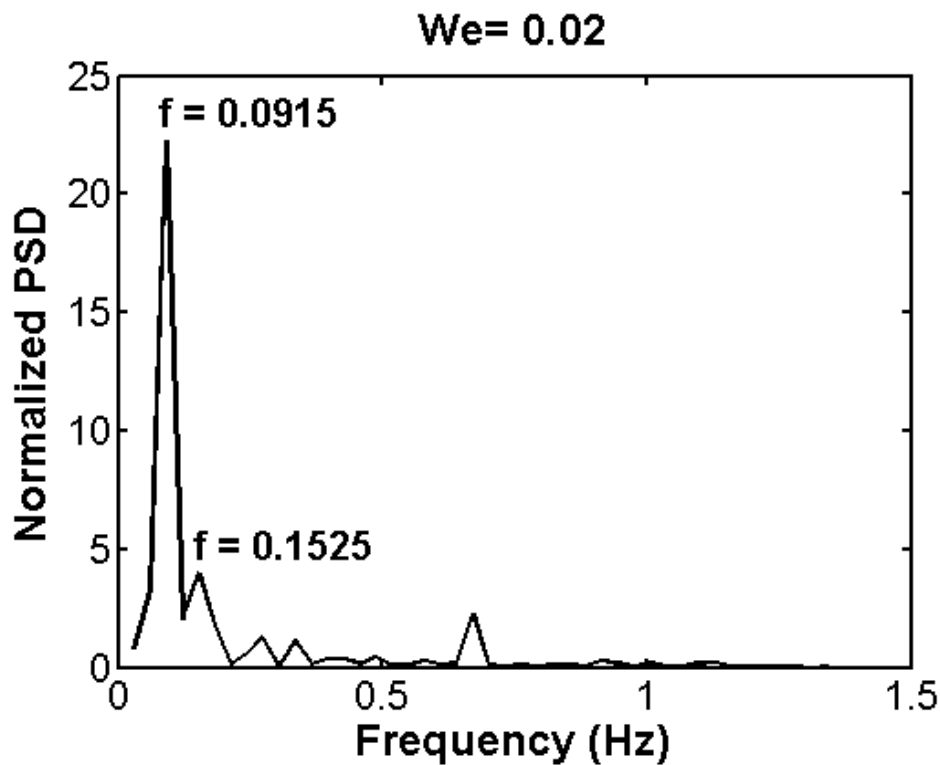
Figure 4. 7 a Lomb Scargle periodogram for P1 behaviour. Here *G*=0.057, *Ka*=0.000562

We= 0.05

f = 0.1215

f = 0.2836
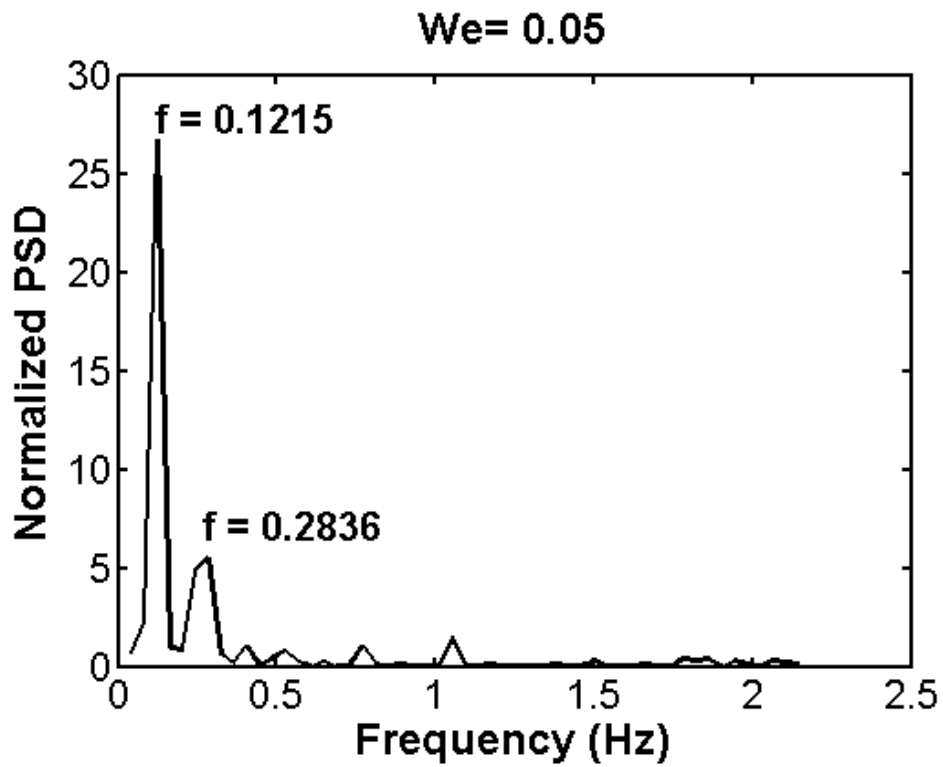
Figure 4.7 b Lomb Scargle periodogram for P1 behaviour. Here *G*=0.057, *Ka*=0.000562

We= 0.1

f = 0.1813

f = 0.3626
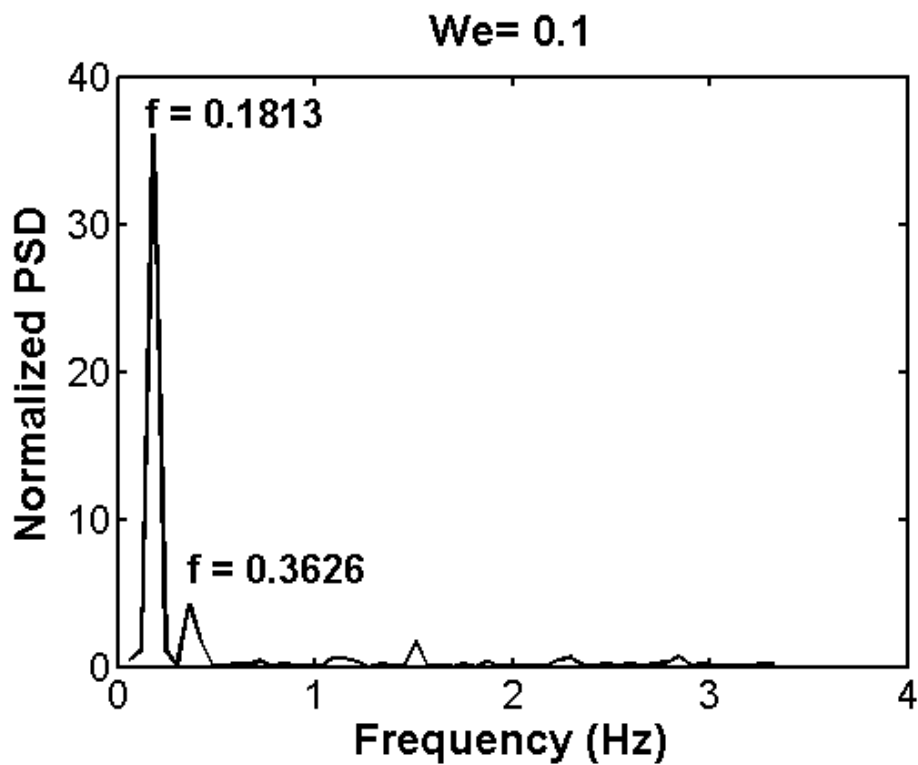
Figure 4.7 c Lomb Scargle periodogram for LC behaviour. Here *G*=0.057, *Ka*=0.000562
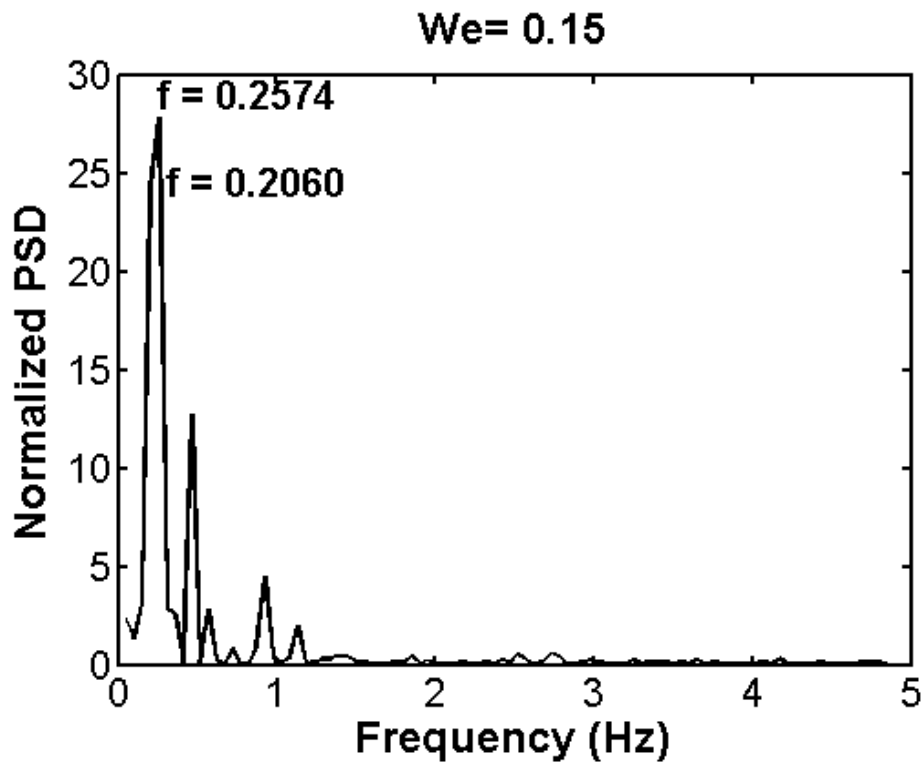
Figure 4.7 d Lomb Scargle periodogram for LC behaviour. Here *G*=0.057, *Ka*=0.000562
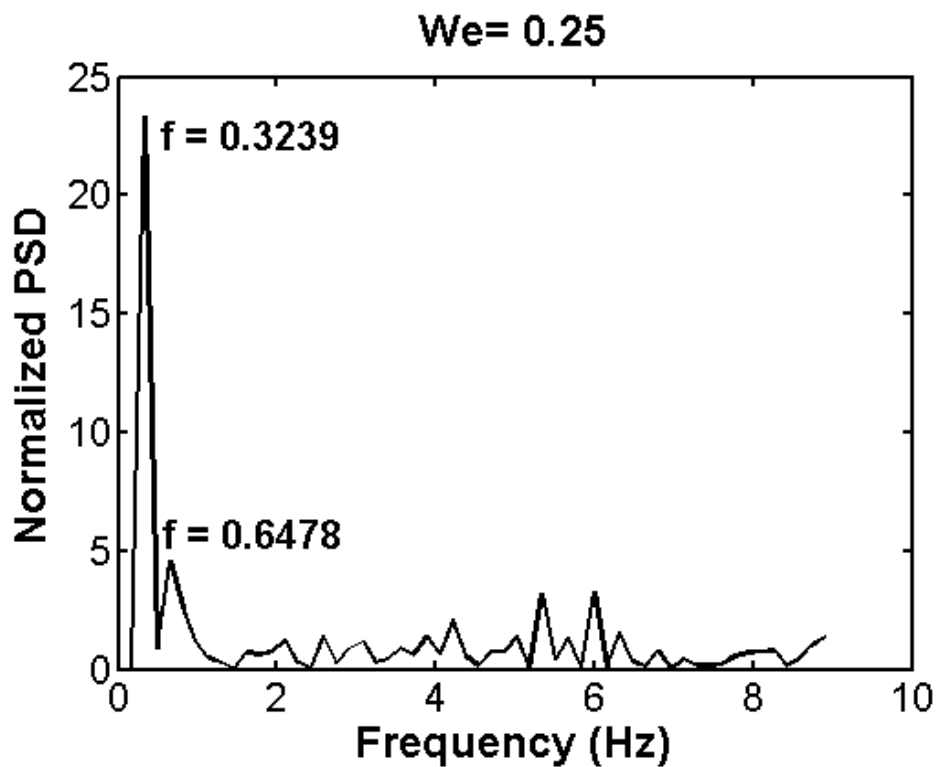
Figure 4.7 e Lomb Scargle periodogram for C behaviour. Here *G*=0.057, *Ka*=0.000562
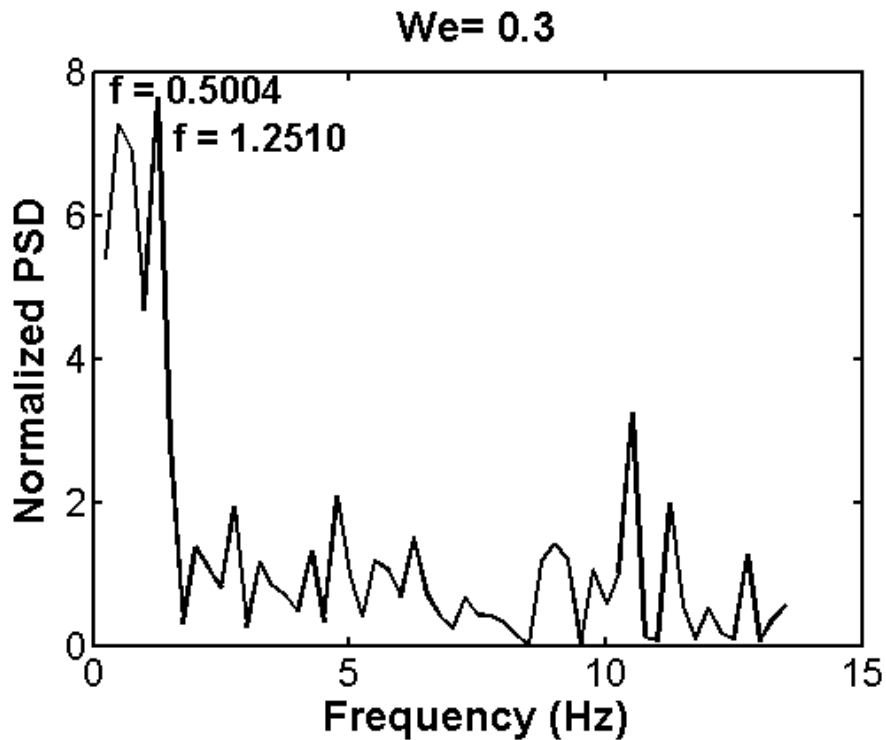
Figure 4.7 f Lomb Scargle periodogram for C behaviour. Here *G*=0.057, *Ka*=0.000562

Although Lomb Scargle periodogram showed in Figure 4.7 (a-f) represents P1 (a, b), LC (c, d), and C (e, f) behaviour, there are no clear evidences or patterns which helps to identify the same behaviour from these plots. To further examine these , the first dominating frequency is plotted against *We* in figure 4.8, which shows that the first dominating frequency value increases as *We* increases. Similar plot for the second dominating frequency is shown in figure 4.9, which shows that the frequency becomes much higher at high *We* but for low *We*, there are no specific patterns and hence it does not give any idea of the dripping mode. Based on these observations, it could be concluded that the Lomb Scargle periodogram does not assist in the identification of dripping modes. An alternative way to identify the dripping behaviour is to plot the time return maps from the breakup time data, as given in the following sub-section.
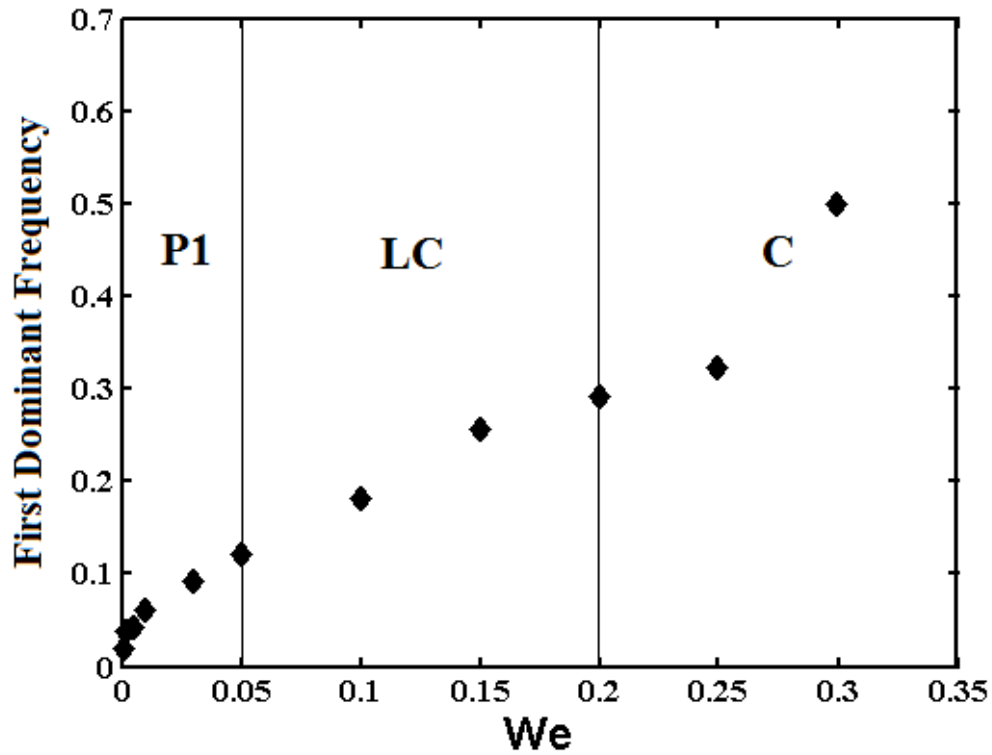
Figure 4.8 First dominating frequency vs We obtained from Lomb Scargle periodogram.
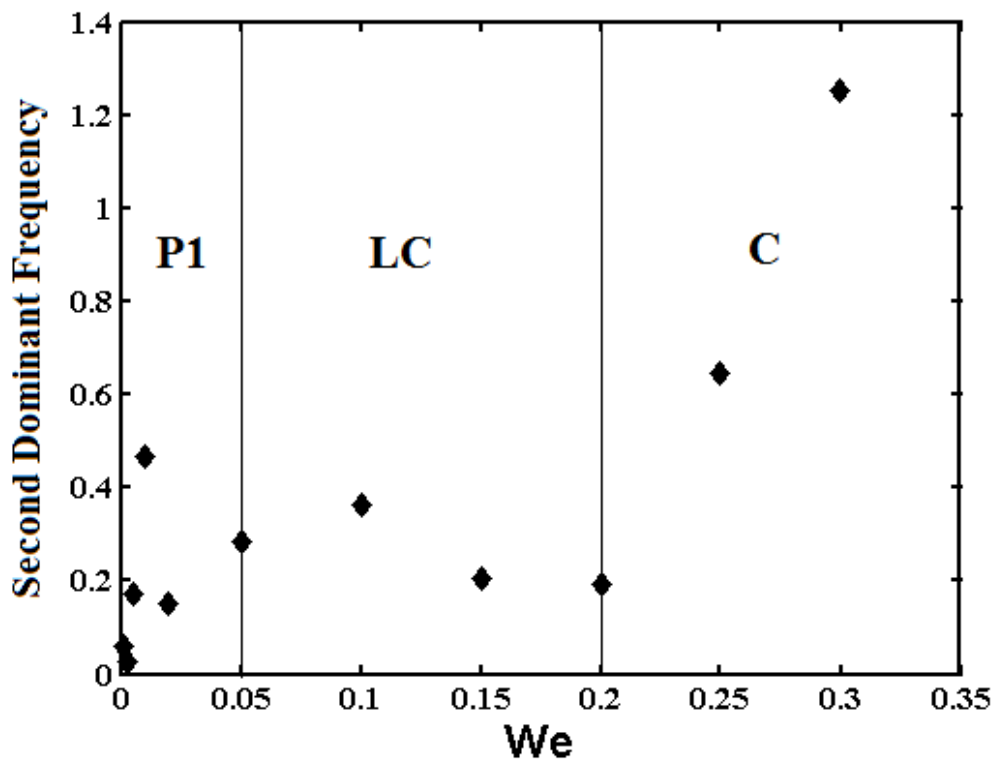
Figure 4.9 Second dominating frequency vs We obtained from Lomb Scargle periodogram.

4.1.2 Time return maps

The time return maps are the plots of time t_n vs. t_{n+1}, where nature of the plot helps to investigate the periodicity of the time series data. Each point on the time return map is determined by the ordered pair (t_n, t_{n+1}) for some n value. Previous researchers (Shaw, 1984; k Martien et al., 1985; D'Innocenzo and Renna, 1996, Subramani *et al*., 2006) have used the time return maps to identify the structures and patterns from the simple plot to define the dripping behaviour. The time return map responses for the same data given in Figure 4.7 (a-f) are given below figure 4.10 for different modes of dripping.

(a)   **(b)**

(c)

(d)

(e)

(f)

(g)

(h)
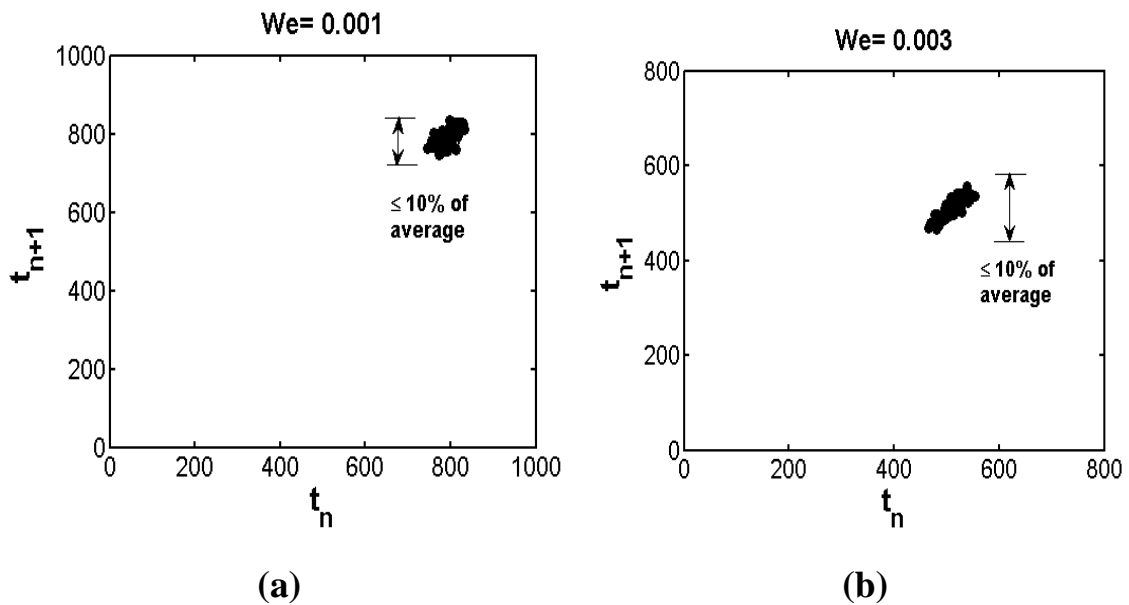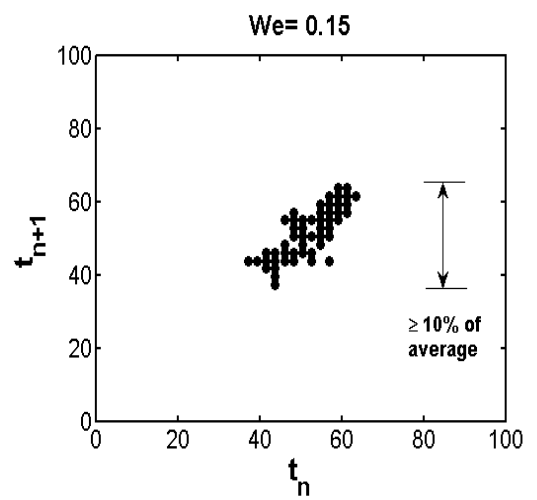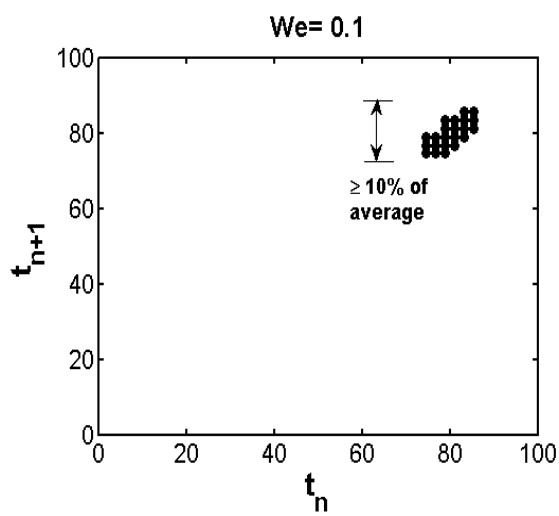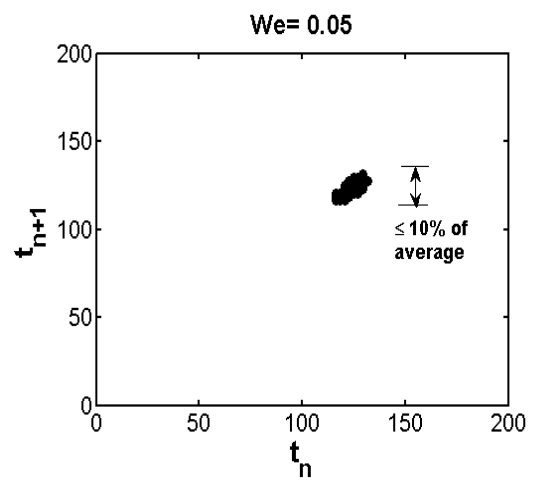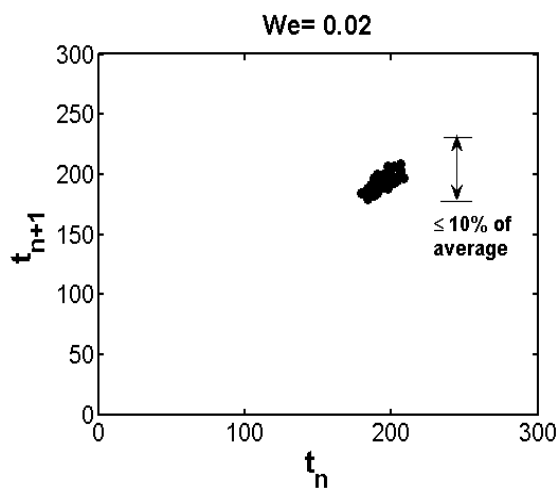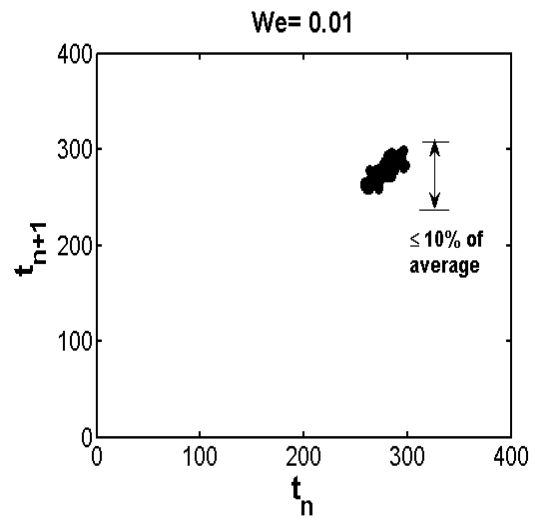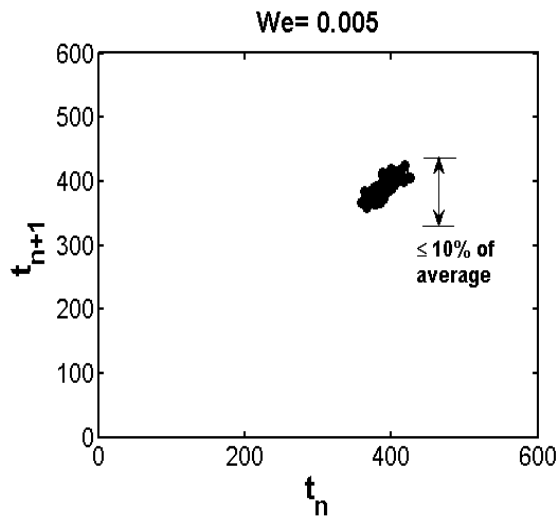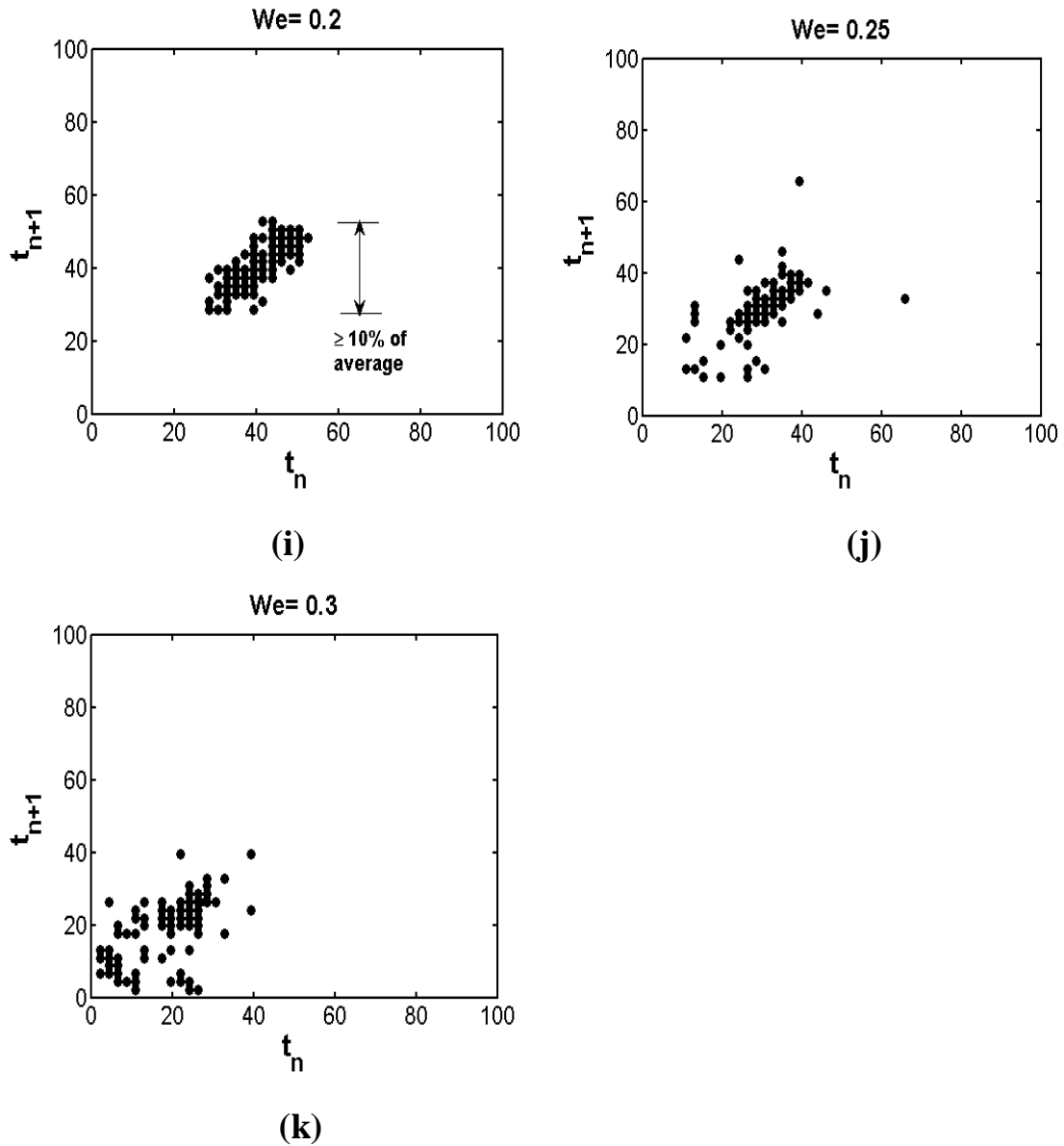
Figure 4.10 Time return maps showing P1 (a-f), LC (g-i), and C (j-k) behaviour. Here *G*=0.057, *Ka*=0.000562.

The time return maps have shown in the figure 4.10 (a-k), represent the trajectories of periodic orbits.   In figure 4.10 (a-f), all the points are clustered together, ideally forming only one point, represents the P1 behaviour. The spread between the data points is within ±10% of the average for P1 regime. For the limit cycle regime, the spread between the data points is more than 10% of average value, but the trajectories repeat itself giving an encircled regime on time return map as shown in figure 4.10 (g-i). At high Weber

number, the points are scattered rather randomly giving C mode of dripping as shown in figure 4.10 (j-k).

The time return maps are shown to give good predictions about the modes of dripping, hence are used in the investigation of modes of dripping for rest of the experimental data. To facilitate discussions, the transition from P1 to LC is deemed to occur at $We = We_{LC}$, and the transition from LC to C occurs at $We = We_c$. These two Weber numbers can be pin-pointed experimentally. As the value of Ka changes, the corresponding values of We_{LC} and We_c also change. The loci of these transitional We are plotted against Ka as a dripping mode phase diagram next.

4.2   Phase diagram

The phase diagrams shown in figure.4.11 (a)-(c) identify the location in the parameter space where the dynamics changes from one mode to another. For a vertical nozzle (figure 4.11 a), at low values of Ka, both We_{LC} and We_c rise sharply as the value of Ka increases. For high values of Ka, the trajectories of We_{LC} and We_c converge, i.e. the transition occurs directly from P1 to C without exhibiting a LC regime. This is known as the "simple dripping" region in the computational phase diagram of Subramani *et al.* (Subramani *et al.*, 2006) when G=0.3. Noting that $Ka=(Oh^4 G)^{1/3}$, their corresponding value of Ka for such "simple dripping" regime is 0.67, nearly an order of magnitude larger than ours. Further, in their work, the P1 region narrows down prior to the "simple dripping" regime, whereas ours do not exhibit this narrowing. Certainly, keeping the P1 region wide at high values of Ka avails greater flexibility for applications. These

differences in the phase diagram highlight the very considerable effect of the value of G on the dripping dynamics, also illustrated by the same authors.

The phase diagrams for an inclined nozzle look similar to that of the vertical nozzle. However, on closer examination, three significant and potentially useful features can be distilled. First, the values of We_c decrease dramatically with θ especially for $Ka \sim 10^{-3}$, suggesting that the asymmetry favors chaotic dripping. This is in line with the findings of *Reyes et al.* (Reyes et al., 2002), which showed that even at $\theta = 5^{\circ}$, the dripping dynamics for low viscosity water turns very complicated. Second, the locus of We_{LC} is not so strongly affected by θ at low values of Ka. It suggests that P1 and LC regimes are influenced more by viscous damping than by asymmetry. A consequence of these two observations is that the LC regime shrinks noticeably with increase in θ. Conceivably at even larger values of θ, the LC region might vanish. However, we could not pursue that in our experiments as the liquid started to wet the outer wall of the nozzle at large inclinations despite the use of a dewetting agent.

At high values of Ka, however, the interaction of asymmetry with strong viscous damping raises the values of We_{LC}, leading to the third observation: The values of We for direct transition from P1 to C increase with θ. This avails an operating option to move the chaotic dripping of a very viscous liquid into the well-defined P1 region simply by tilting the nozzle. The modest increase in the values of this direction transition We against the corresponding values for the vertical nozzle suggest that the effect of θ is most likely a higher order effect and thus difficult to deduce from scaling arguments, as was done for the jetting transition (Subramani et al., 2006).

65
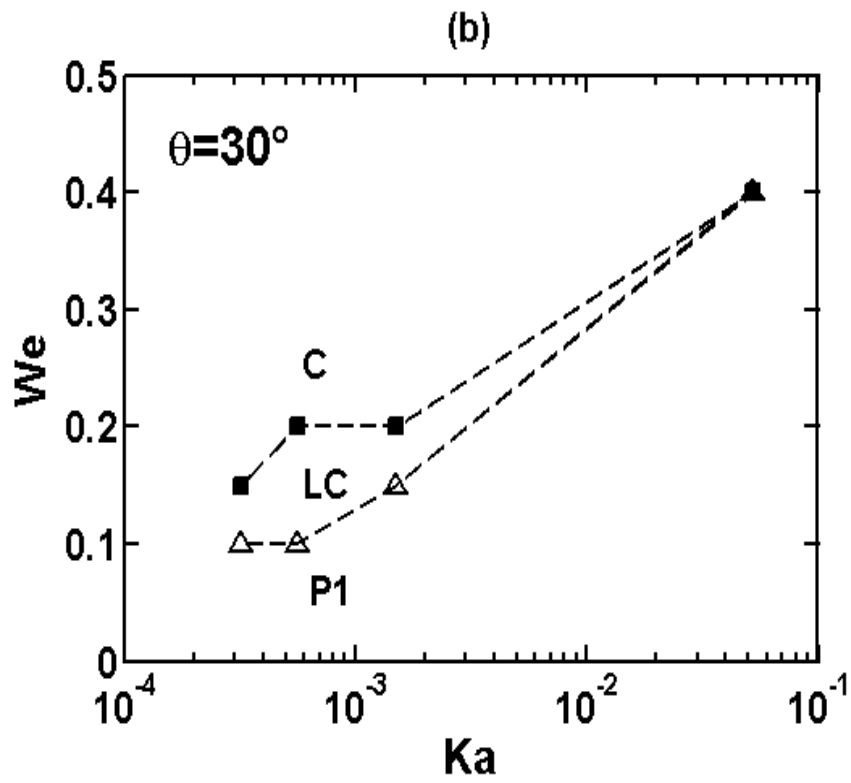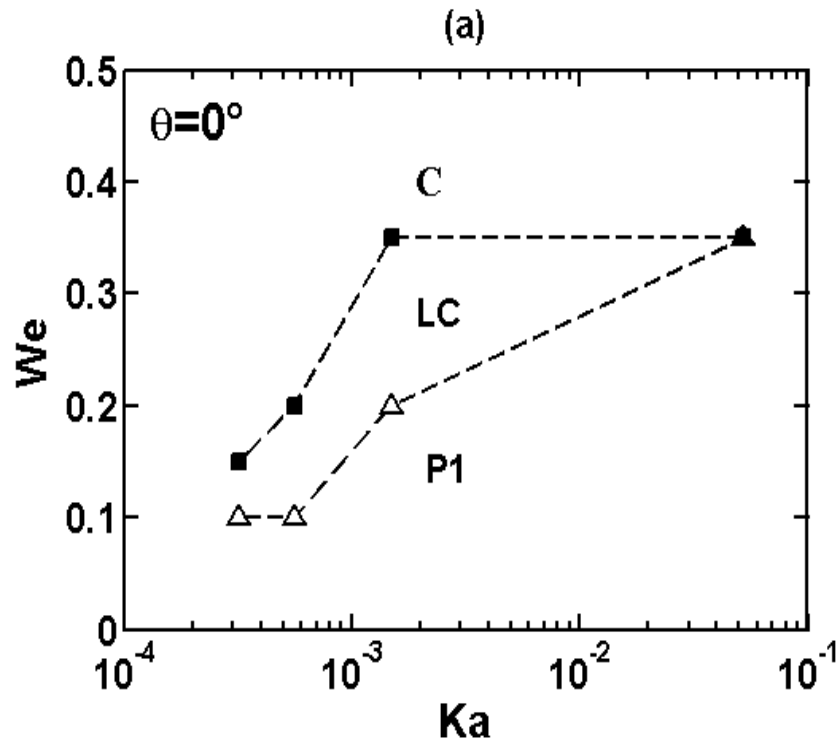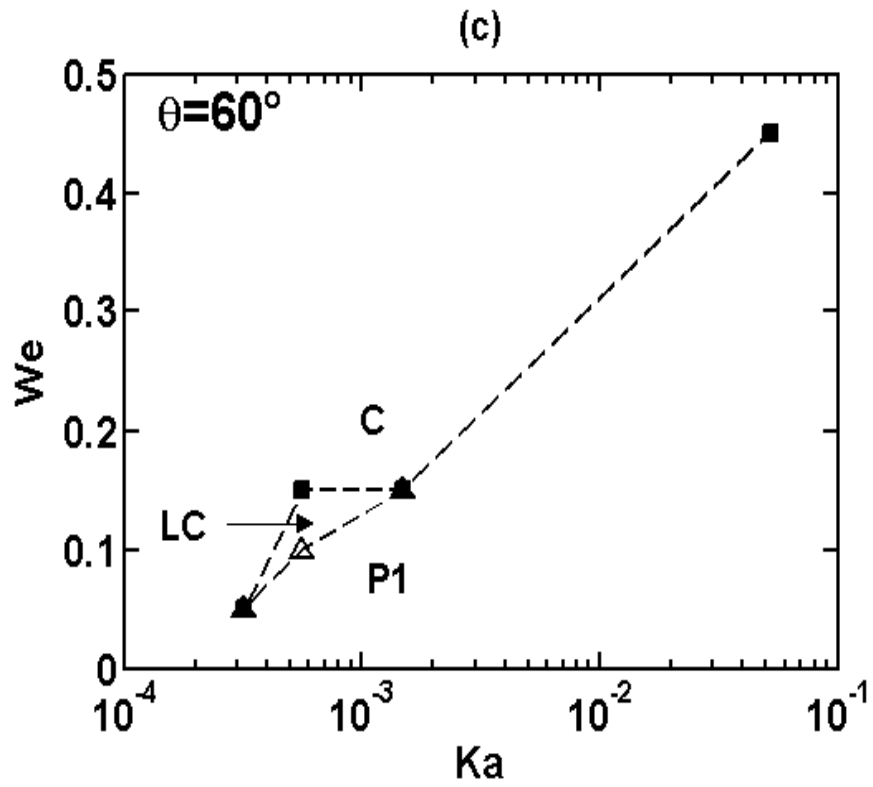
Figure 4.11 An experimental phase diagram in (*We*, *Ka*) space at θ=0° (a), θ=30° (b), θ=60° (c), showing transitional Weber numbers $-\triangle-\mathrm{We_{LC}}-\blacksquare-\mathrm{We_c}$. Here G=0.062.

4.3   Effect of nozzle inclination on drop breakup time at low Weber number

Further insight into the dripping dynamics of an inclined nozzle can be gained by examining the drop breakup times t_b for different nozzle inclination angle θ. As shown in figure 4.12, the value of t_b at a given We decreases with increasing θ. As discussed earlier, the t_b values are unaffected by θ in the LC regime, but the number of repeating trajectories for the LC regime at a given total time decreases with increase in θ as shown in figure 4.13. The observation in figure 4.12 was further investigated at other values of We, as represented by closed symbols in figure 4.14 (a). Clearly the values of t_b decrease with increasing θ when G=0.053. As the t_b values in figure 4.14 are the average values with a maximum of ±10% spread (the value of spread decreases with increase in viscosity), it is critical to determine if two sets of data at different angles were indeed statistically different. Assuringly, using the Student's t-test, the probability of having indistinguishable values of t_b (as the angle changed) is very low (p value approximately 10^{-8}). Analogous behaviour is found even at ten times greater value of G (G=0.52) shown by open symbols in figure 4.14 (b) as well as for different viscosities of the liquids, as in figure 4.14 (c) and (d). In short, t_b decreases with increasing θ for all values of G, We, and Ka investigated.
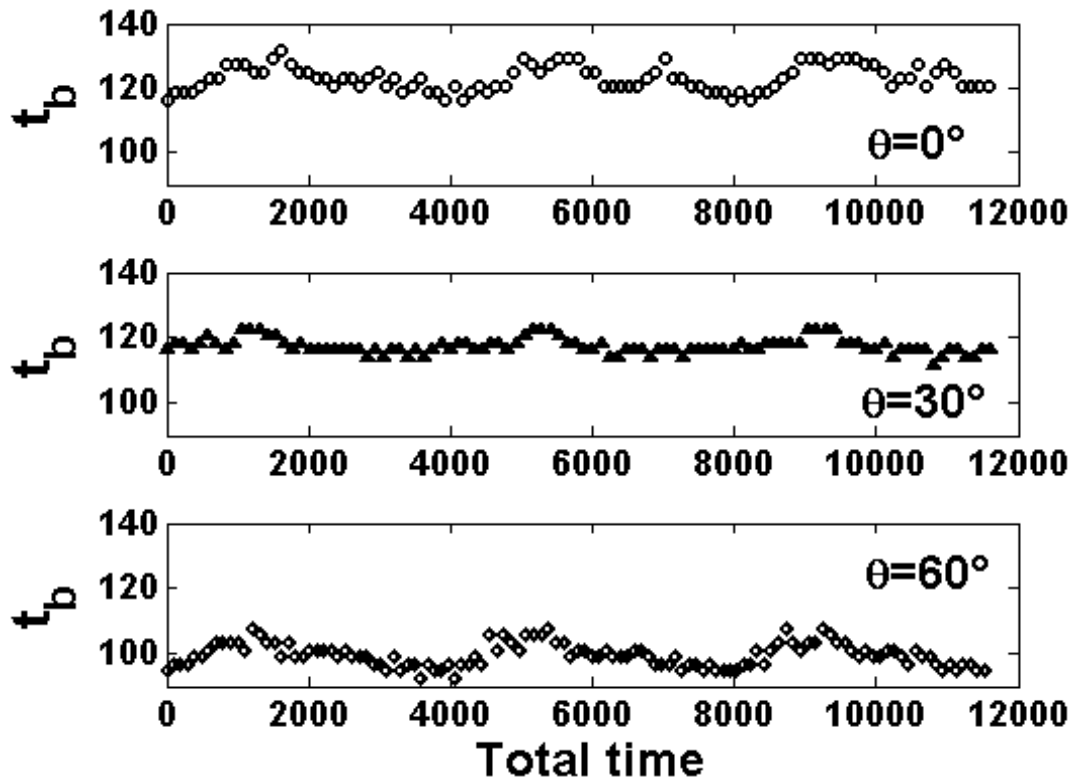
Figure 4.12 Breakup time t_b at different angle of inclination θ for P1 behaviour. The experiments were performed at G=0.057, Ka=0.000562 and We=0.05.
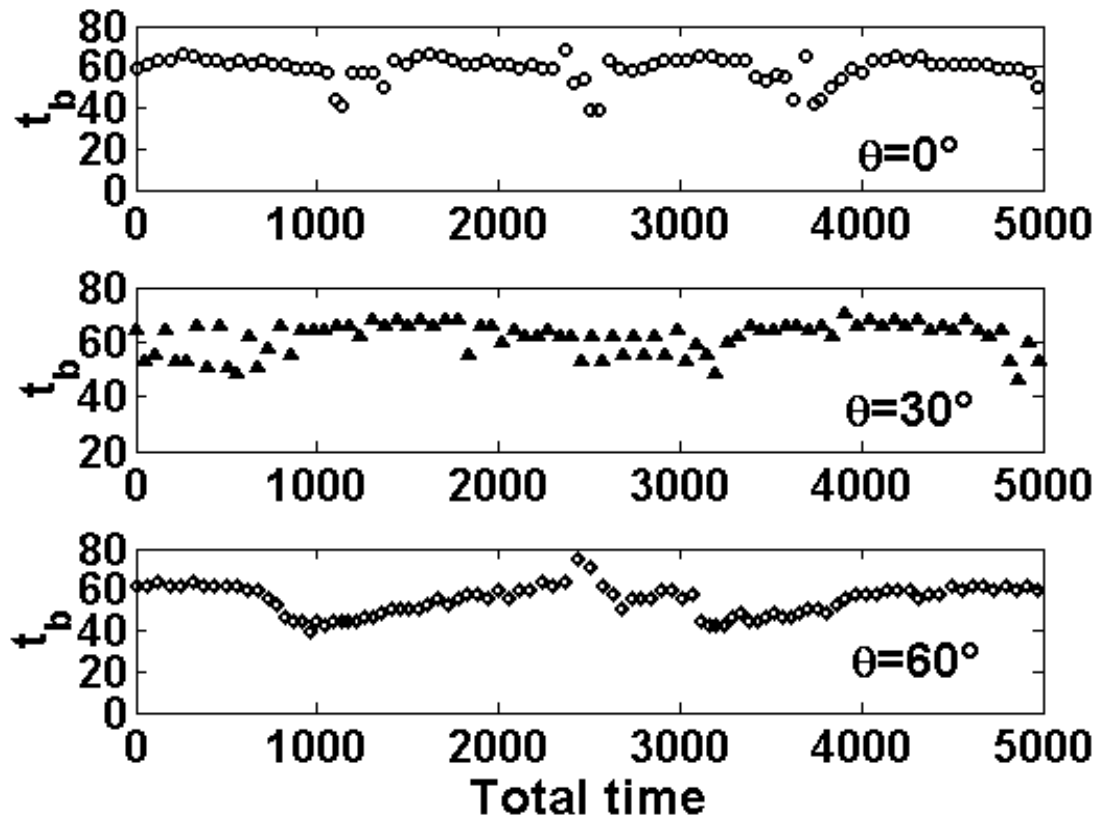
Figure 4.13 Breakup time t_b at different angle of inclination θ for LC behaviour. The experiments were performed at G=0.057, Ka=0.000562 and We=0.15.

(a)

G=0.053

▼--S0,N1,0°
●--S0,N1,30°
▲--S0,N1,60°

(b)

▽--S0,N3,0°
○--S0,N3,30°
△--S0,N3,60°

G=0.52
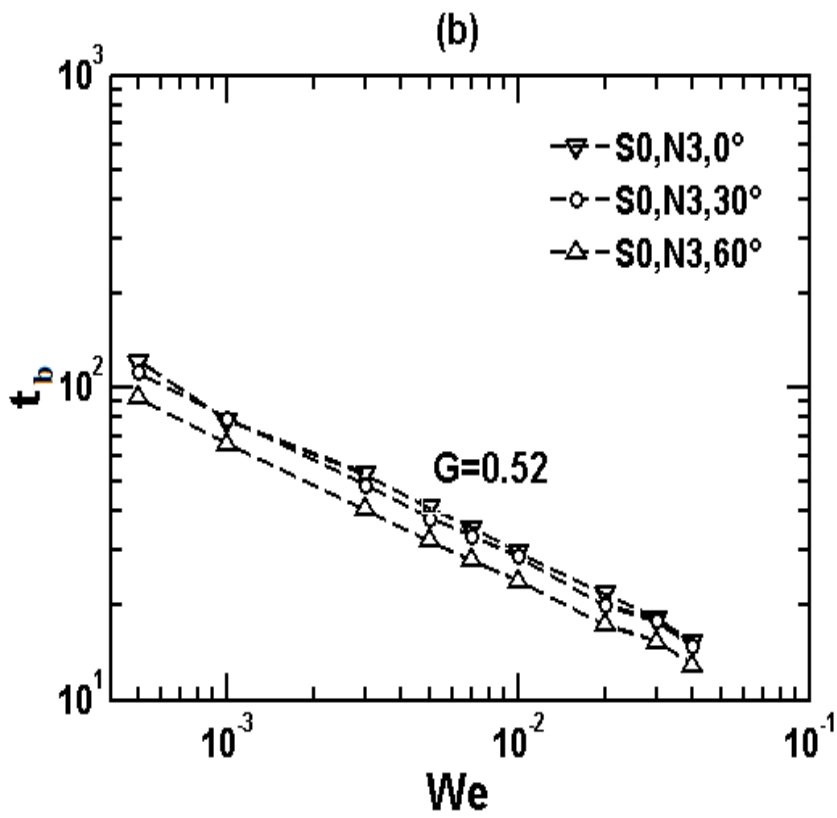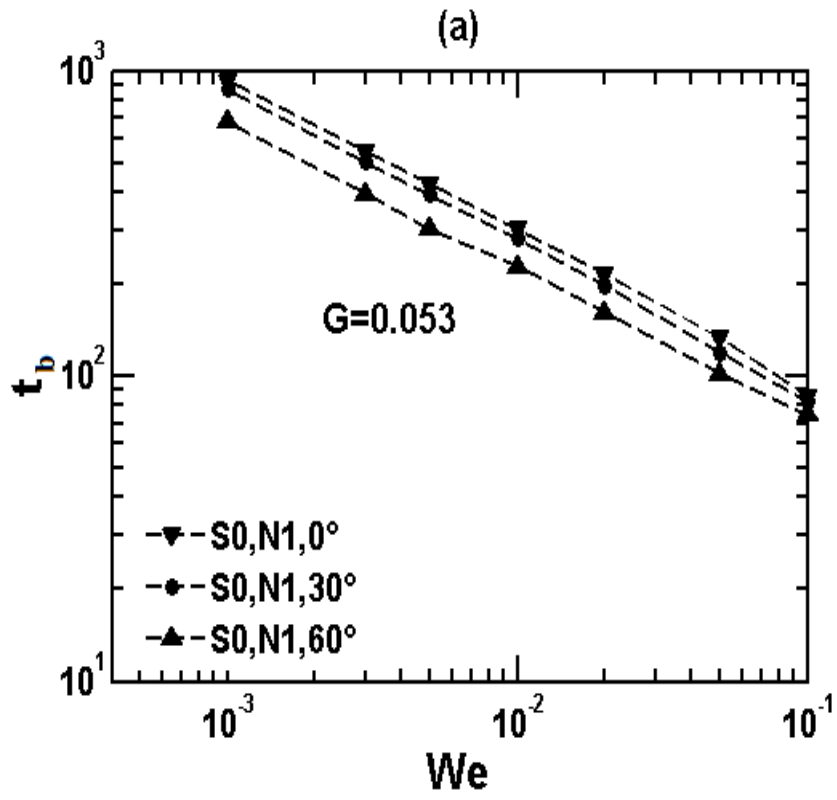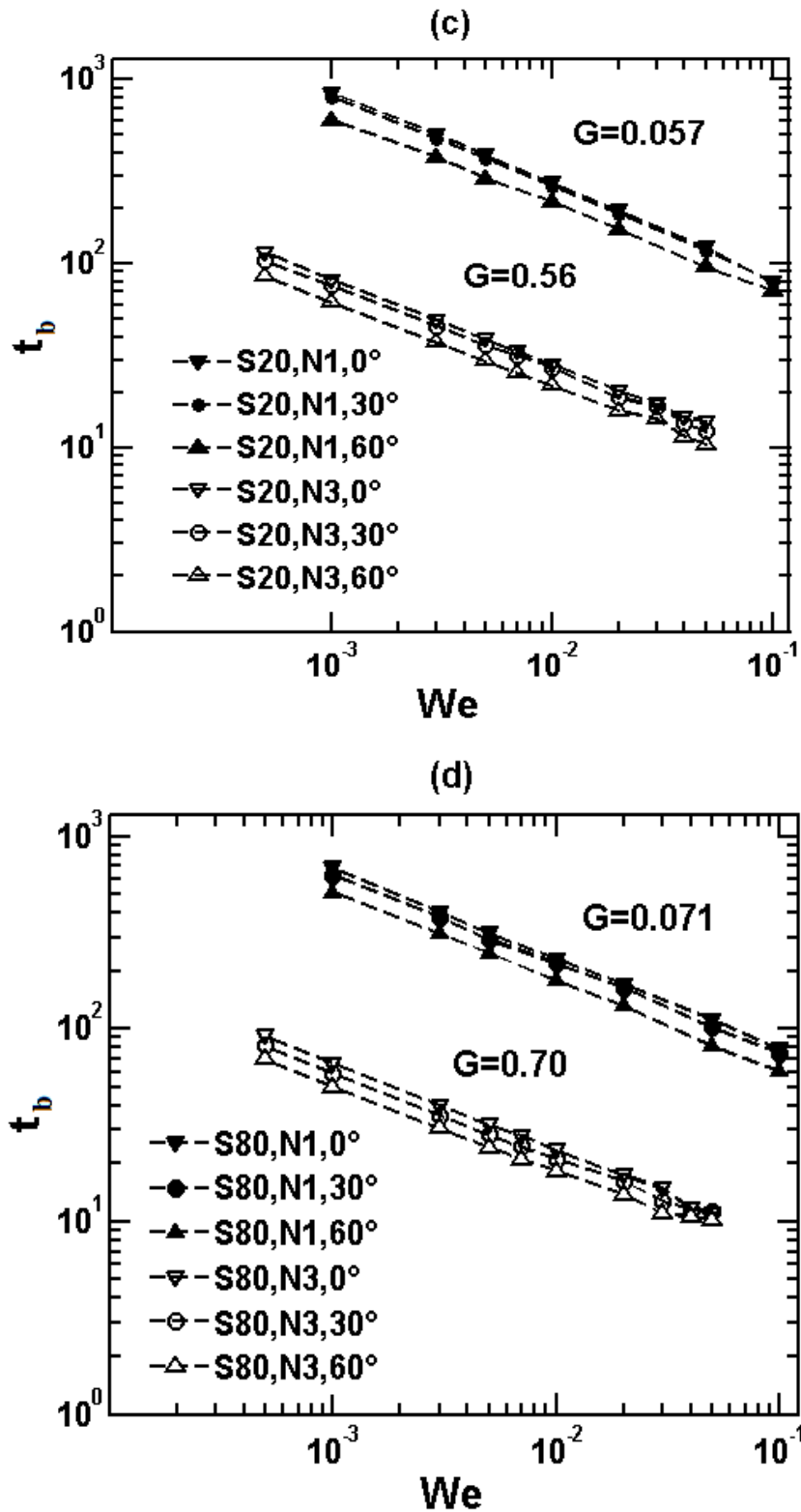
Figure 4.14 Breakup times as a function of Weber number. Here S0, S20 and S80 represent 0% (a, b), 20% (c), and 80% (d) glycerol by weight respectively. N1 represents the nozzle of OD 1.25 mm, and N3 is the largest nozzle of OD 3.92 mm.

Table 4.1 Magnitude of the slopes of the lines obtained from Fig. 4.14

	0°	30°	60°	G
S0N1	0.5	0.5	0.5	0.053
S20N1	0.5	0.5	0.5	0.057
S80N1	0.5	0.5	0.5	0.071
S0N2	0.5	0.5	0.4	0.52
S20N2	0.5	0.5	0.4	0.56
S80N2	0.4	0.4	0.4	0.70

Figure 4.14 suggests that $t_b \propto We^{-m}$. To examine the variability of the values of the slope -m due to the ±10% scatter inherent in the data points (representing averages), two lines representing the worst-case scenario were drawn as follows: first a line connecting the minimum (-10%) t_b at the lowest We and the maximum (+10%) t_b at the highest We; second a line connecting the maximum (+10%) t_b at the lowest We with the minimum (-10%) t_b at the highest We. The magnitudes of slopes for such two lines for each experimental set are in between 0.4 and 0.6, suggesting that the values of the slopes in figure 4.14 are accurate to the first significant digit only. Recognizing this observation, Table 4.1 collects the magnitudes of the slopes for all the lines in figure 4.14. Most of the values are approximately 0.5, suggesting

$$t_b \propto \frac{1}{We^{0.5}}$$ (4.1)

Equation (4.1) leads to a rather counter-intuitive finding. It can be rewritten in the dimensional form as, $t_b \propto \frac{1}{v}$, where v is the velocity of the emanating fluid. Rearranging and multiplying both sides by the internal cross sectional area A of the nozzle results in $Av\tilde{t}_b = AK$, where K is the proportionality constant dependent on G, Ka and θ. The left hand side is approximately the volume $\tilde{V}$ of the detached liquid droplet; this approximation is very good when the volume of pendant drop does not change significantly. Random sampling of the recorded images suggested that this assumption is very reasonable. This relationship offers a startling conclusion that the detached drop volume in P1 dripping is rather independent of the flow rate. It also avails a very convenient route to obtain the experimental drop volumes without analyzing the complicated asymmetric drop images.

To compactly quantify this finding, by making $\tilde{V}$ dimensionless with the volume of an equivalent sphere based on the outer nozzle radius R, a power law correlation was tested:

$$V = c_1 G^{c_2} Ka^{c_3} (\cos\theta)^{c_4}$$ (4.2)

The choice of cosine of θ was mainly suggested by the component of gravity along the axis of the nozzle. A nonlinear least squares regression of Eq. (4.2) using all data points in the P1 regime yielded the coefficients:

$$V = 1.3G^{-1}Ka^{0.02}(\cos\theta)^{0.37} \qquad\qquad (4.3)$$

The dimensionless volumes V of the liquid droplets predicted are within 10% of experiments, as plotted in figure 4.15. A similar regression analysis that included *We* gave a very small (0.009) exponent for *We*, without any significant improvement in the accuracy of predictions, further justifying its omission in Eq. (4.3). It is noteworthy that figure 4.14 covers the widest ranges of parameters than previously reported, with θ up to 60°, *Ka* spanning three orders of magnitude and *G* one order of magnitude. Eq. (4.3) is also significant as the first ever correlation for the droplet volume for P1 dripping from a tilted nozzle. Further, it includes dripping from a vertical nozzle as a special case, valid beyond vanishingly small values of Weber number (unlike the correlation in Yildirim *et al.*) (Yildirim et al., 2005). It also shows that the *1/G* dependence as hinted in figure 7 of Ambravaneswaran *et al*. (Wilkes et al., 1999) remains valid for dripping from a tilted nozzle.
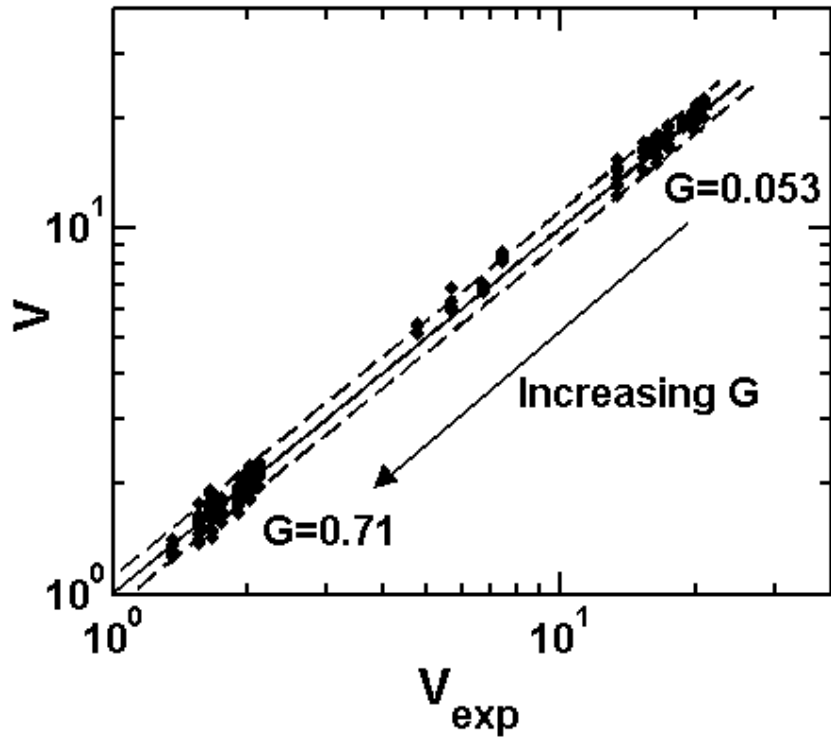
Figure 4.15 Predicted volume V vs experimental volume V_{exp}. The dashed lines represent ±10% error in volume. Here $0.0005 \leq We \leq 0.1$, $3.22 \times 10^{-4} \leq Ka \leq 5.26 \times 10^{-2}$ and $\theta = 0°$, $30°$, $60°$.

4.4 Interrogating the origin of the effect of the angle of tilt on t_b

As the angle of inclination increases, the component of gravity along the axis of the nozzle decreases. Intuitively this should result in a decrease in the driving force for drop formation as the gravitational pull on the emanating liquid has been weakened. At low flow rates in which the inertial force is not dominating, surface tension forces should then resist drop detachment for a longer time, giving an increased value of the breakup time t_b, and hence an increased drop volume. In contradiction, the experimental results showed that the t_b values decreased with increasing θ. This suggests that despite the weaker axial component of gravity, the surface tension force is being weakened even more by the asymmetric air-liquid interface. To probe the detailed interplay between these forces will require a full 3-dimensional unsteady state simulation of the free surface motion which is out of the scope of this work. In lieu of this, an alternative approach was pursued as described below.

A pendant drop, which is pinned to the end of a nozzle, assumes a stable shape as long as the drop volume is below a critical value, beyond that it becomes unstable leading to its deformation and eventual breakup. At low Weber numbers typical of P1 dripping, the key forces remain gravity and surface tension, whether the nozzle is tilted or not. Inertial forces come into play only in the necking of the droplet in the last moments (Wilkes et al., 1999), often comprising just a small fraction of the overall breakup time. This similarity suggests that the drop formation process in slow P1 dripping is closely related to the limits of stability of a static pendant drop. Specifically, we hypothesize that if the

largest volume of the static pendant drop that could be supported with a tilted nozzle becomes smaller, the corresponding dynamic drop formation should also require a shorter breakup time.

Here, the largest volume for a stable pendant drop pinned to the nozzle tip is denoted as the critical volume, V_c. The value of V_c was determined experimentally as follows. An incremental volume of liquid was pushed very slowly with the syringe pump to form a pendant drop at the tip of a nozzle, followed by a long pause to observe its stability. More volume was added if the drop was stable. The stable shapes of the drops were recorded in the camera and the pendant drop volumes calculated using the image analysis tool in MATLAB. The last stable volume was assigned as V_c. The experiments were done at θ=0°, 30° and 60°.

A computational approach was made to further cross-check the experimental results obtained on pendant drop stability. Simulations were performed with *Surface Evolver* (*SE*) (SEFIT software, retrieved on 10 July 2013), an open source software. In *SE* computations, a pendant drop of prescribed volume was pinned to a unit circle on a ceiling. The orientation of the gravity (θ) can be varied in the simulations. The experimental Bond number was used for the simulation. An incremental volume was added until the pendant drop was destabilized and detached over simulated time. The value of V_c was then refined by using a smaller volume (decrements of about 2% of the total volume) that resulted in a stable pendant drop. The simulations were repeated for θ=0°, 30° and 60°. The associated shapes of the pendant drops at V_c for different θ are shown in figure 4.16 (a-c). The asymmetry in the shape of the drops due to nozzle inclination is apparent mainly near the contact line.

77
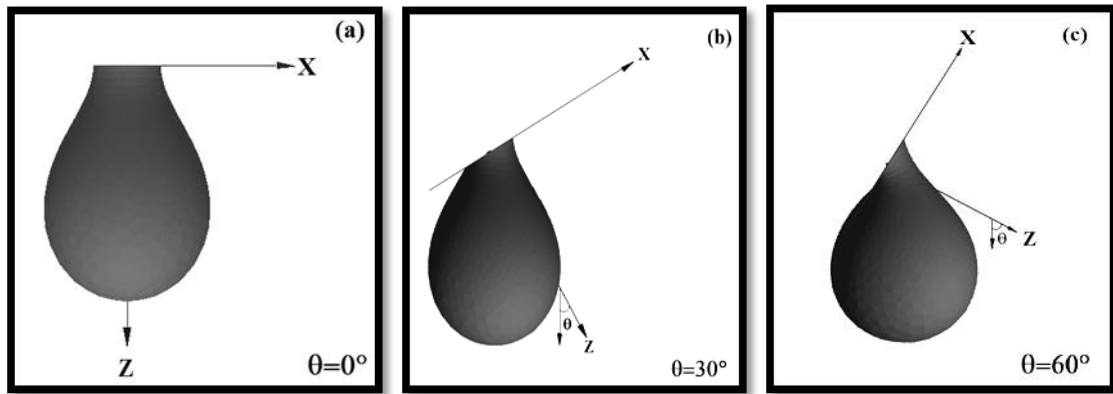
Figure 4.16 Stable drop shapes pinned on a circular roof at different θ, side view, at G=0.06. The roof is in the X-Y plane and gravity is acting along the vertical downward direction.

The values of V_c from both experiments and simulations were made dimensionless using the volume V_o of an equivalent sphere with the corresponding nozzle radius, then plotted against θ as shown in figure 4.17. The error bars demarcate uncertainties in edge detection of the experimental images of the pendant drops. The agreement between experiments and simulations is very good. The experimental values were understandably below those of simulations as the theoretical limit could be attained only under zero perturbations. The most critical observation is that the dimensionless critical drop volume decreases with an increase in θ. It strongly suggests that the increasing asymmetry of the gas-liquid interface has a pronounced weakening effect on the capillary forces in resisting the pull of gravity. We suspect that the component of gravity perpendicular to the nozzle axis contributes in a subtle manner, e.g. by opening up a "second front" in the tussle with capillary forces. In experiments involving small flow rates, the same effects carry over, resulting in shorter breakup times.
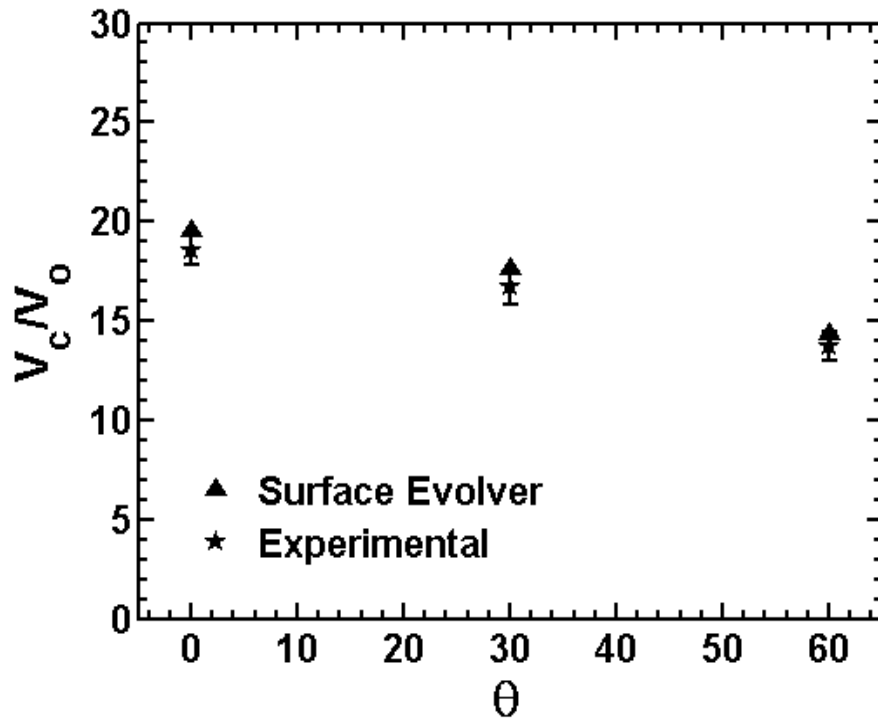
Figure 4.17 Experimental and computed variation of the dimensionless critical volume V_c/V_o with θ.

4.5   Volume of primary drops from image analysis

A number of theoretical and experimental predictions on drop volume of primary drops detaching from a vertical nozzle is available and already mentioned in the literature review. In this section a comparison of volume obtained from a correlation developed in previous subsection and volume obtained from image analysis is made for P1 regime. Also for all three modes of dripping, the volume of individual drops obtained from image analysis is compared with drop breakup time in another subsection. Here the volume comparison is done for three different nozzle inclination angles.

4.5.1   Comparison of drop volume obtained from correlation developed and from image analysis

A correlation developed in section above represented by equation 4.3, gives the dimensionless volume V. In the equation 4.3, the dimensionless volumes are actually the average volumes for a particular *We*. Hence the volumes used in image analysis calculations are also the average volumes for same *We*. These volumes are made dimensionless with the volume of an equivalent sphere based on outer radius R. Figure 4.18 compares the volume V_{img} obtained from image analysis and predicted volume V obtained from equation 4.3 for $\theta=0°$ for different *We* values in P1 regime. The open square represents dimensionless volume obtained from image analysis and closed diamond represents predicted dimensionless volume from equation 4.3. Although the experimental method of measuring drop volume i.e. image analysis method always have error in the measurements (errors are $\leq5\%$ and are smaller than the marker size in the plot

4.18), the predicted values of drop volume are relatively good agreement with the experimental results, with a maximum relative deviation of 15%. Similar plots for inclination angle θ=30˚, and 60˚ are shown in the same figure (figure 4.18 b and 4.18 c respectively) also having maximum relative deviation of 15% in the experimental and predicted dimensionless drop volumes. The values measured in the experiments are consistently smaller than that of predicted and their deviation decreases at high *We* value within P1 regime.
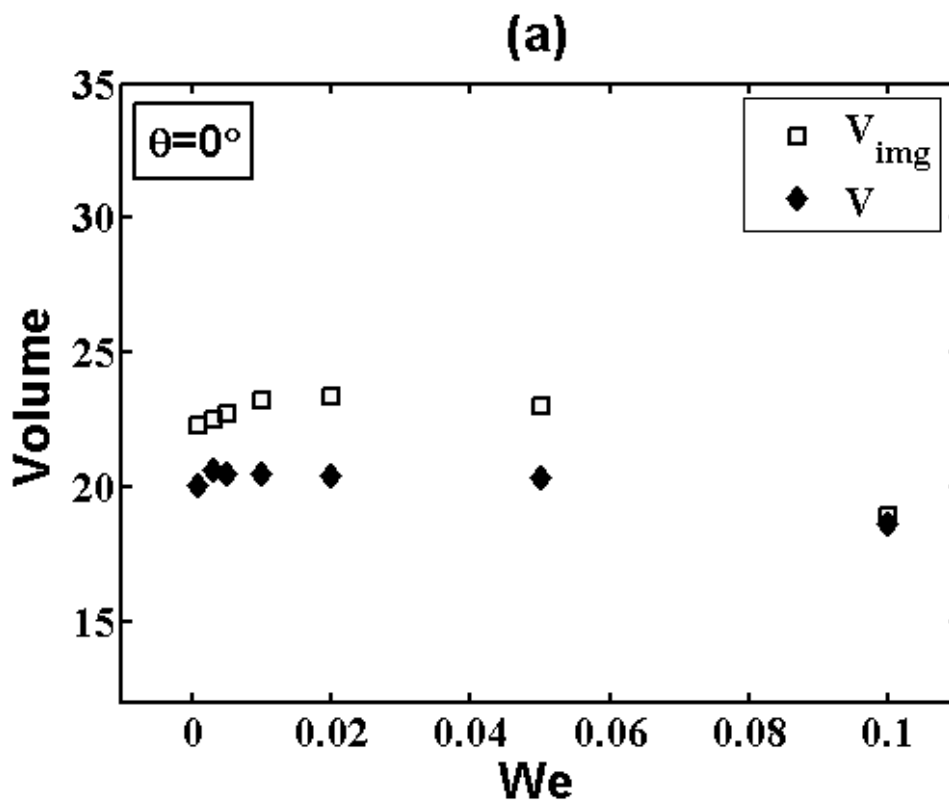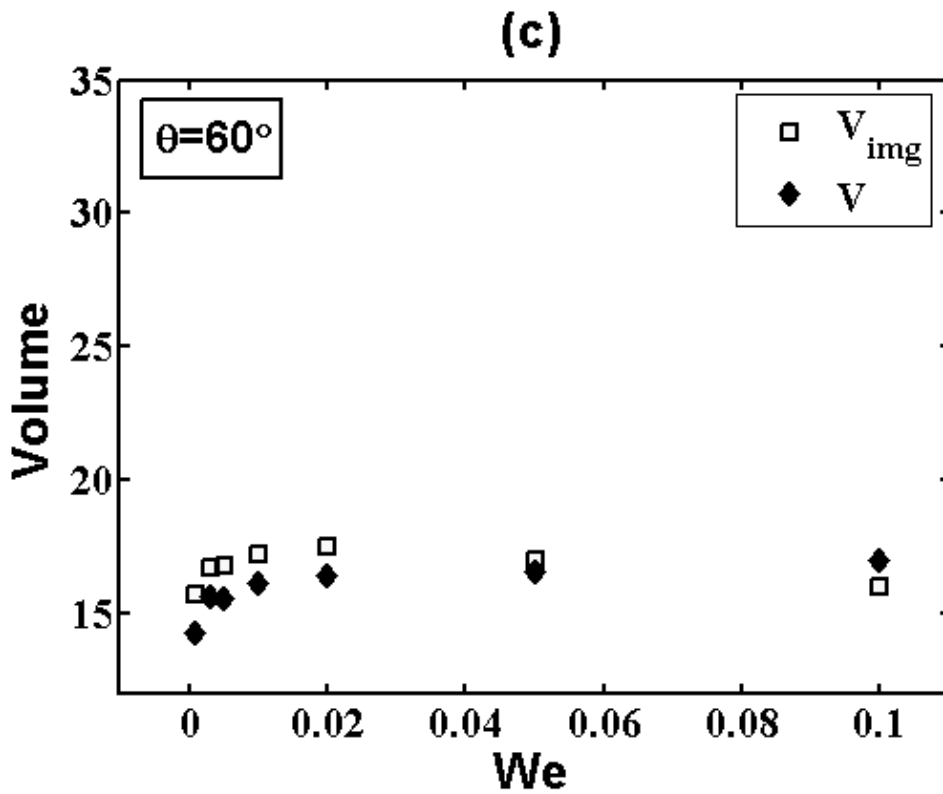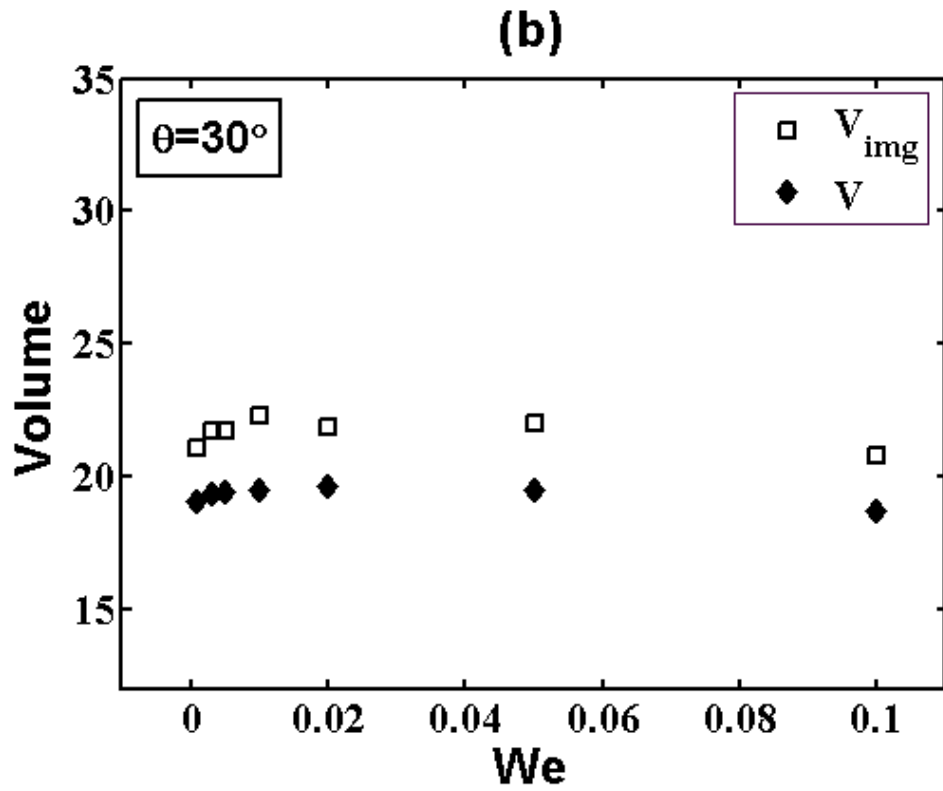
Figure 4.18 Predicted volume V and image analysis volume V_{img} change with *We* in P1 regime for $\theta=0°$ (a), $\theta=30°$ (b), $\theta=60°$ (c).The experiments were performed at *G*=0.057 and *Ka*=0.000562.

The plots given in this subsection compares the average volumes in P1 regime for experiments and predictions. As the P1 regime represents the mode of dripping where the drop breakup time are within 10% of its average value, comparison of average values of volume for experiments and prediction may not have much error in the measurements. For LC and C mode of dripping, the breakup times are always more than 10% of its average value, so we cannot simply take average of volumes and compare it. It is very important to know the volume of every single drop in LC and C regime and how it changes with the drop breakup time t_b. In next subsection, the volumes of every single drop measured by image analysis method are plotted with drop number for all three modes of dripping. On the same plot, the breakup time t_b with drop number is overlapped, so that we can compare the change in volume and t_b, with drop number.

4.5.2 Comparison of breakup time and drop volume with drop number

Although the nature of drop formation process is qualitatively similar from one situation to the next, as shown by the experimental observations made on drop elongation and breakup by Zhang and Basaran (Zhang and Basaran, 1995), drop breakup volume vary considerably with the various parameters. Large breakup time t_b indicates that, the drop is taking long time to break. In that case the primary drop volume should have increased. Similarly the primary drop volume should have decreased if the t_b values are small. The variation of the drop breakup time t_b and drop breakup volume V_{img} with the drop number is qualitatively expected to be similar. In contradiction to the above statements, the drop breakup time t_b and drop breakup volume V_{img} does not always show similar variation with the drop number is shown in the paragraph below.

Figure 4.19 (a-f) represents the t_b vs drop number (in subplot-1) and V_{img}, vs drop number (in subplot-2) for P1 regime for a vertical nozzle. For P1 regime the drop breakup time t_b and drop breakup volume V_{img} plots do not accord well with each other. Also another interesting feature is that the spread in drop volume V_{img} is always smaller ($\leq$ 5% of average) than the spread in t_b ($\leq$ 10% of average) values.
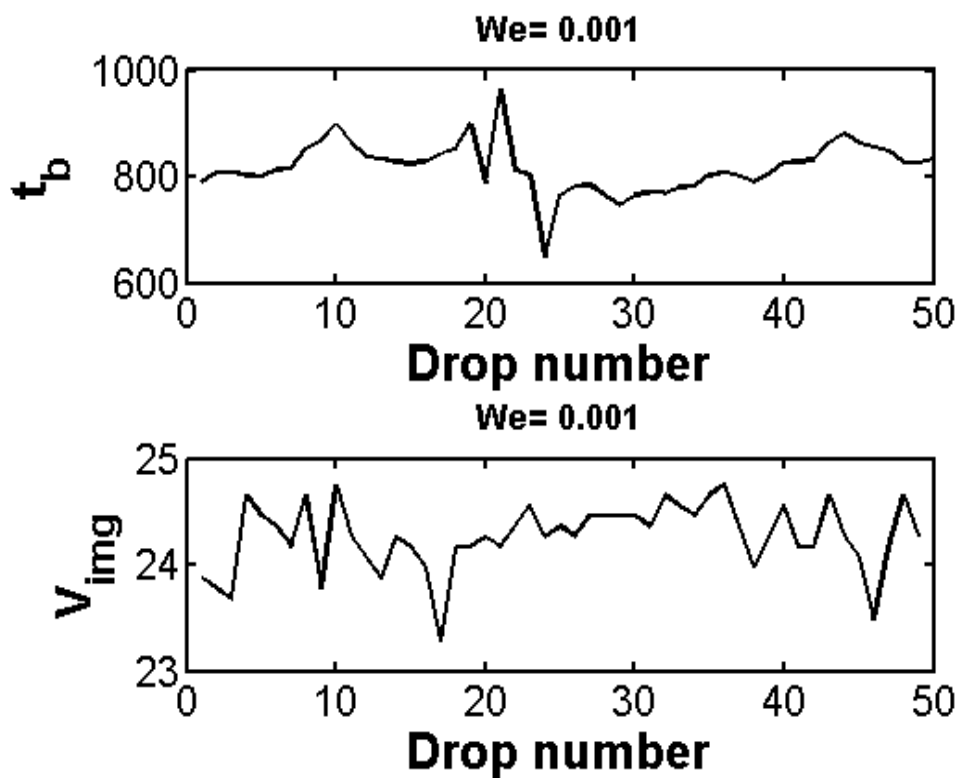
Figure 4.19 a Comparison of drop breakup time t_b and volume V_{img} with drop number for P1 mode. Here G=0.057, Ka=0.000562, and θ=0˚.
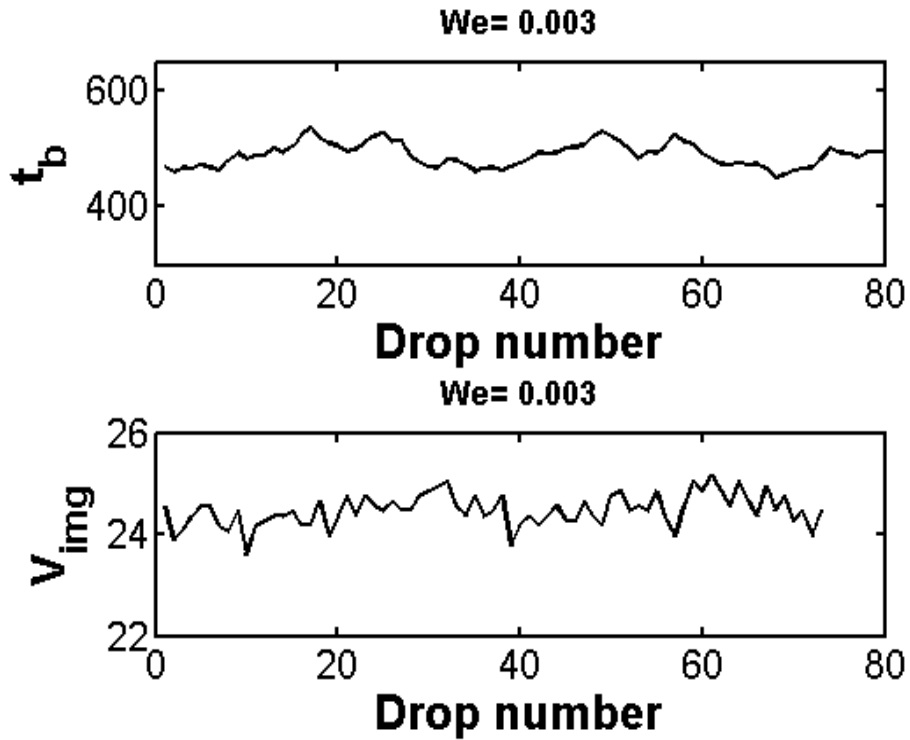
Figure 4.19 b Comparison of drop breakup time t_b and volume V_{img} change with drop number for P1 mode. Here $G=0.057$, $Ka=0.000562$, and $\theta=0°$.
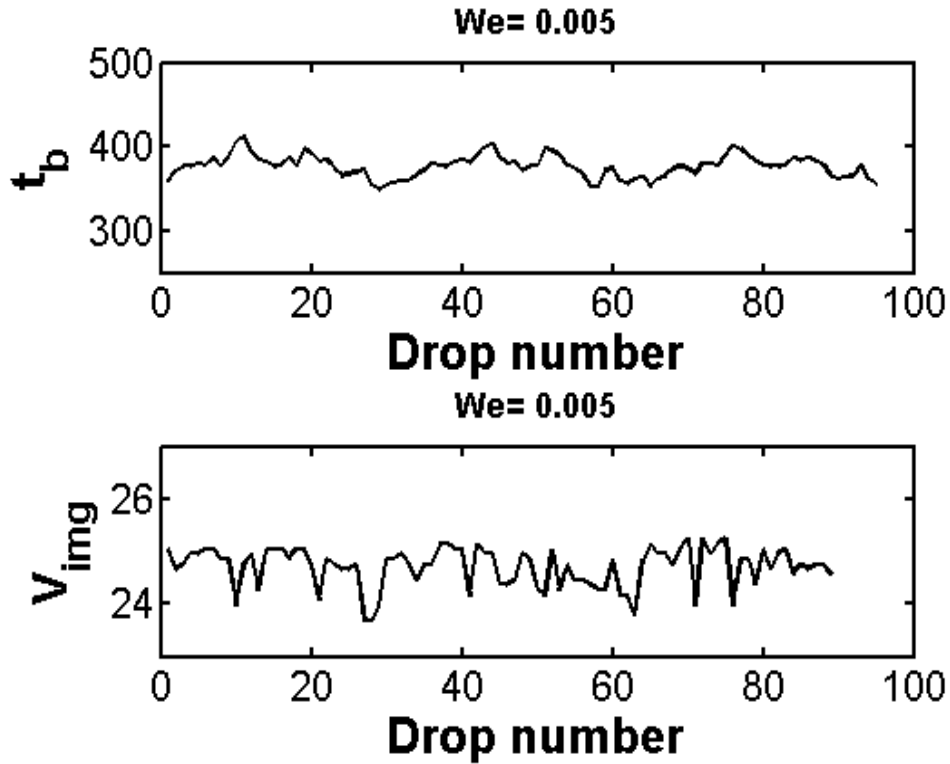
Figure 4.19 c Comparison of drop breakup time t_b and volume V_{img} with drop number for P1 mode. Here $G=0.057$, $Ka=0.000562$, and $\theta=0°$.
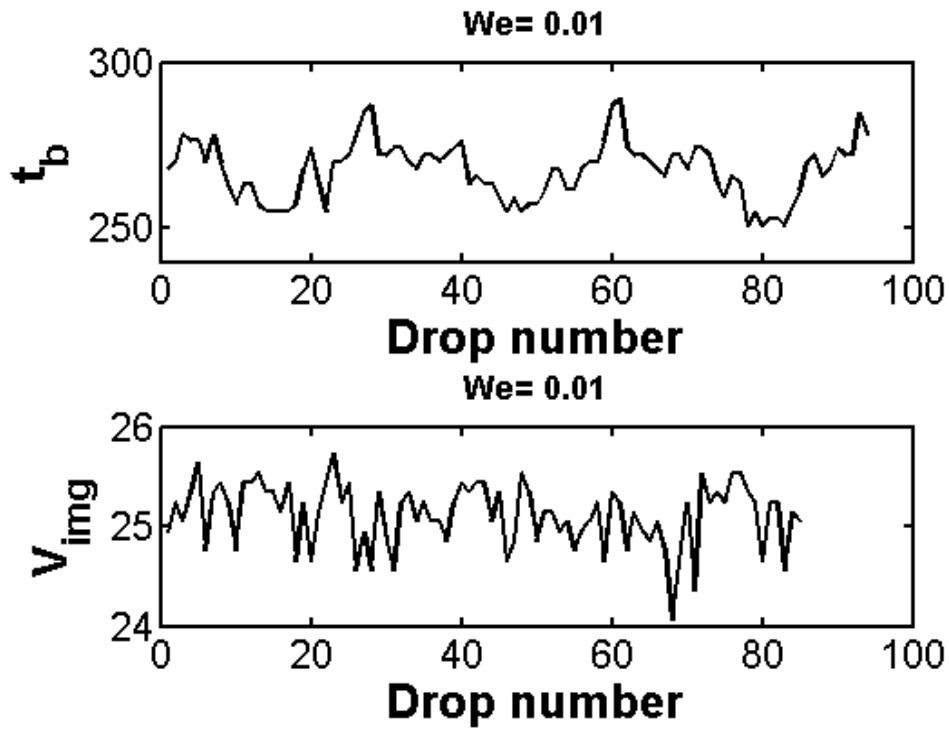
Figure 4.19 d Comparison of drop breakup time t_b and volume V_{img} with drop number for P1 mode. Here G=0.057, Ka=0.000562, and θ=0°.
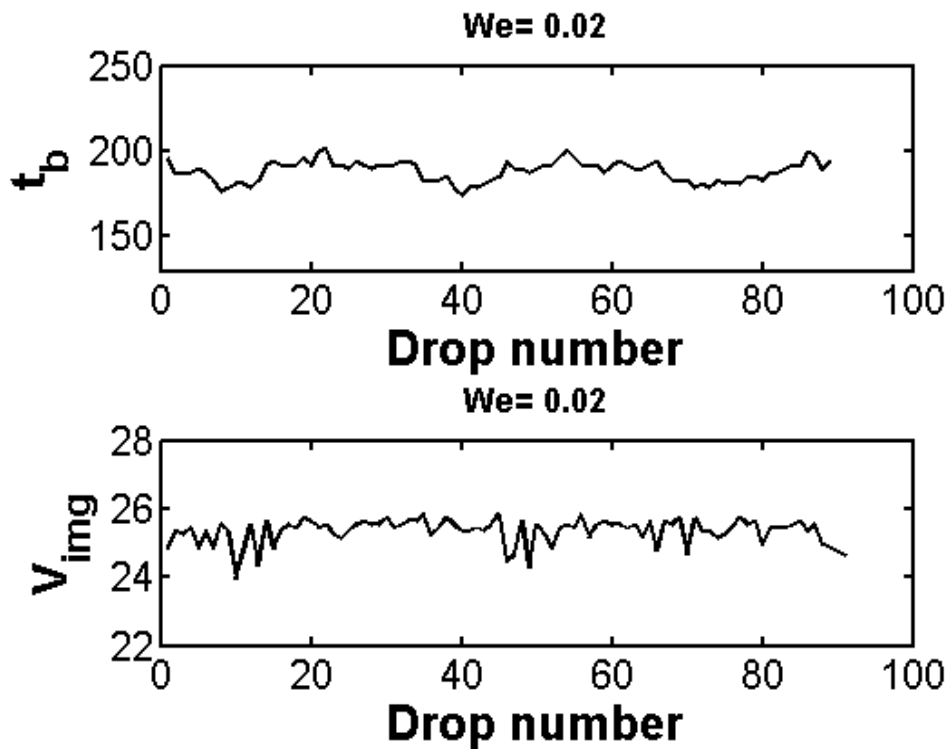
Figure 4.19 e Comparison of drop breakup time t_b and volume V_{img} change with drop number for P1 mode. Here G=0.057, Ka=0.000562, and θ=0°.
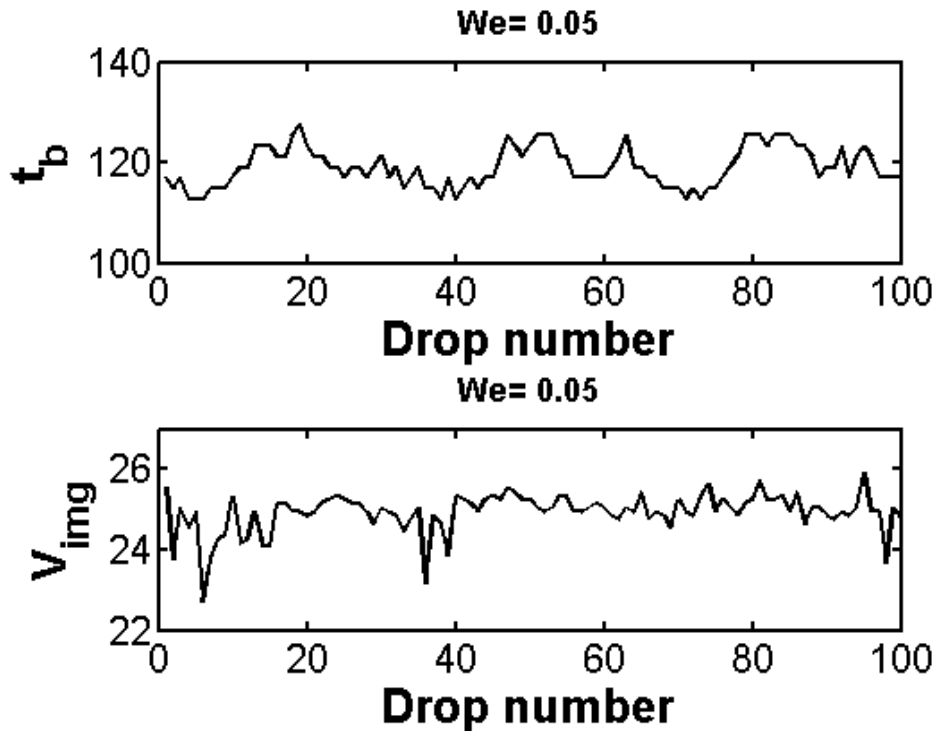
Figure 4.19 f Comparison of drop breakup time t_b and volume V_{img} with drop number for P1 mode. Here $G=0.057$, $Ka=0.000562$, and $\theta=0°$.

For moderate *We*, the similar plots are shown for LC regime as represented by figure 4.20 (a-c). In the LC regime, the drop breakup time t_b and drop breakup volume V_{img} change with drop number visually look in good agreement. This trend is further examined at the end of this section. In LC regime also, the spread for volume V_{img} change is small ($\leq10\%$of average) compared to spread in t_b values ($\geq10\%$of average) for lower *We* values. As We increases within the LC regime the spread in both V_{img} and t_b values is $\geq10\%$ of average.
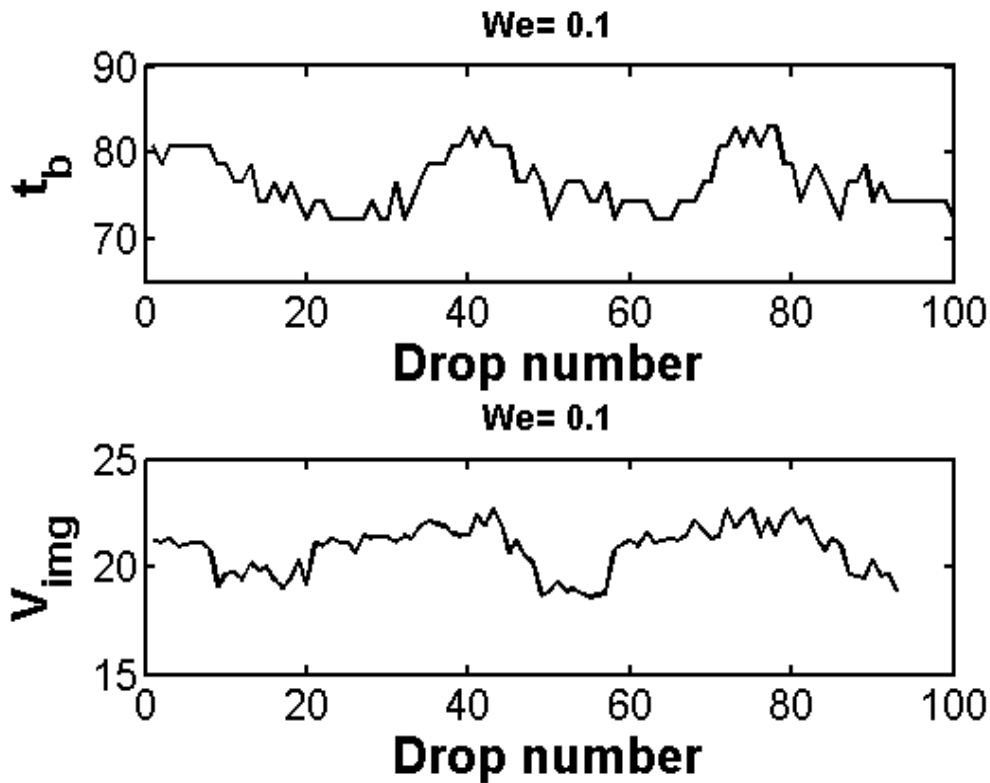
Figure 4.20 a Comparison of drop breakup time t_b and volume V_{img} with drop number for LC mode. Here G=0.057, Ka=0.000562, and θ=0˚.
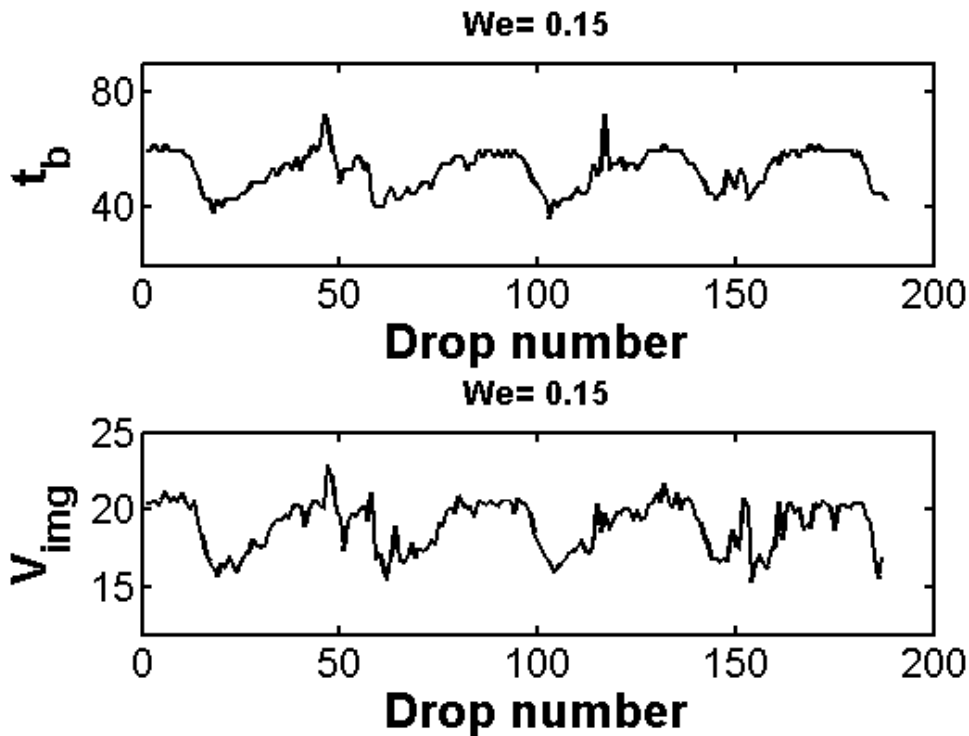
Figure 4.20 b Comparison of drop breakup time t_b and volume V_{img} with drop number for LC mode. Here G=0.057, Ka=0.000562, and θ=0˚.
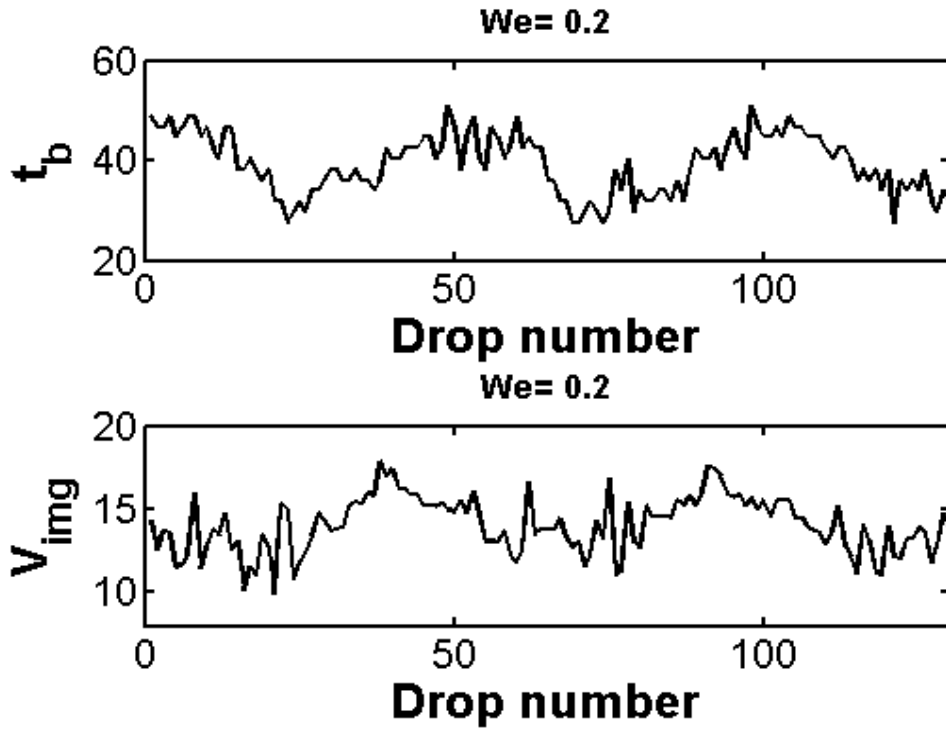
Figure 4.20 c Comparison of drop breakup time t_b and volume V_{img} with drop number for LC mode. Here G=0.057, Ka=0.000562, and θ=0˚.

Further increasing the *We* gives the chaotic regime of dripping, for which the similar plots are shown in figure 4.21. There is good agreement between the variation of drop breakup time t_b and drop breakup volume V_{img} with drop number except at a few points in the chaotic mode of dripping.
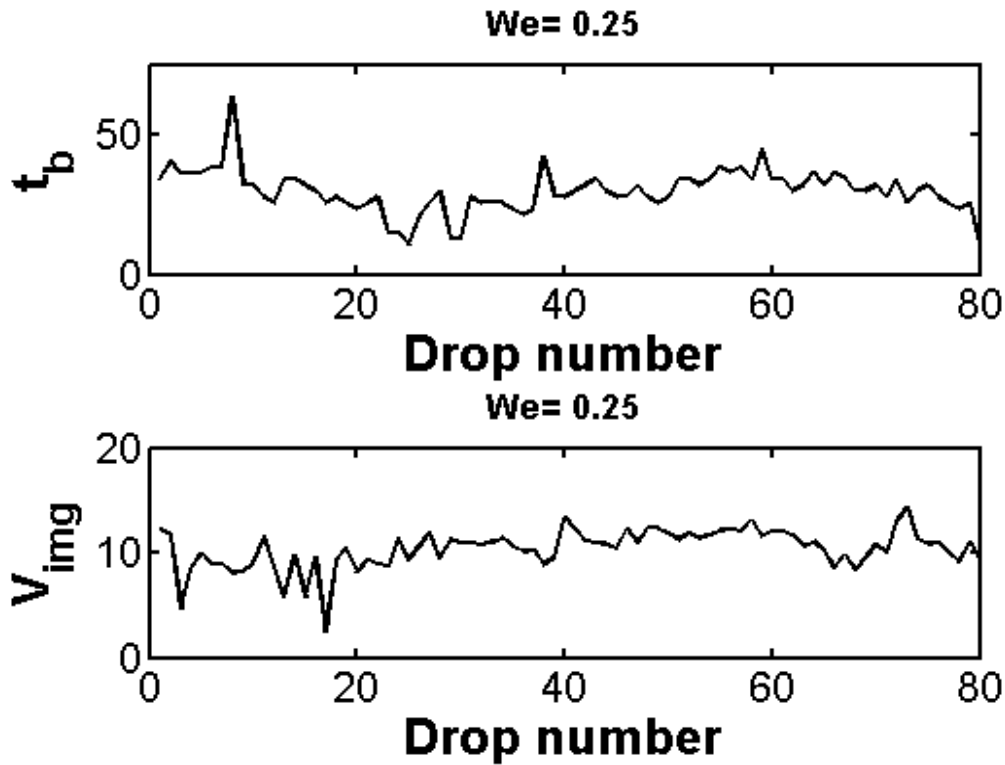
Figure 4. 21 Comparison of drop breakup time t_b and volume V_{img} with drop number for C mode. Here G=0.057, Ka=0.000562, and θ=0°.

Similar behaviour is noticed for θ=30° and θ=60° as shown in figure 4.22 (a-c) and figure 4.23 (a-c) respectively. This indicates that the observations made for comparison of volume and t_b are independent of nozzle inclination angle θ. Here only one sample figure for all three modes of dripping i.e. P1 (a), LC (b), and C (c) are shown in figure 4.22 and figure 4.23.

(a)

We= 0.05

We= 0.05

(b)

We= 0.15

We= 0.15

(c)

We= 0.25

We= 0.25
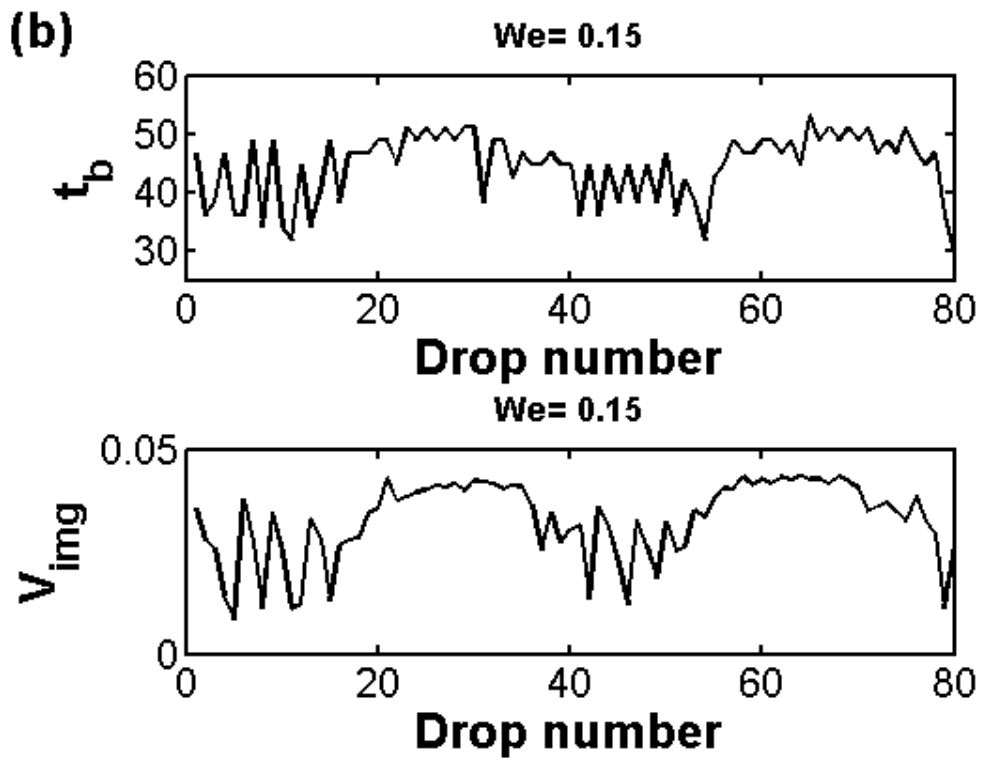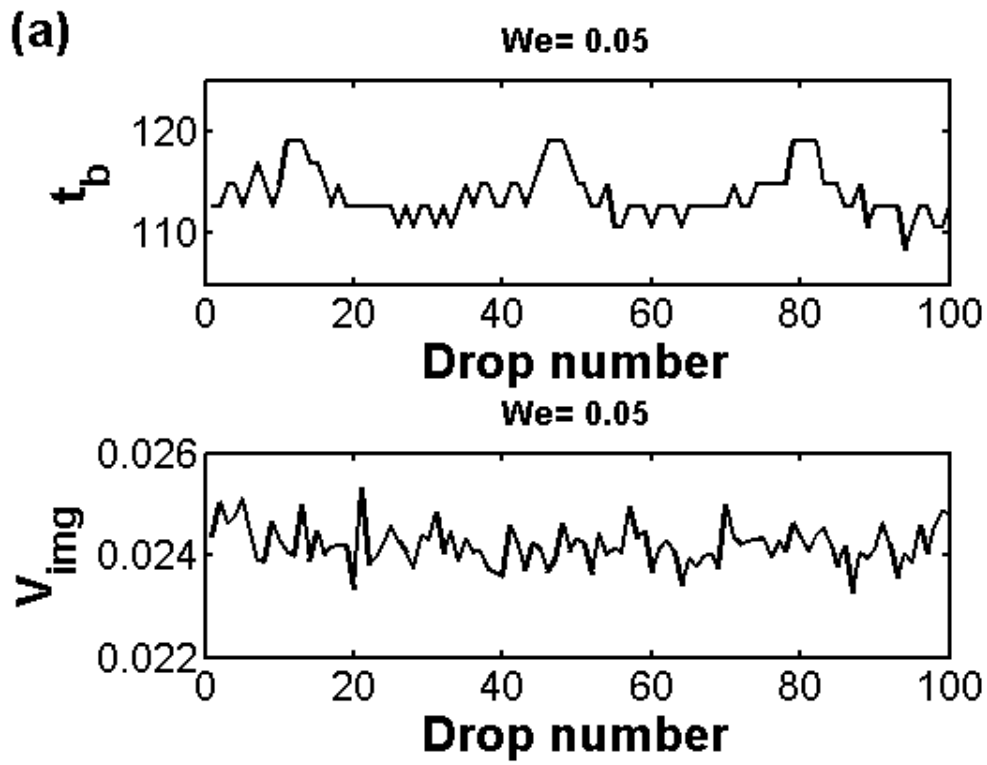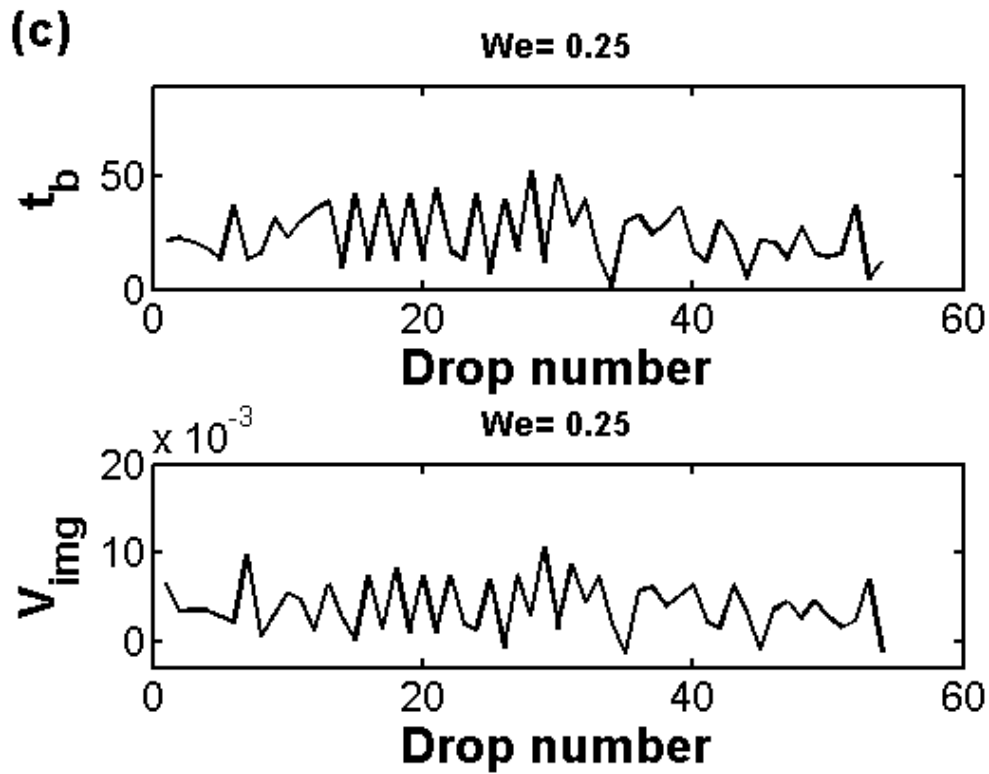
Figure 4.22 Comparison of drop breakup time t_b and volume V_{img} with drop number for P1 mode (a), LC mode (b), and C mode (c). Here G=0.057, Ka=0.000562, for θ=30˚.

(a)

We= 0.05

We= 0.05

(b)

We= 0.15

We= 0.15

(c)

We= 0.25

We= 0.25
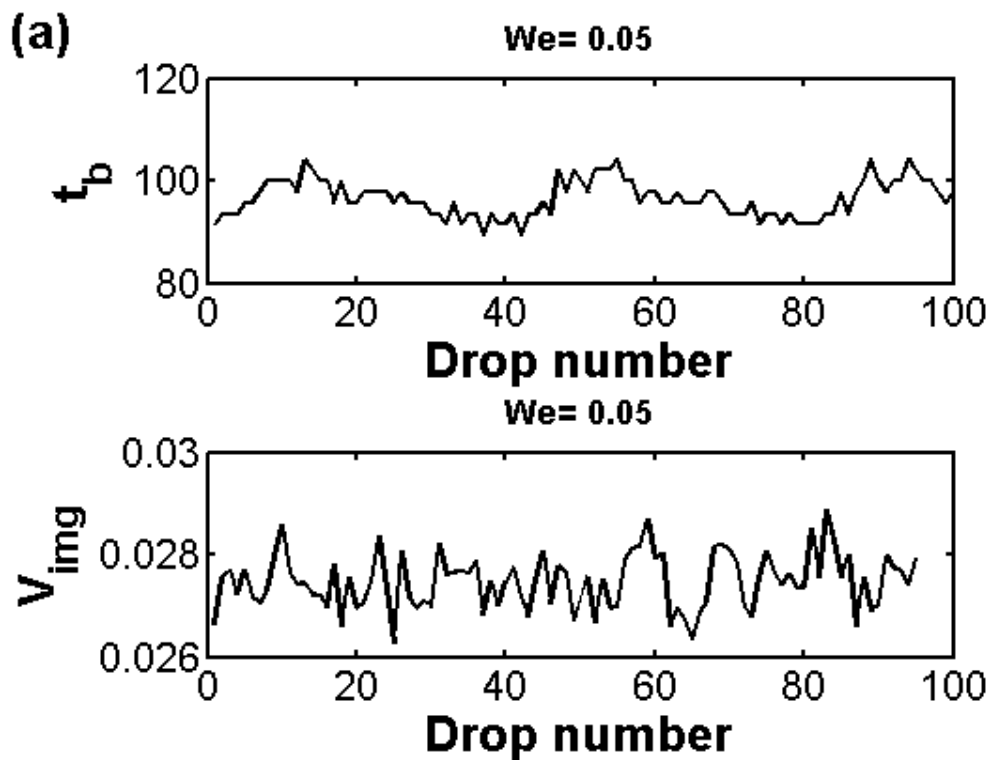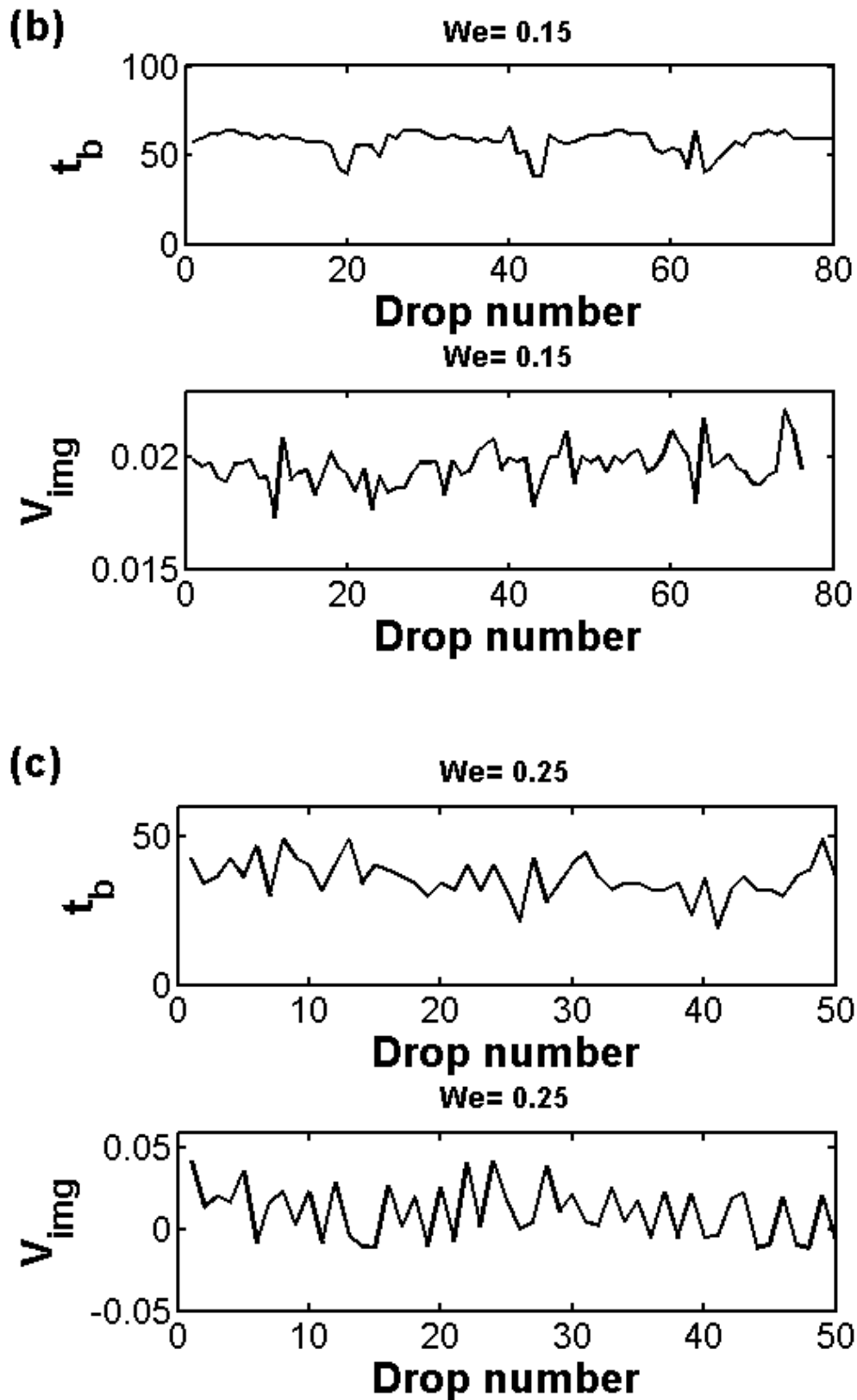
Figure 4.23 Comparison of drop breakup time t_b and volume V_{img} with drop number for P1 mode (a), LC mode (b), and C mode (c). Here G=0.057, Ka=0.000562, for θ=60°.
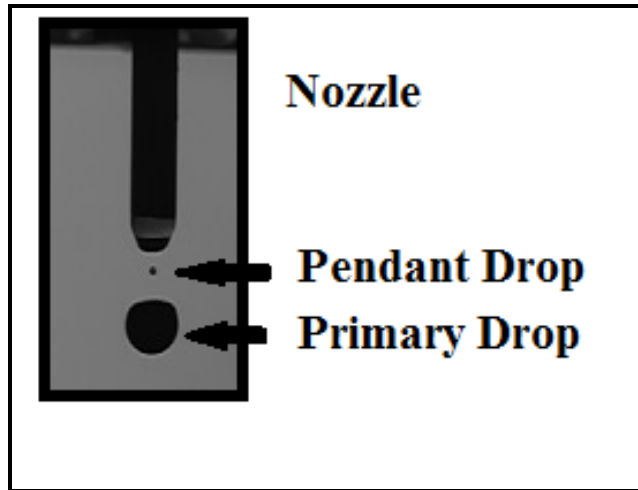
Figure 4.24 Comparison of pendant drop and primary drop volume

Table 4.2 Correlation function *f* values.

We	*F*		
	$\theta=0°$	$\theta=30°$	$\theta=60°$
0.001	-6.5×10^{-4}	-1.1×10^{-4}	-1.6×10^{-4}
0.003	-4.7×10^{-4}	-8.5×10^{-4}	-2.8×10^{-4}
0.005	-5.8×10^{-4}	-5.0×10^{-4}	-8.4×10^{-4}
0.01	-2.3×10^{-4}	-6.8×10^{-4}	-1.9×10^{-3}
0.02	-3.9×10^{-4}	-2.9×10^{-4}	-6.3×10^{-3}
0.05	-6.7×10^{-4}	-5.5×10^{-4}	-5.7×10^{-2}
0.1	3.5×10^{-3}	6.0×10^{-3}	6.4×10^{-3}
0.15	1.2×10^{-2}	4.8×10^{-3}	6.1×10^{-3}
0.2	1.6×10^{-2}	4.9×10^{-2}	2.6×10^{-3}
0.25	1.8×10^{-2}	3.6×10^{-2}	1.7×10^{-3}

These figures for all nozzle inclination angles clearly show that the trend of volume in the dripping experiments is not in synchrony with the drop breakup time for P1 mode of dripping. This difference in the P1 mode indicates that the pendant drop does not have the same volume every time the primary drop detaches from it. It is challenging to obtain

experimental evidence for this hypothesis, because the pendant drop is very small compared to the main drop as shown in figure 4.24, and a difference in one pixel alone can add major error to the volume measurement. To quantify the observed trends between the volumes and breakup times for LC and C modes of dripping, a cross correlation function f , similar to the evaluation of Reynolds stress in turbulence, is defined as (Pope, 2000),

$$f = \overline{\alpha\beta} \tag{4.4}$$

Where $\alpha = t_b\text{-}t_{avg}$ is breakup time fluctuation and $\beta = V\text{-}V_{avg}$ is breakup volume fluctuation, where t_{avg} and V_{avg} are average breakup time and average breakup volume respectively. Here both α and β are normalized against mean breakup time and mean breakup volume respectively. Function f is a averaged value over total experimental time. A positive value of f indicates that the breakup time and breakup volume are moving in the same direction with time and a negative value indicates that they are moving in opposite directions. The negative but very small value of f indicates that they are not very well correlated, and if any, their trend is in opposite direction. Zero value of function f simply indicates that the breakup time and breakup volume does not move in synchrony. Table 4.2 gives the values of f for different values of We and θ. The small negative values at low We indicates that the correlation is much weaker in P1 mode of dripping compared to high values of We, nearly 100 times smaller than those in the LC and C modes of dripping. These cross correlation function f values clearly support the visual observations made on plots for comparison of breakup time and breakup volume with drop number.

Aside from this, the spread in the volume is small for low We in P1 and LC mode of dripping. If the spread in the volume is less compared to the spread in t_b values for same

experimental data, the LC modes of dripping can be counted as P1 modes of dripping if the volume spread is below 10% of its average. So the modes of dripping based on t_b values will have slightly different phase diagrams than that based on drop volume spread. So this finding opens an option to define modes of dripping on the basis of volume change in the dripping experiments. In our experiments, the modes of dripping are decided on the basis of t_b values as the error in t_b measurements are much smaller than the error in volume calculations.

5 Conclusion

This is the first systematic exploration of the phase diagram for dripping from an inclined nozzle. According to the experimental results, the global dripping behaviour from an inclined nozzle is qualitatively similar to that from a vertical nozzle, where at low values of *We* and *Ka* the system shows a transition from P1 to LC before C occurs. The phase diagram is however modified in which an increase in the angle of inclination θ results in narrowing of the LC regime and giving an extended P1 region. This finding has implications to applications involving droplet formation, for example, the dripping modes for a desired operation can be obtained by changing the nozzle inclination instead of its size.

This study also uncovers an unexpected behaviour that increasing the nozzle inclination shortens the drop breakup time in the P1 mode regardless of the values of *G*, *Ka*, and *We*. It highlights the significant role of asymmetry due to nozzle inclination in weakening the surface tension forces to resist gravity. This was further supported by both experiments and computations which showed that the maximum volume of a stable pendant drop decreases noticeably with θ.

The predicted average volumes of the primary drops are compared with the average volumes obtained from image analysis and found within 15%. Further the volume change of primary drops is visually in good agreement with the breakup time change for LC and C mode of dripping, but they do not agree in P1 mode of dripping, suggesting that the

pendant drop has different volume for every drop breakup. The spread of volume is always smaller compared to the spread of the breakup time in P1 mode dripping.

Further, it was found that the drop volume in the P1 mode is reasonably independent of the flow rate. This has potential ramifications in applications, as the same drop size could be produced at a greater rate. This finding was summarized in a correlation accurate to within 10% for the dimensionless breakup volume V over wide ranges of G, Ka and θ.

Future efforts could be directed to uncover the underlying reasons such as why pendant drop volume changes for every drop for low We.

References

Ambravaneswaran, B., Phillips, S. D., & Basaran, O. A. (2000). Theoretical analysis of a dripping faucet. *Physical review letters, 85*(25), 5332.

Ambravaneswaran, B., Subramani, H. J., Phillips, S. D., & Basaran, O. A. (2004). Dripping-jetting transitions in a dripping faucet. *Physical review letters, 93*(3), 034501.

Basaran, O. A. (2002). Small scale free surface flows with breakup: Drop formation and emerging applications. *AIChE Journal, 48*(9), 1842-1848.

Bloomfield, P., *Fourier analysis of time series: an introduction*. 2004: John Wiley & Sons.

Clasen, C., Bico, J., Entov, V., & McKinley, G. (2009). 'Gobbling drops': The jetting-dripping transition in flows of polymer solutions. *Journal of Fluid Mechanics, 636*, 5.

Clasen, C., Phillips, P. M., & Palangetic, L. (2011). Dispensing of rheologically complex fluids: The map of misery. *AIChE Journal, 58*(10), 3242-3255.

Cooper-White, J., Fagan, J., Tirtaatmadja, V., Lester, D., & Boger, D. (2002). Drop formation dynamics of constant low-viscosity, elastic fluids. *Journal of non-newtonian fluid mechanics, 106*(1), 29-59.

D'Innocenzo, A., Paladini, F., & Renna, L. (2004). Effects of geometrical parameters on dripping from cylindrical nozzles. *Physica A: Statistical Mechanics and its Applications, 338*(1), 272-276.

D'Innocenzo, A., & Renna, L. (1996). Dripping faucet. *International Journal of Theoretical Physics, 35*(5), 941-973.

D'Innocenzo, A., Paladini, F., & Renna, L. (2002). Experimental study of dripping dynamics. *Physical Review E, 65*(5), 056208.

D'Innocenzo, A., Paladini, F., & Renna, L. (2004). Asymmetrical dripping. *Physical Review E, 69*(4), 046204.

Dravid, V. (2006). *Drop formation in newtonian and non-newtonian liquid jets*: ProQuest.

Eggers, J. (1997). Nonlinear dynamics and breakup of free-surface flows. *Reviews of modern physics, 69*(3), 865.

Eggers, J. (2006). A brief history of drop formation *Nonsmooth mechanics and analysis* (pp. 163-172): Springer.

Eggers, J., & Dupont, T. F. (1994). Drop formation in a one-dimensional approximation of the navier–stokes equation. *Journal of fluid mechanics, 262*, 205-221.

Freitas, S., Merkle, H. P., & Gander, B. (2005). Microencapsulation by solvent extraction/evaporation: Reviewing the state of the art of microsphere preparation process technology. *Journal of Controlled Release, 102*(2), 313-332.

Furbank, R. J., & Morris, J. F. (2004). An experimental study of particle effects on drop formation. *Physics of fluids, 16*, 1777.

German, G., & Bertola, V. (2010). Formation of viscoplastic drops by capillary breakup. *Physics of fluids, 22*(3), 033101-033101-033111.

Goedde, E., & Yuen, M. (1970). Experiments on liquid jet instability. *Journal of Fluid Mechanics, 40*(03), 495-511.

Guthrie, F. (1863). On drops. *Proceedings of the Royal Society of London, 13*, 444-457.

Haenlein, A. (1931, as cited by reference 6.). Disintegration of a liquid jet. *N.A.C.A. Technical Memorandum No 659*.

Image J software download site from softonic.com, retrieved on 10 August 2012 from http://imagej.en.softonic.com/.

Kippax, P., & Fracassi (2003), J. Particle size characterisation in nasal sprays and aerosols.

Lake, J. R. (1977). The effect of drop size and velocity on the performance of agricultural sprays. *Pesticide Science, 8*(5), 515-520.

Laurell, T., Nilsson, J., & Marko-Varga, G. (2001). Silicon microstructures for high-speed and high-sensitivity protein identifications. *Journal of Chromatography B: Biomedical Sciences and Applications, 752*(2), 217-232.

Le, H. P. (1998). Progress and trends in ink-jet printing technology. *Journal of Imaging Science and Technology, 42*(1), 49-62.

Lenard, P. (1887). *Ann. Phys. Chem., 30*, 209, as cited by reference 219.

Li, H., & Sundararaj, U. (2008). Does drop size affect the mechanism of viscoelastic drop breakup? *Physics of fluids, 20*, 053101.

Liu, Q., & Orme, M. (2001). High precision solder droplet printing technology and the state-of-the-art. *Journal of materials processing technology, 115*(3), 271-283.

Martien, P., Pope, S., Scott, P., & Shaw, R. (1985). The chaotic behavior of the leaky faucet. *Physics Letters A, 110*(7), 399-404.

MATLAB code for Lomb Scargle method is obtained on 15 January 2013 from http://w3eos.whoi.edu/12.747/notes/lect07/l07s05.html.

McKinley, G. H., & Renardy, M. (2011). Wolfgang von ohnesorge. *Physics of Fluids (1994-present), 23*(12), 127101.

Pimbley, W., & Lee, H. (1977). Satellite droplet formation in a liquid jet. *IBM Journal of Research and Development, 21*(1), 21-30.

Plateau, J. (1843). *Acad. Sci. Bruxelles, 16*, 3, as cited by reference 6.

Plateau, J. (1849). *Acad. Sci. Bruxelles, 23*, 5, as cited by reference 19.

Pope, S. B. (2000). *Turbulent flows*: Cambridge university press.

Rayleigh, L. (1879). On the capillary phenomena of jets. *Proceedings of the Royal Society of London, 29*(196-199), 71-97.

Rayleigh, L., & Strutt, J. W. (1879). On the instability of jets. *Proceedings of the Royal Mathematical Society London*, 4-13.

Reyes, M., Pinto, R., Tufaile, A., & Sartorelli, J. (2002). Heteroclinic behavior in a dripping faucet experiment. *Physics Letters A, 300*(2), 192-198.

Ruf, T. (1999). The lomb-scargle periodogram in biological rhythm research: Analysis of incomplete and unequally spaced time-series. *Biological Rhythm Research, 30*(2), 178-201.

Rutland, D., & Jameson, G. (1971). A nonlinear effect in the capillary instability of liquid jets. *J. Fluid Mech, 46*(2), 267-271.

Sachs, E. M., Haggerty, J. S., Cima, M. J., & Williams, P. A. (1994). Three-dimensional printing techniques: US Patent 5,340,656.

Savart, F. (1833). *Ann. Chim. Phys, 53*(337), 1833, as cited by reference 1836.

Scheele, G. F., & Meister, B. J. (1968). Drop formation at low velocities in liquid- liquid systems: Part i. Prediction of drop volume. *AIChE Journal, 14*(1), 9-15.

SE-FIT software, retrived on 10 July 2013 from http://se-fit.com/downloads.

Shaw, R. (1984). The dripping faucet as a model chaotic system.

Shi, X., Brenner, M. P., & Nagel, S. R. (1994). A cascade of structure in a drop falling from a faucet. *Science-New York then Washington* 219-219.

Subramani, H. J., Yeoh, H. K., Suryo, R., Xu, Q., Ambravaneswaran, B., & Basaran, O. A. (2006). Simplicity and complexity in a dripping faucet. *Physics of fluids, 18*, 032106.

Takahashi, T., & Kitamura, Y. (1969). Effect of nozzle length on breakup length of liquid jet. *Memoirs of the School of Engineering, Okayama University, 4*(1), 57-64.

Walstra, P. (1993). Principles of emulsion formation. *Chemical Engineering Science, 48*(2), 333-349.

Wilkes, E. D., Phillips, S. D., & Basaran, O. A. (1999). Computational and experimental analysis of dynamics of drop formation. *Physics of Fluids (1994-present), 11*(12), 3577-3598.

Worthington, A. M. (1881). On pendent drops. *Proceedings of the Royal Society of London, 32*(212-215), 362-377.

www.aciscience.org. (1967). Physical properties of glycerine and its solution

Yildirim, O. E., Xu, Q., & Basaran, O. A. (2005). Analysis of the drop weight method. *Physics of Fluids (1994-present), 17*(6), 062107.

Zhang, X., & Basaran, O. A. (1995). An experimental study of dynamics of drop formation. *Physics of fluids, 7*, 1184.

A.1 MATLAB code for t_b calculations

```matlab
function time_periodicity1(a,b,x,y,fps);

%a= starting image,  b=number of images to be analysed
% y= its a column on image which is at the center of the nozzle from which
% intensity measurements has to start
% x= subsequent rows starting from center of nozzle till droplet
%a=49; b=100;
%x=321; y=165;
somefile= 'G:\Work\Images\S1N1,30deg\We=0.2,S1N1,30deg\'; % maisource
%subname= 'view000'; % image name (incomplete)
%maximum=max(size(m));

while a<=b; % Takes images in sequence from given folder mentioned in
following two lines.

    if a<=9;
        subname= 'view0000'; % This is to read images by subname

    elseif (9<a)&& (a<100);
        subname= 'view000';
    elseif (99<a)&& (a<1000);
        subname= 'view00';
    elseif (999<a) && (a<10000);
        subname= 'view0';
    elseif (9999<a) && (a<100000);
        subname= 'view';
    end

    str= num2str(a);

    images= strcat(somefile,subname,str,'.tif'); %
C:\MATLAB701\work\snapshots\: is the path or directory for images. %
view00, str and .tif completes the name of image

    img= imread(images); % reads image in matlab


    img= rgb2gray(img); % converts image to gray scale
    level = graythresh(img);
    img= im2bw(img,level);

    A= size(img); % matlab reads image in matrix form so A is size of image
which is a matrix
    %whos %

    k=1; % Changing k does not make much difference
    j=x; % x axis
```

```matlab
    %count=0;
        i=y; % y axis
        val1 = img(i,j,k); % point on nozzle (dark intensity)
        val2 = img(i+10,j,k); % point in air (light intensity)
        val3 = img(i+30,j,k);  % point on a drop (dark intensity)

        if val1>val2;
            diff1= abs(val1-val2);
        else
            diff1= abs(val2-val1);
        end

        if val2>val3;
            diff2= abs(val2-val3);
        else
            diff2= abs(val3-val2);
        end


    while diff1 >.50 && diff2>.50 ; % the threashold value can vary

        imnumb=a;
        strtimg1(a)=imnumb-1;
        strtimg1(strtimg1==0)=[];

        g= [strtimg1];

            for m = 2:length(g);
                num(m)= abs((g(m)-g(m-1)));
                time(m)= num(m)/fps
                dlmwrite('C:\MATLAB701\work\strtimg1.m',strtimg1);
                dlmwrite('C:\MATLAB701\work\time.m',time);
                strtimg1
            end
            a=a+5;
            break
    end


    a=a+1;
end

end
```

A.2 MATLAB code for breakup volume calculations

```matlab
function Volume_simpsons_v14
clear all;


    [strtimg]=[6,13,19,20,29,35,43,48,54,60,65,72,80,95,100,106,113,116,1
    22,129,135,141,143,147,153,156,160,164,174,181,185,187,189,193,196,20
    3,209,212,217,220,224,228,230,232,236,238,243,248];% list outs the
    drop break up image for angle 1
  for imn=1:length(strtimg);

     for h=1:2;


    [r1,r2,strty1,endy1,kk,rng]=Volume_simpsons_v13(180,240,151,300,imn,s
    trtimg,h);%Calling file Volume_simpsons_v13 which is given at the end
    of this code which give two different radius r1 and r2 as a output
    for the volume calculations. %r1 is the radius based on vertical half
    section of a asymmetric drop and r2 is for another half vertical
    section.


    strtimg1=[15,22,28,29,38,45,52,57,63,69,74,81,89,104,109,115,122,125,
    131,138,144,150,152,156,162,165,169,173,183,190,194,196,198,202,205,2
    12,218,221,226,229,233,237,239,241,245,247,252,257];
    % list outs the drop break up image for angle 1


    [r11,r22,strty11,endy11]=Volume_simpsons_v12(180,240,151,300,kk,h,imn
    ,strtimg1);%Calling file Volume_simpsons_v12 which is given at the
    end of this code which give two different radius r11 and r22 as a
    output for the volume calculations.%r11 is the radius based on
    verticle half section of a asymmetric drop and r22 is for another
    half verticle section.


       p=length(rng);
       z=mod(p,2);

         if z==0 % Use of Simpsons 1/3 rd rule


         vol1(imn)=(pi*h/3).*((r1(strty1).*r11(strty11))+(r1(endy1).*r11
         (endy11))+(4*sum(r1(strty1+h:2*h:endy1-
         h).*r11(strty11+h:2*h:endy11-
         h)))+(2*sum(r1(strty1+2*h:2*h:endy1-
         2*h).*r11(strty11+2*h:2*h:endy11-2*h))));% volume based on r1
         and r2


         vol2(imn)=(pi*h/3).*((r2(strty1).*r22(strty11))+(r2(endy1).*r22
         (endy11))+(4*sum(r2(strty1+h:2*h:endy1-
         h).*r22(strty11+h:2*h:endy11-
```

```matlab
            h)))+(2*sum(r2(strty1+2*h:2*h:endy1-
            2*h).*r22(strty11+2*h:2*h:endy11-2*h)))));% volume based on r11
            and r22

        else


            vol1(imn)=((pi*h/3).*((r1(strty1).*(r11(strty11))+(r1(endy1-
            4*h).*r11(endy11-4*h))+(4*sum(r1(strty1+1*h:2*h:endy1-
            5*h).*r11(strty11+1*h:2*h:endy11-
            5*h)))+(2*sum(r1(strty1+2*h:2*h:endy1-
            6*h).*r11(strty11+2*h:2*h:endy11-
            6*h)))))+(((pi*3*h)/8).*((r1(endy1-3*h).*r11(endy11-
            3*h))+(r1(endy1).*r11(endy11))+(3*r1(endy1-2*h).*r11(endy11-
            2*h))+(3*r1(endy1-1*h).*r11(endy11-1*h)))));

            vol2(imn)=((pi*h/3).*((r2(strty1).*(r22(strty11))+(r2(endy1-
            4*h).*r22(endy11-4*h))+(4*sum(r2(strty1+1*h:2*h:endy1-
            5*h).*r22(strty11+1*h:2*h:endy11-
            5*h)))+(2*sum(r2(strty1+2*h:2*h:endy1-
            6*h).*r22(strty11+2*h:2*h:endy11-
            6*h)))))+(((pi*3*h)/8).*((r2(endy1-3*h).*r22(endy11-
            3*h))+(r2(endy1).*r22(endy11))+(3*r2(endy1-2*h).*r22(endy11-
            2*h))+(3*r2(endy1-1*h).*r22(endy11-1*h)))));

        end
            avgvol(imn) = (vol1(imn)+vol2(imn))/2; %taking average of vol1
            and vol2

        if h<=1;
            dumvol1(imn)=avgvol(imn);
        else
            dumvol2(imn)=avgvol(imn);
        end
    end

    es(imn)=abs((dumvol1(imn)-dumvol2(imn))/15);

    truevol(imn)=(dumvol1(imn)+es(imn))*(5.694241982*10^-6)%this factor
    results from the pixel to ml calculations

    dlmwrite('C:\MATLAB701\work\vol.m',truevol);

    errorinpercent=((100*es)/truevol) ; % Gives error percent in the true
    volume calculations


end
end
```

Function which is being called in programme Volume simpsons v14 above

```matlab
function [r11,r22,strty11,endy11]=
Volume_simpsons_v12(strtx,endx,strty,endy,kk,h,imn,strtimg1);


% strtx:Starting point on x axix very near to nozzle end from where pixel
reading starts
% endx:end point on x axix in the air where pixel reading ends
% strty:Starting point on y axix in air from where pixel reading starts
% endy:end point on y axix in air from where pixel reading ends
% strty11:After detecting the drop, first pixel on y axis on actual drop
% endy11:After detecting the drop, last pixel on y axis on actual drop


somefile= 'H:\Final work\final\Images\Angle-60 deg\Nozzle-1\S1\Angle-
1\We=0.3,S1N1,60deg\';  %calling file


    if strtimg1(imn)<=9;
        subname= 'view0000';
    elseif (9<strtimg1(imn))&&(strtimg1(imn)<100);
        subname= 'view000';
    elseif (99<strtimg1(imn))&& (strtimg1(imn)<1000);
        subname= 'view00';
    elseif (999<strtimg1(imn))&& (strtimg1(imn)<10000);
        subname= 'view0';
    elseif (9999<strtimg1(imn))&& (strtimg1(imn)<100000);
        subname= 'view';
    end

    str= num2str(strtimg1(imn));
    images= strcat(somefile,subname,str,'.tif');
    img = imread(images);
    img= rgb2gray(img);
    level = graythresh(img);
    img= im2bw(img,level+0.1);


     hh=h;

        if hh<=1;
            rng=strty:endy;
        else
            rng= strty:2:endy;
        end

        rr= zeros(length(rng));
        r11= zeros(size(rng));
        r22= zeros(length(rng));
        kk1= 0;

        for i= rng;

            j1=0;j2=0;
            for j =strtx:endx;
                val1= img(i,j,1);
```

```matlab
            val2= img(i,j+1,1);

            if val1>val2;
                diff= abs(val1-val2);
            else
                diff= abs(val2-val1);
            end

            if val1>val2 && diff > .5;
                j1=j+1; % j+1 is the black pixel and j is white pixel
            elseif val2>val1 && diff > .5;
                j2=j;
            end

        end

        rr(i) = (j1 + j2)/2;
        if  rr(i)==0 && rr(i-h)>0
            endy1=i-h;
        break

        end

        dummyj2(i)= j2;
        dummyj1(i)= j1;
    end

        strty11=endy1-(kk)+1;
        kk1=kk ;
        endy11=endy1;


    for i= strty11:h:endy11;

        meanr= mean(rr(strty11:h:endy11));

        r11(i)= abs(meanr-dummyj1(i));
        r22(i)= abs(dummyj2(i)-meanr);

        if r11(i)<=0;
            r22(i)=abs(r11(i))+r22(i);
            r11(i)=0;
        elseif r22(i)<=0;
            r11(i)=abs(r22(i))+r11(i);
            r22(i)=0;

        end

    end
end
```

Function which is being called in programme Volume simpsons v14 above

```
function [r1,r2,strty1,endy1,kk,rng]= Volume_simpsons_v13
(strtx,endx,strty,endy,imn,strtimg,h);

% strtx:Starting point on x axix very near to nozzle end from where pixel
reading starts
% endx:end point on x axix in the air where pixel reading ends
% strty:Starting point on y axix in air from where pixel reading starts
% endy:end point on y axix in air from where pixel reading ends
% strty1:After detecting the drop, first pixel on y axis on actual drop
% endy1:After detecting the drop, last pixel on y axis on actual drop




somefile= 'H:\Final work\final\Images\Angle-60 deg\Nozzle-1\S1\Angle-
1\We=0.3,S1N1,60deg\'; %calling file

    strtimg(imn)

    if strtimg(imn)<=9;
        subname= 'view0000';
    elseif (9<strtimg(imn))&&(strtimg(imn)<100);
        subname= 'view000';
    elseif (99<strtimg(imn))&& (strtimg(imn)<1000);
        subname= 'view00';
    elseif (999<strtimg(imn))&& (strtimg(imn)<10000);
        subname= 'view0';
    elseif (9999<strtimg(imn))&& (strtimg(imn)<100000);
        subname= 'view';
    end

    str= num2str(strtimg(imn));
    images= strcat(somefile,subname,str,'.tif');
    img = imread(images);
    img= rgb2gray(img);
    level = graythresh(img);
    img= im2bw(img,level+0.1);


        if h<=1;
            rng=strty:endy;
        else
            rng= strty:2:endy;
        end
        meanr=zeros(length(rng));
        rr= zeros(length(rng));
        r1= zeros(length(rng));
        r2= zeros(length(rng));
        j1= zeros(length(rng));
        j2= zeros(length(rng));
        dummyj1= zeros(length(rng));
        dummyj2= zeros(length(rng));
        kk= 0;


        for i= rng;
```

```matlab
j1=0;j2=0;
for j =strtx:endx;
    val1= img(i,j,1);
    val2= img(i,j+1,1);

    if val1>val2;
        diff= abs(val1-val2);
    else
        diff= abs(val2-val1);
    end

    if val1>val2 && diff > .5;
        j1=j+1; % j+1 is the black pixel and j is white pixel
    elseif val2>val1 && diff > .5;
        j2=j;
    end

end

rr(i) = (j1 + j2)/2;
dummyj2(i)= j2;
dummyj1(i)= j1;

if  rr(i)==0 && rr(i-h)>0
    endy1=i-h;
    break

end
end

for i=strty:h:endy1;

    meanr= mean(rr(strty:h:endy1));

    rad1(i)= (meanr-dummyj1(i));
    rad2(i)= (dummyj2(i)-meanr);
    dia(i)=(rad1(i)+rad2(i))/2;

    if (dia(i-(4*h))>dia(i-(3*h))) && (dia(i-(3*h))>=(dia(i-
2*h)))&& (dia(i-(2*h))<=(dia(i-1*h))) &&(dia(i-1*h)<(dia(i)));
    strty1=i-2*h;
    break

    elseif(dia(i-(8*h))>dia(i-(7*h)))&&(dia(i-(7*h))>=dia(i-(6*h)))
&& (dia(i-(6*h))>=(dia(i-(5*h))) && (dia(i-(5*h))>=(dia(i-
4*h)))&& (dia(i-(4*h))<=(dia(i-3*h))) &&(dia(i-3*h)<=(dia(i-
2*h))) && (dia(i-(i-2*h))<=dia(i-1*h)) &&(dia(i-1*h)<(dia(i)));
    strty1=i-4*h;

    break

    elseif (dia(i-(6*h))>dia(i-(5*h))) && (dia(i-(5*h))>=(dia(i-
4*h)))&& (dia(i-(4*h))>=(dia(i-3*h))) &&(dia(i-3*h)<=(dia(i-
2*h))) && (dia(i-(i-2*h))<=dia(i-1*h)) &&(dia(i-1*h)<(dia(i)));
    strty1=i-3*h;

    break
```

```matlab
        elseif (dia(i-(3*h))>(dia(i-(2*h)))) &&(dia(i-2*h)<=(dia(i-
        1*h))) && (dia(i-1*h)<(dia(i)));
        strty1=i-1*h;
        break

        end

    end

    for i= strty1:h:endy1;
        r1(i)= (meanr-dummyj1(i));
        r2(i)= (dummyj2(i)-meanr);


    end
    kk=(endy1-strty1+1);
```

A.3 MATLAB code for FFT calculations

```matlab
clc
clear

% To use real data (y-axis in time domain)
data =[
];%copy the data of breakup time here

N = length(data);       % number of data points
t_tot= sum(data(:));    % total sampling time
fs   = N/t_tot;         % sampling frequency

% Create the time vector (x-axis in time domain)
t = zeros(N, 1);
t(1) = data(1);
     for i = 2:N
         t(i) = data(i) + t(i-1);
     end


% Watch out for the effects
%NFFT = 2^nextpow2(N);    % Next power of 2 from the length of data
NFFT = N;


Y = fft(data, NFFT);


% Both forms are equal:
%f = (fs/2)*linspace(0,1,NFFT/2+1);
f = (1:NFFT/2)*fs/NFFT;
mag=abs(Y(2:NFFT/2+1));
% Plot single-sided amplitude spectrum.
% First point of fft is excluded
figure(1)
plot(f, log(mag))
%title('Single-Sided Amplitude Spectrum of y(t)')
xlabel('Frequency (Hz)')
ylabel('Amplitude')
```

A.4 MATLAB code for Lomb Scargle periodogram calculations

```matlab
clc
clear

% Call the data file, remember to change the assignment of y below
drop_dataS1N1_breakuptime1_ang_0_oil;

% Select the desired data point from the Weber number vector
      for point =1:length(we_no);

      point
      % Assign the data and the Weber number
      y  = we_ang_0{point};
      We = we_no(point);
      d = we_ang_0{point};
      lny=length(y)
      N = length(y);        % number of data points
      t_tot = sum(d(:));    % total sampling time
      fs = N/t_tot;         % sampling frequency

      % Create the time vector (x-axis in time domain)
      t = cumsum(d);
      length(y)
      length(t)
      lnt=length(t)


      % Now do compute the Lomb normalized periodogram
      % first create a vector of frequency bins
      NFFT = N;
      f = (1:NFFT/2)*fs/NFFT;
      lnf=length(f)
      [Pn Prob] = lomb(t,y,f);



      % plot the periodogram, to also indicate the peaks
      figure(point)
      ylim([0 15]);
      %axis([0 1 0 80]);
      %b=horzcat('4,4,',num2str(point))
      subplot(1,1,1)
      h=plot(f,Pn,'k'); set(h,'LineWidth',2);

      % sort for smallest values first
      % (i.e. those points least likely to be random)

      [p,ind] = sort(Prob);
      pos = ind(1:last);
      ANS=[f(pos)' Pn(pos)' Prob(pos)'];

      fprintf('For We = %.3f,\n', We)
```

```
        display('The probably non-random frequencies:')
        display(' ')
        display('Frequency in Hz     PSD      Probability')
                for row = 1:last
                fprintf('  %.4f         %.4f        %.4f\n', ANS(row,:))
                end

    % show the top 3 peaks
            for j = 1:2
    text(f(pos(j)),         Pn(pos(j)),          sprintf('f         =        %.4f',
    f(pos(j))),'FontSize',16,'FontWeight','bold')
          end

    xlabel('Frequency                (Hz)','FontSize',18,'FontWeight','bold');
    ylabel('Normalized PSD','FontSize',18,'FontWeight','bold');
    title(sprintf('We= %g',we_no(point)),'FontSize',18,'FontWeight','bold');
    set(gca,'LineWidth',2,'FontSize',16);


    end
```

Function which is being called in of Lomb Scargle method above

```
%
%   [Pn, Prob] = lomb(t, y, freq)
%
%       Uses Lomb's method to compute normalized
%       periodogram values "Pn" as a function of
%       supplied vector of frequencies "freq" for
%       input vectors "t" (time) and "y" (observations).
%       Also returned is probability "Prob" of same
%       length as Pn (and freq) that the null hypothesis
%       is valid.
%       x and y must be the same length.

function [Pn, Prob] = lomb(t, y, f)

%       check inputs
        if length(t) ~= length(y); error('t and y not same length');
          exit;
        end;

        %   subtract mean, compute variance, initialize Pn
        z = y - mean(y);
        var = std(y);
        N=length(f);
        Pn=zeros(size(f));

        %   now do main loop for all frequencies
        for i=1:length(f)
            w=2*pi*f(i);
            if w > 0
                twt = 2*w*t;
                tau = atan2(sum(sin(twt)),sum(cos(twt)))/2/w;
```

114

```matlab
        wtmt = w*(t - tau);
        Pn(i) = (sum(z.*cos(wtmt)).^2)/sum(cos(wtmt).^2) + ...
           (sum(z.*sin(wtmt)).^2)/sum(sin(wtmt).^2);
      else
    Pn(i) = (sum(z.*t).^2)/sum(t.^2);
      end
end
%
%   and normalize by variance, compute probs
Pn=Pn/2/var.^2;
Prob = 1-(1-exp(-Pn)).^N;
for i=1:length(Pn)      % accomodate possible roundoff error
    if Prob(i) < .001
    Prob(i) = N*exp(-Pn(i));
    end

end
```
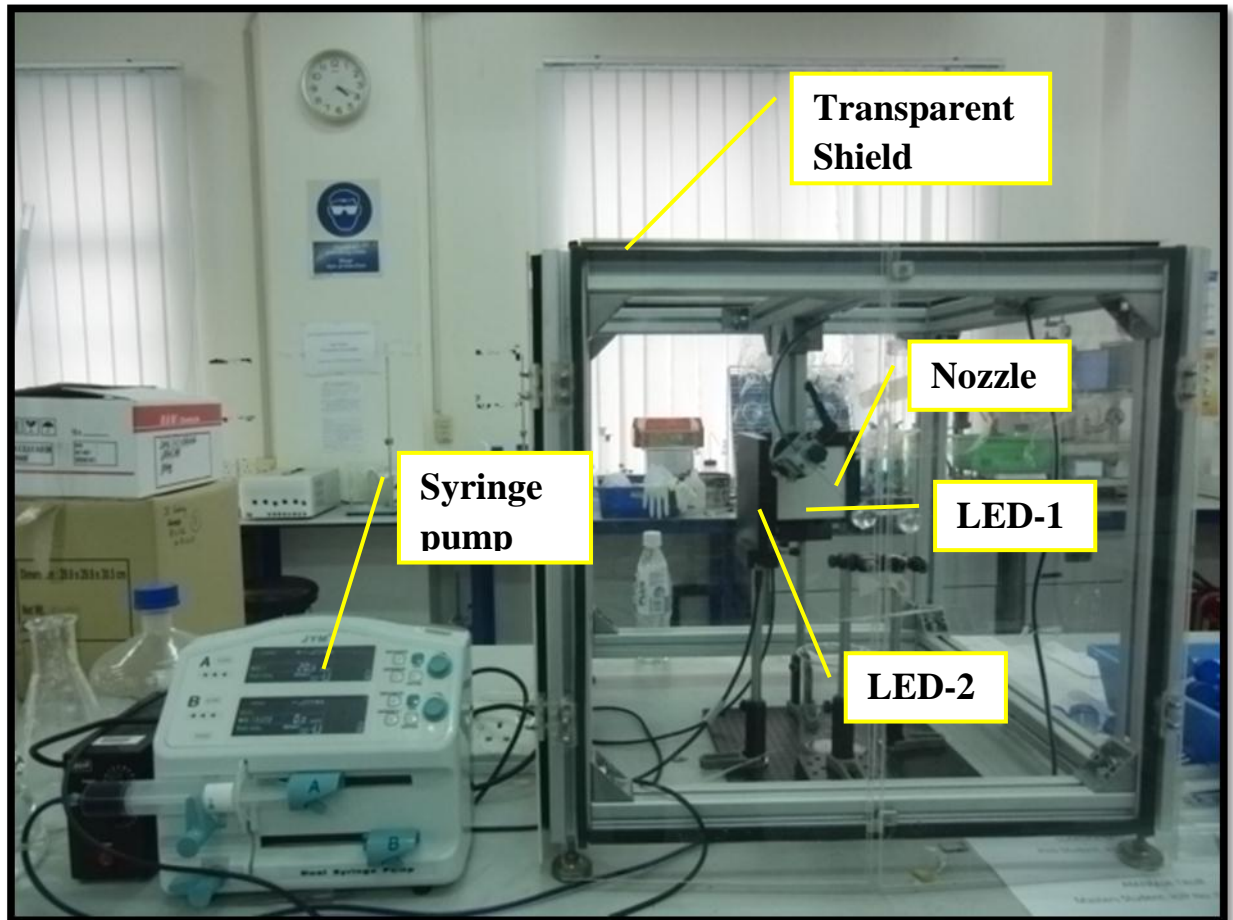
Appendix B- Experimental set-up images

Figure B.1 Experimental set-up photograph
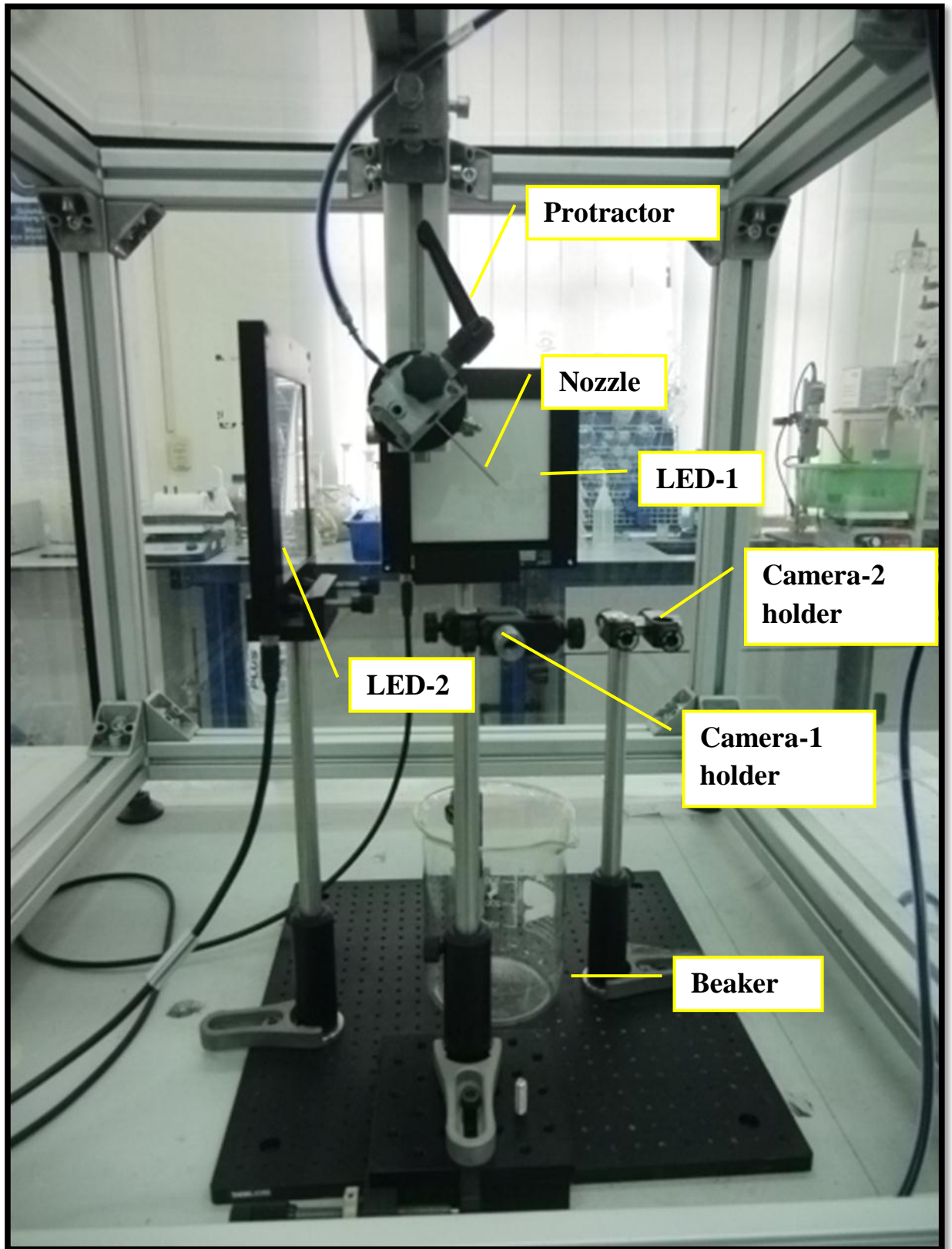
Figure B.2 Experimental set-up near nozzle
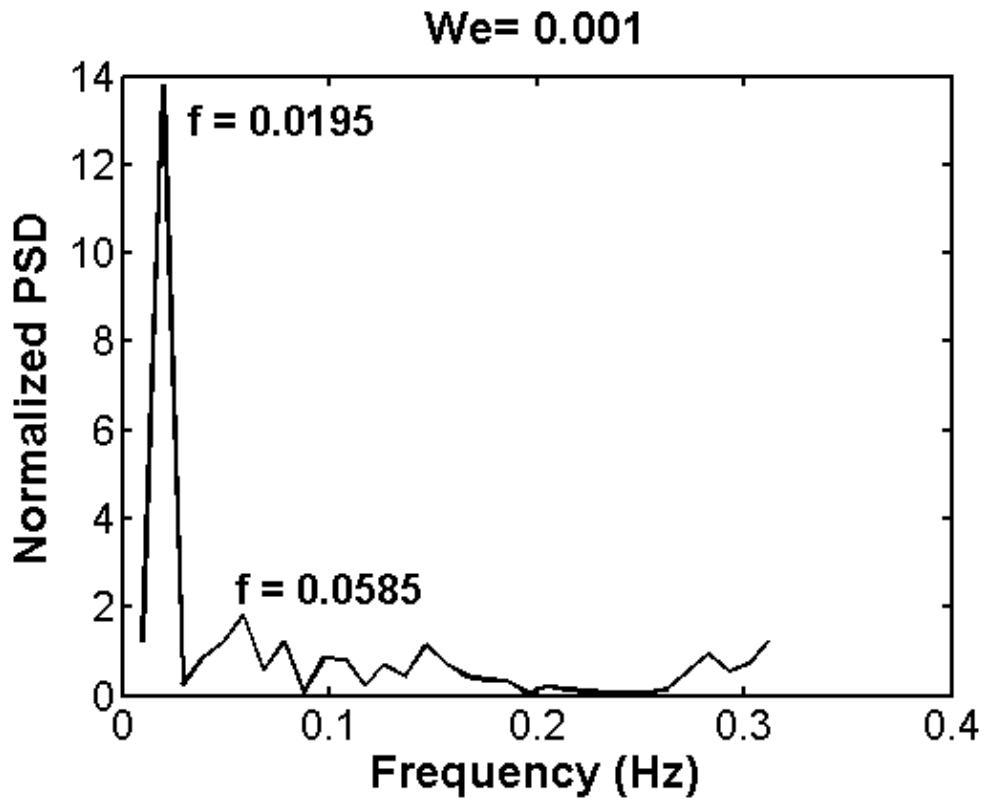
Appendix C-Lomb Scargle periodogram plots

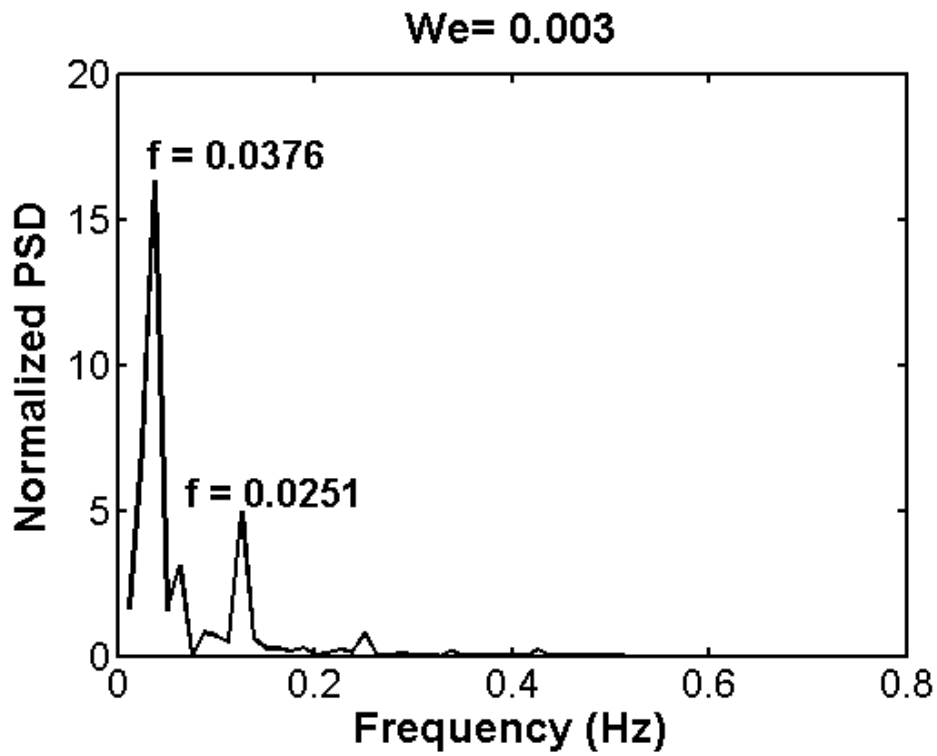Figure C.1 Lomb Scargle periodogram for P1 behaviour. Here *G*=0.057, *Ka*=0.000562

Figure C.2 Lomb Scargle periodogram for P1 behaviour. Here *G*=0.057, *Ka*=0.000562
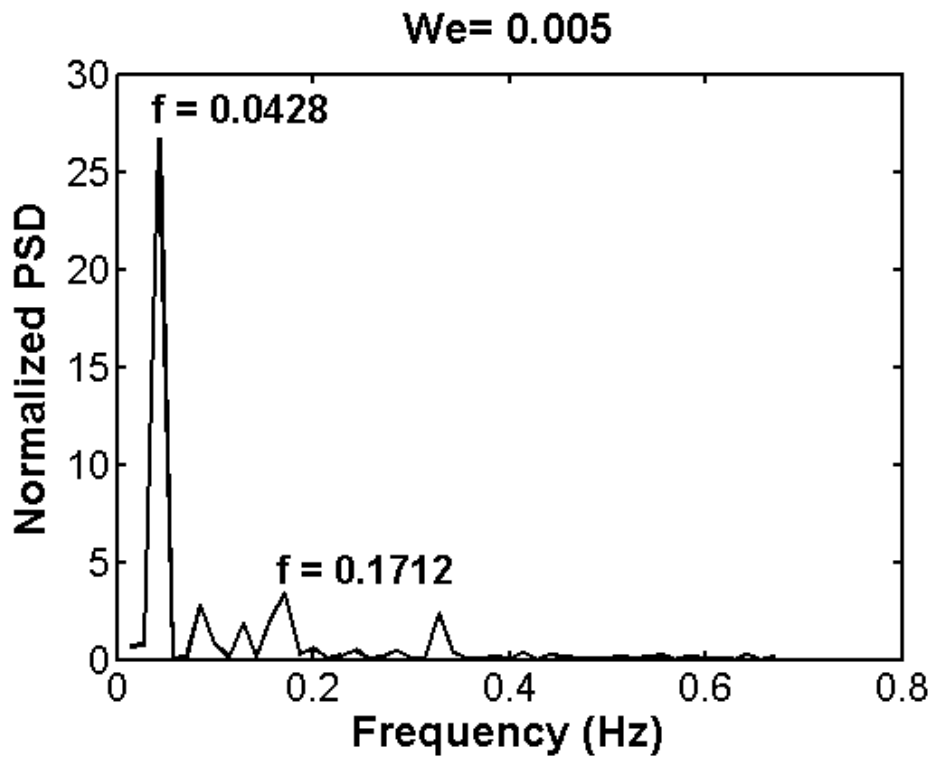

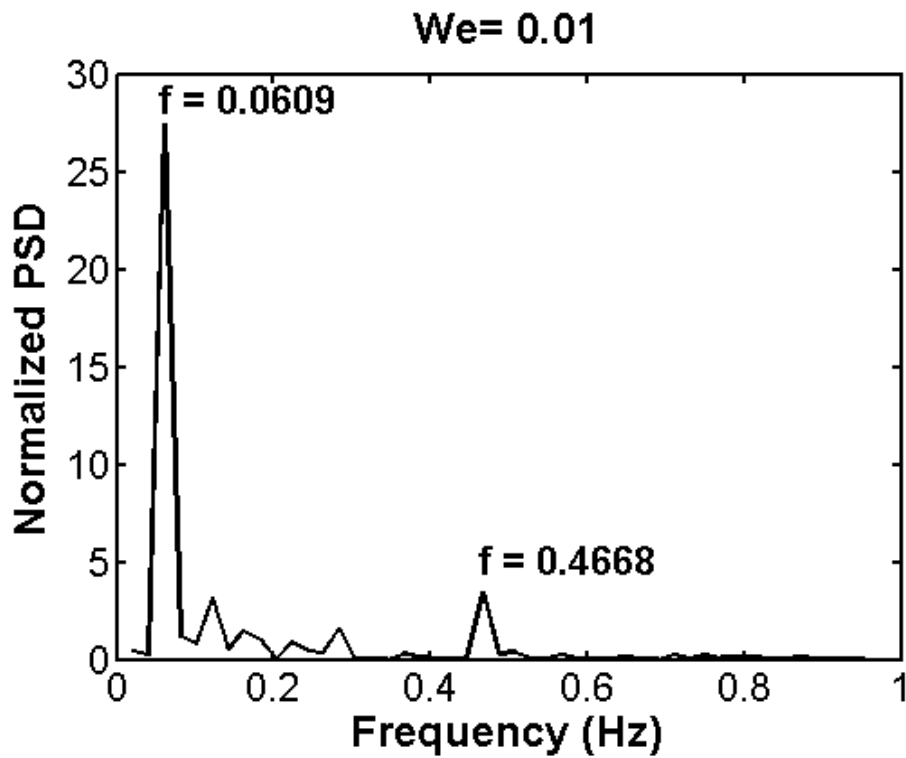Figure C.3 Lomb Scargle periodogram for P1 behaviour. Here *G*=0.057, *Ka*=0.000562

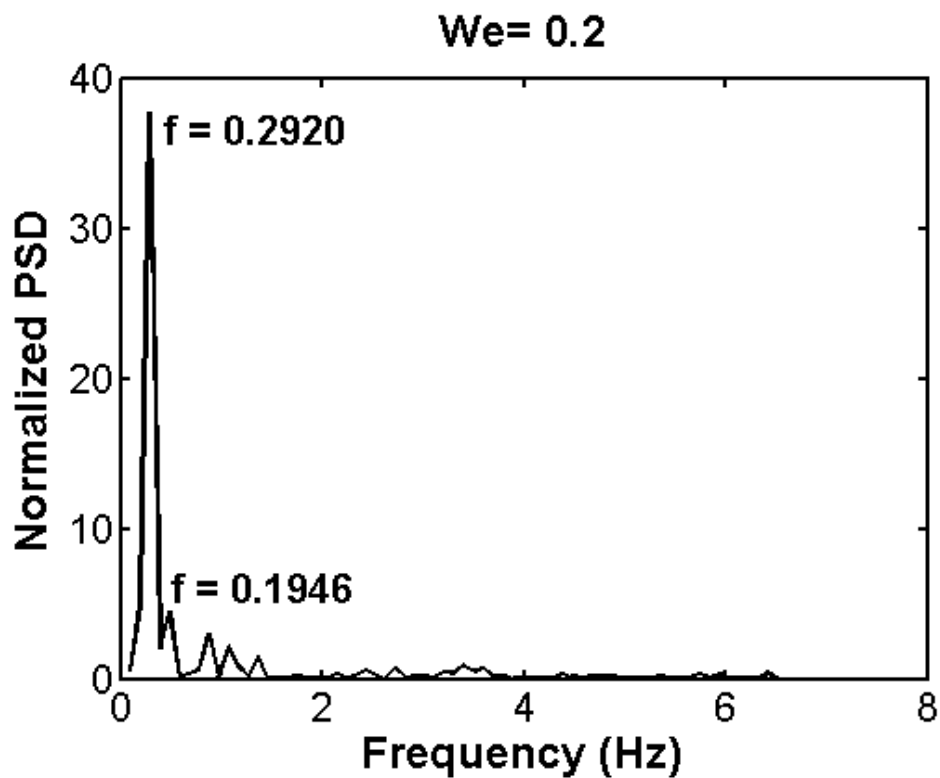Figure C.4 Lomb Scargle periodogram for P1 behaviour. Here *G*=0.057, *Ka*=0.000562

Figure C.5 Lomb Scargle periodogram for LC behaviour. Here *G*=0.057, *Ka*=0.000562

Appendix D- List of Publications and Conferences Attended

a) Submitted a paper titled "Dripping Modes of Newtonian Liquids: The Effect of Nozzle Inclination" to the ICFMT 2013: International Conference on Fluid Mechanics and Thermodynamics. The paper was selected for an oral presentation on 17 December 2013.

b) Submitted a manuscript titled "Dripping Dynamics of Newtonian Liquids from a tilted Nozzle" to Journal of Mechanics B/Fluids. This paper is currently under revision by reviewers.